Dissertation

submitted to the

Combined Faculty of the Natural Sciences and Mathematics

of the Ruperto Carola University Heidelberg, Germany

for the degree of

Doctor of Natural Sciences

presented by

Yingying Fu, M. Agr.

born in: Zhumadian, China

Oral examination: 13.11.2018

Modulation of capsid protein expression of *Mastomys natalensis* papillomavirus as a mechanism to circumvent adaptive immunity in a preclinical model

Referees:

Prof. Dr. Martin Müller

Prof. Dr. Frank Rösl

Eidesstattliche Erklärung

Ich erkläre hiermit, dass ich die vorliegende Dissertation selbst verfasst und mich keiner anderen als der von mir ausdrücklich bezeichneten Quellen und Hilfsmittel bedient habe. Diese Dissertation wurde in dieser oder anderer Form weder bereits als Prüfungsarbeit verwendet, noch einer anderen Fakultät als Dissertation vorgelegt. An keiner anderen Stelle ist ein Prüfungsverfahren beantragt.

Heidelberg, den 07.08.2018

Yingying Fu

Table of contents

Summary

A remarkable feature of cancer-associated Human papillomavirus (HPV) types (e.g. HPV16/18) is that the open reading frame (ORF) of the major capsid protein L1 comprises alternative translation initiation codons, thereby potentially encoding different isoforms. Notably, the same can be found within the genome of *Mastomys natalensis* papillomavirus (MnPV), an etiological agent for non-melanoma skin cancer in the rodent *Mastomys coucha*.

Capsid formation of these L1 variants was tested using both baculovirus and pseudovirus production systems. L1 translated from the first and second ATG (referred as L1LONG and L1MIDDLE) inefficiently induced capsid formation. In contrast, virions could be efficiently formed with capsomeres derived from L1SHORT protein starting from the third ATG. Even after adding L1SHORT and L2 proteins, L1LONG and L1MIDDLE were still unable to form the spherically correct virus particles.

Analysis of MnPV-infected animals during early infection revealed strong serological responses against MnPV L1LONG and L1MIDDLE protein, but these antibodies were not protective. Contrary, neutralizing antibodies against conformational epitopes of L1SHORT only appeared during the late phase of infection, apparently enabling the virus to accumulate. Therefore, the additional N-terminal part of L1LONG might play a decisive role in capsid formation and form a loop which prevents the assembly of correct capsomeres *in vivo*. Such a transitory conformational epitope is apparently only recognized during early infection, allowing the virus to escape from humoral immune surveillance. Moreover, using competition assays during pseudoviruses formation revealed that L1LONG protein could interfere with the capsid forming process in the presence of L1SHORT. This could be also shown by changes in intracellular localization when L1LONG or L1MIDDLE is co-expressed with L1SHORT.

In summary, these data provide evidence of an adaptive immune escape initial after infection by avoiding the production of protective antibodies. Since other “high-risk” mucosal and cutaneous HPVs can also encode such L1 isoforms, these results may have important implications in the establishment of a persistent viral infection and the outcome of the disease.

Zusammenfassung

Eine bedeutsame Eigenschaft krebsassoziierter humaner Papillomavirus (HPV)-Typen (z.B. HPV16/18) ist es, dass der offene Leserahmen (ORF) des Hauptkapsidproteins L1 mehrere alternative Translationsinitiationscodons enthält. Somit können potentiell verschiedene L1 Isoformen synthetisiert werden. Dieselbe Konstellation findet man auch im Genom des *Mastomys natalensis* papillomavirus (MnPV), dem ätiologischen Agens für die Entstehung von nicht-melanozytären Hautkrebs im Nagetier *Mastomys coucha*.

Die Rolle dieser L1-Varianten bei der Bildung intakter Kapside wurde sowohl in einem Baculovirus- als auch in einem Pseudovirus-Produktionssystem getestet. L1 Varianten welche ab dem ersten bzw. zweiten ATG Startcodon translatiert werden (als $L1_{LONG}$ und $L1_{MIDDLE}$ bezeichnet) bilden nur sehr ineffizient virale Kapside aus. Im Gegensatz dazu können Kapsomere mit dem dritten ATG beginnenden $L1_{SHORT}$-Proteins sehr effizient infektiöse Partikel ausbilden. Auch nach Zugabe von $L1_{SHORT}$- und L2- Proteinen sind $L1_{LONG}$ und $L1_{MIDDLE}$ nicht in der Lage korrekte Viruspartikel zu bilden.

Biologisch relevant sind diese Ergebnisse deshalb, da die Analyse von MnPV-infizierten Tieren während frühen Phasen der Infektion ergab, dass trotz starker serologischer Reaktion gegen $L1_{LONG}$ und $L1_{MIDDLE}$ Proteine keine neutralisierende Antikörper gebildet werden. Diese werden nur im späteren Infektionszyklus gegen Konformationsepitope von $L1_{SHORT}$ gebildet und erlaubt daher den Viren sich in der frühen Phase zu vermehren. Dabei spielt der zusätzliche N-terminale Teil von $L1_{LONG}$ eine entscheidende Rolle da sich dadurch die Konformation ändert welche die Bildung von korrekten Kapsomeren *in vivo* verhindert. Ein solches Konformationsepitop wird offenbar nur während einer frühen Infektionsphase synthetisiert, sodass das Virus der humoralen Immunantwort entgeht. Darüber hinaus zeigten Kompetitionsassays, dass das $L1_{LONG}$-Protein das „Assembly“ zu intakten Kapsiden in Gegenwart von $L1_{SHORT}$ stört. Dies konnte auch durch Veränderungen in der intrazellulären Lokalisation gezeigt werden, wenn $L1_{LONG}$ oder $L1_{MIDDLE}$ mit $L1_{SHORT}$ co-exprimiert wurden.

Zusammenfassend zeigen diese Daten, dass MnPV durch die Synthese unterschiedlicher L1 Isoformen die adaptive Immunantwort umgeht indem es die Produktion von protektiven Antikörpern in der frühen Infektionsphase verhindert. Da auch andere "risikoreiche" mukosale und kutane HPVs solche L1-Isoformen kodieren können, könnten ähnliche Mechanismen vorliegen was virale Persistenz und damit die Entstehung von Tumoren begünstigt.

1. Introduction

1.1 Papillomaviruses

Papillomaviruses (PVs) are a diverse cluster of small non-enveloped DNA viruses that infect a range of different species including reptiles, birds, marsupials, and mammals [1]. Up to date more than 300 papillomaviruses types were identified including 210 human papillomaviruses (HPVs) as well as 170 animal papillomaviruses (PaVE: Papillomavirus Episteme) [2]. They are divided into different genera based on the nucleotide sequence comparison (at least 10 percent difference), which are named with Greek letter: alpha, beta, gamma, mu and nu for HPV and pi, omicron, xi, lambda, kappa, iota, theta, eta, zeta, epsilon and delta etc. for animal papillomaviruses [3, 4].

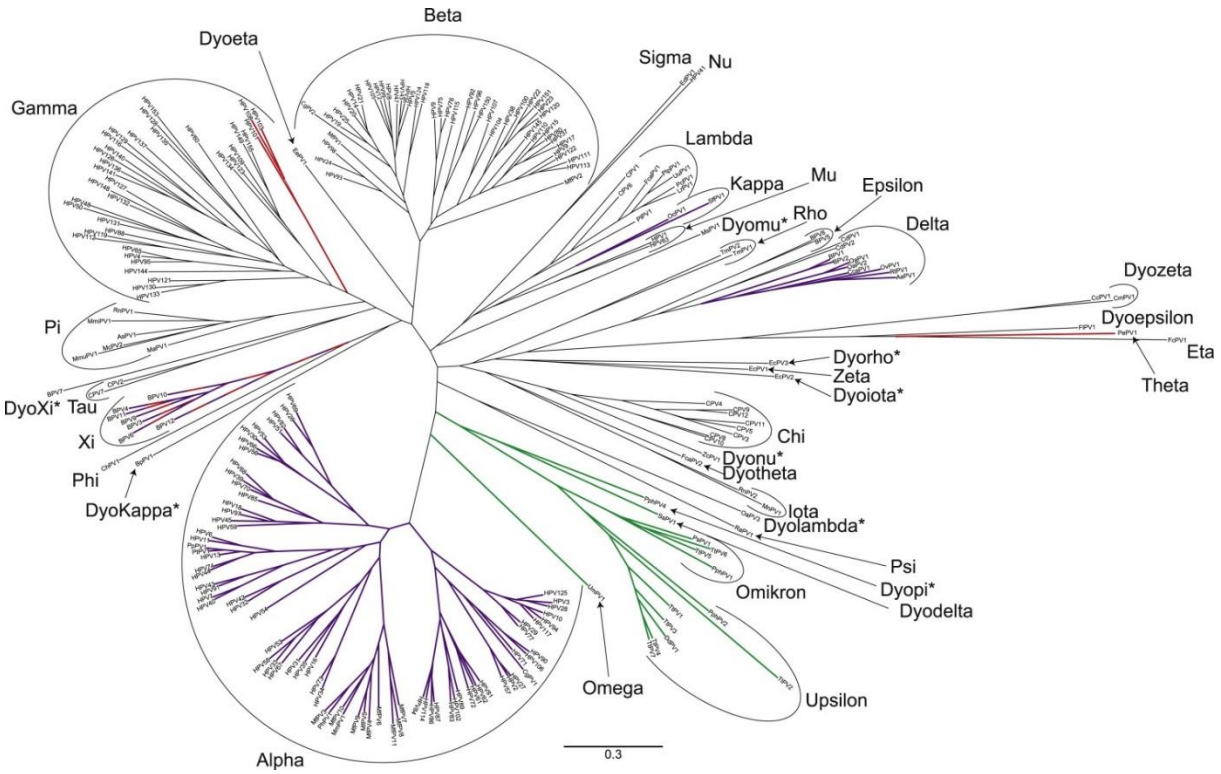

Figure 1.1: Papillomavirus phylogenetic tree [5]. E1, E2, L1 and L2 genes from 241 papillomaviruses were downloaded from PaVE and aligned for construction of the phylogenetic tree. The colors represent presence or absence of adaptive proteins. Red clades lack an E6 ORF, green clades lack E7 protein and purple clades lack E5 gene. *Mastomys natalensis* papillomavirus (MnPV) belongs to iota-papillomavirus family and *Mastomys coucha* papillomavirus 2 (McPV2) is classified to pi-papillomavirus family.

1.2 Human papillomaviruses

In general, HPV infections can be potentially cleared by immune system. However, for some instances, HPVs can cause benign hyper-proliferative lesions such as warts or asymptomatic

lesions at particular anatomic sites, which in some cases can progress to invasive malignant cancer [6]. The cutaneous HPVs facilitate benign papillomas in the skin, of which most manifestations are common plantar and flat warts [7]. The genital HPVs, which are responsible for benign warts or malignancies in penile, vulvar and anal, are considered to be the causative agents of most cervical cancers [8]. According to clinical pathologies, HPVs are classified into ‘‘low risk’’ cutaneous type (e.g. HPV 3, HPV 10 and HPV61 etc.); “low risk” mucosal type (e.g. HPV 6, HPV11 and HPV 13 etc.) and “high risk” type (e.g. HPV 16, HPV 18 and HPV 45 etc.). On the basis of epidemiological data, HPV 16, 18, 31, 33, 35, 39, 45, 51, 52, 56, 58 59, 69, 73 and 82 are confirmed as “ human carcinogens ”, which are responsible for 99.7% cervical cancer [9, 10]. Especially, HPV 16 and HPV 18 are the most prevalent pathogens causing 50% and 20% of all cervical cancer cases. Cervical cancer, a major burden worldwide, is the fourth most frequent cancer in women causing 528,000 cases and 266,000 deaths every year [10]. In a small group of infected women, continuous infection leads to low or high grade cervical interepithelial neoplasia (CIN), and eventually results in invasive cancer, where the viral genome integrate into the host genome [11]. The virus-like-particle (VLPs) based vaccines e.g. Cervarix (HPV16 and 18), Gardasil (HPV 6, 18, 11 and 16) and Gardasil-9 (additionally HPV 6, 18, 11, 16, 31, 33, 45, 52 and 58) are the current strategy to prevent cervical cancer.

1.3 The papillomaviruses genome

Papillomaviruses have a double stranded circular DNA genome, which ranges from 6953 bp [Chelonia mydas papillomavirus type 1 (CmPV1)] to 8607 bp [Canine papillomavirus type 1 (CPV1)] in length [5]. The genome is normally associated with the cellular histones [12] and contains three regions: the upstream regulatory region (URR), the early region and the late region. The URR encompasses several cis-regulatory elements including early promoter, viral origin of replication and various transcriptional regulatory sites for cellular and viral transcription factors.

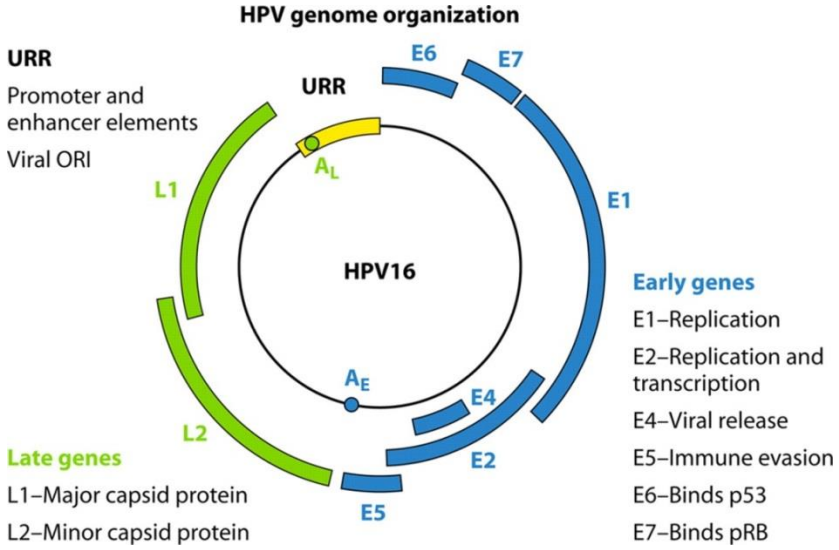

Figure 1.3: The typical mucosal high-risk HPV genome [13]. The HPV 16 genome with a size of 8 kb contains early region (E1, E2, E4, E5, E6 and E7), late region (L1 and L2) and the upstream regulatory region (URR). The early genes E1 and E2 play a role in the viral replication and transcription, whereas E6 and E7 oncogenes are essential for transformation. The late region encodes viral structural L1 and L2 proteins, which modulate capsid assembly and encapsidation of viral genome. The URR harbors cis-regulatory elements such as promoter, replication origin and transcription factor binding sites. A_L: polyA (late); A_E: polyA (early).

The early region contains five to six open reading frames (ORFs): E1, E2, E4, E5, E6 and E7, while the cutaneous PV types typically miss E5 gene [14]. The replication origin is comprised of a palindromic E1 binding region, two to three E2 binding sites and an A/T rich region [15-17]. The hexameric DNA helicase E1 is thought to be an essential protein for initiation and catalysis of viral DNA synthesis in the nucleus of infected keratinocytes. E1 unwinds DNA at the origin ahead of replication fork and mediates with cellular DNA replication factors by assembly into its enzymatically active form - a double hexamer [18]. For most PV types, E2 acts as a molecular enhancer to initiate DNA replication by directing E1 helicase onto the origin [19, 20]. E2 can engage in the binding to the sequence motifs in the viral genome, which can activate or repress the transcription. E2 represses the transcription by the competition with a short form of E2 for binding to binding sites or recruitment of repressor complexes to viral DNA [21-23]. E4 gene is entirely located within the E2 ORF, which is often expressed from a spliced mRNA and present as E1^E4 transcript. Despite E4 protein is expressed before the late genes, it always serves as a biomarker of active virus infection due to its frequency expression at the late stages of the viral life cycle, around the time that genome amplification is initiated. E1^E4 protein mainly contributes to the virus release and transmission by its disruption of cellular keratin network and formation of

the cornified envelope [24, 25]. The transmembrane E5 protein engages in multiple interactions with cellular growth receptors such as PDGF β receptor and EGF receptor, thus facilitating transformation and the development of carcinomas [26]. The oncoproteins E6 and E7, which induce the degradation of the host cell tumor suppressors p53 and retinoblastoma (Rb) protein, are the primary reason for tumorigenesis [8]. These two factors act cooperatively in the development of HPV-induced cancers. As the key regulators of S phase genes, Rb protein controls the activity of E2F transcription factors [27]. Thus, the efficient binding of Rb and E7 could promote premature S phase entry and DNA synthesis, leading to inhibited cell growth and apoptosis, as well as driving productive viral life cycle for tumor progression [28]. However, the block of Rb function by E7 results in increased levels of p53, and E6 correspondingly disrupts p53 for degradation allowing avoidance of apoptosis [29]. This gives rise to the accumulation of DNA damage and mutations that can promote transformation and carcinogenesis.

1.4 The open reading frame of L1

The L1 gene expression is restricted to the late phase of the viral life cycle, which occurs in the differentiated keratinocytes in the *Stratum granulosum* [30]. L1 transcripts are generated from the polycistronic mRNA isoforms under the control of URR and generally mediated by the late promoter within E7 gene. During the late gene expression, the early gene mRNAs are removed by viral RNA splicing when the transcriptional machinery passes through the early region and fails to recognize the early polyadenylation signal [31].

For many PV types, especially the high-risk HPVs, L1 protein contains several alternative translation initiation codons, which can potentially synthesize several isoforms of L1. Many well-established cervical carcinomas associated types, such as HPV16, 18, 45, 52, 54 and 58, contain the additional ATGs. However, the alternative upstream ATG is absent in “low-risk” types linked with genital warts such as HPV 6b, 11, 13, 42, 44 and 55, as well as HPV 3, 7, 9, 10, 12, 36 and 37 which associate with benign lesions [32]. Therefore, it is attempted to speculate that the capability to synthesize different isoforms of L1 protein might contribute to the development of carcinomas. The alignment of L1 proteins from different PV types indicates that there is a consensus MxxWx_7YLPP motif at N-terminal region. It is reported that virus-like particles (VLPs) can only

be efficiently assembled from the short L1 version of which the methionine is close to this Wx7YLPP motif [33].

Figure 1.4: The alignment of L1 sequence (adapted from Dr. Sabrina Vinzón, modified according to [33]). L1 proteins N-terminus sequences from 28 PV types were aligned by the Clustal Omega online. The red boxes indicate the highly conserved sequences (MxxWx7YLPP) at the N-terminus of L1 sequence. The different genera of the PVs are marked. Both MnPV and McPV2 contain three translation initiation codons at the N-terminal sequences of L1.

1.5 The L1 monomer structure

The L1 monomer contains a canonical "jelly roll" β sandwich (eight-strand β barrel: BIDG-CHEF), five α helices (h1 - h5) and six loops (BC, CD, DE, EF, FG, and HI), five of which (besides CD) are the surface loops of capsomere [34]. Eight antiparallel stranded β jellyrolls form the core structure of L1, with the strands linked with loops on the top of pentamer knob, where the most neutralizing antibodies bind. There are several interpentameric and intrapentameric disulfide bonds between the neighboring subunits, which play an important role in the interaction with pentamers within the particles, thus facilitating capsid stability. For example, the HI surface loop from one monomer intertwines with the neighboring anticlockwise FG and EF loops. The helices h2 and h3 form a V-shape groove, which has a hydrophobic interface with the neighbor monomer h4. The G1 segment strand of the BIDG β barrel from one L1 monomer connects with the neighboring monomer CHEF β sheet. The N-terminal and C-terminal domain of L1, as the "invading arm", form the interpentameric contacts by invading the arms to the adjacent pentamers [35, 36]. The residues 1-20 of the N-terminal arm are conserved in all papillomaviruses and are thought to fill the gap in the virions shell, which is essential for maintaining the capsid

stability [35]. The deletions of up to 30 residues of the C-terminus as well as the addition sequences to C-terminus do not interrupt the pentamer structure [37-39]. The residues at C-terminus (approximately after residue 474) return to the L1 pentamer origin. Two conserved cysteines Cys175 and Cys428 are involved in the intercapsomeric disulfide bridge, which facilitate the formation of intact virus capsid [31, 34].

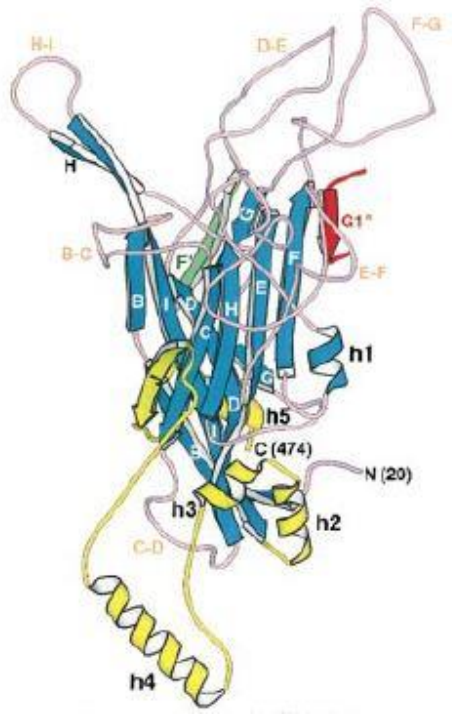

Figure 1.5: The HPV16 L1 monomer with residues from 20 to 474 [36]. The β "jelly roll" strands and h1 helix are in blue. The helices h2 - h5 and βJ strand are marked in yellow. The G1 strand segment is in red. The F strand of the clockwise neighbor is in green. The six BC, CD, DE, EF, FG, and HI loops are in pink.

1.6 The papillomaviruses capsid

Papillomavirus capsid is a 50-60nm in diameter icosahedral particle that is composed of multiple copies of major capsid protein L1 and minor capsid protein L2 [40]. The major capsid protein L1, with molecular mass of around 55 kDa, could spontaneously self-assemble into virus like particles (VLPs) [41], without viral DNA encapsidation. These VLPs can be produced in insect cells by the baculovirus expression system and in yeast, which result in particles presenting an exterior surface virtually indistinguishable from native virions [41-43]. Five copies of L1 monomer spontaneously self-assemble into the pentameric capsomere, which presents mushroom-like protrusions (11-12nm in diameter) along with five-points star-shaped heads [44]. Seventy-two capsomeres with small amounts of L2 proteins in the proximal pocket form infectious virus

particles with the icosahedral lattice symmetry T = 7. Even though it is not necessary to form VLPs with the participation of L2 proteins, it is reported that twelve L2 proteins are incorporated into native viral capsid by the hydrophobic C-terminal arm [45]. However, the abundance of L2 within capsid can be arranged up to 72 molecules, which presents an icosahedral L2 density beneath the axial lumen per L1 capsomere [46]. The internal diameter of the viral capsid shell is around 42 - 46nm [34, 44]. Twelve pentavalent pentamers, each surrounded by five other pentamers, are centered on 5-fold symmetry axes. However, 60 hexavalent pentamers, each of which is surrounded with six other capsomeres, are centered at 6-coordinated positions [44] [47]. Therefore, each hexavalent lattice point is encompassed by five hexavalent points and one pentavalent point. A twelve pentameric icosahedral particle (T = 1, small VLP) was formed by N-terminus truncated L1 proteins, indicating that N-terminal polypeptides (1-20 residues) might play an important role in the intercapsomeric contacts by blocking the C-terminal arm from returning to pentamer of origin [36].

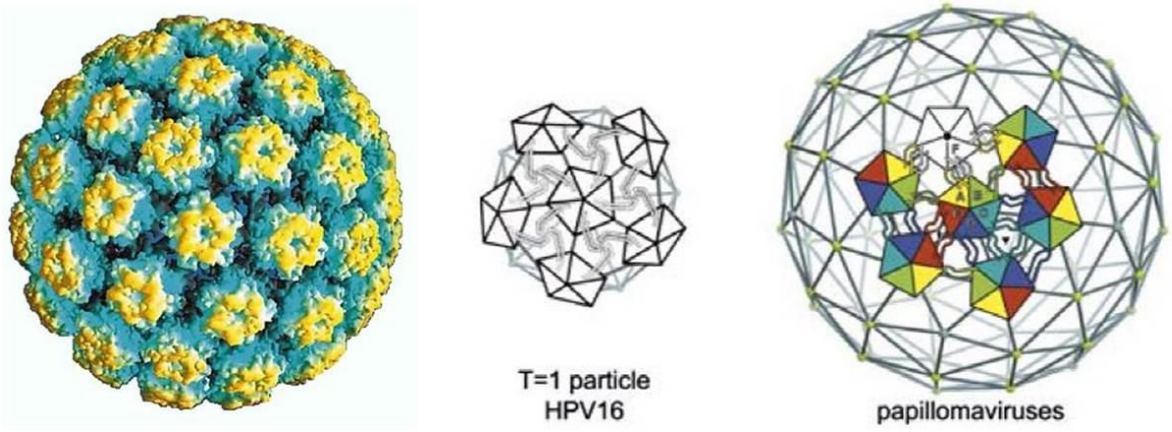

Figure 1.6.1: The papillomavirus capsid structure [35, 47]. The papillomavirus capsid consists of major capsid protein L1 and minor capsid protein L2. The N-terminal truncated L1 proteins (ΔN-10) form a small 12 - pentamer icosahedral particle (T = 1). 360 copies of L1 with twelve L2 form a T = 7 papillomavirus capsid. Each hexagon is surrounded by five hexagons and one pentagon.

For a T = 7 lattice, there is a left T = 7 *laevo* or a right T = 7 *dextro* handed enantiomorph. However, it is assumed that particle structures only have the same hand among the viral capsids within a particular virus strain. For example, apart from cottontail rabbit papillomavirus (CRPV), which is the only T = 7 *laevo* capsid, other papovaviruses, such as simian virus 40, murine polyomavirus and human papillomavirus, are all T = 7 *dextro* icosahedral particles. The triangulation number of papillomavirus particle (T = 7) is defined by the arrangement of lattice points between adjacent pentavalent points. A T = 7 lattice exhibits a "two steps (h) starting from a

pentavalent point forward onto two neighboring hexagons followed by one step (k) to the left or right pentavalent point" pattern. Therefore, the triangulation number of icosahedron is calculated by the formula: $T = h^2 + hk + k^2$ [44].

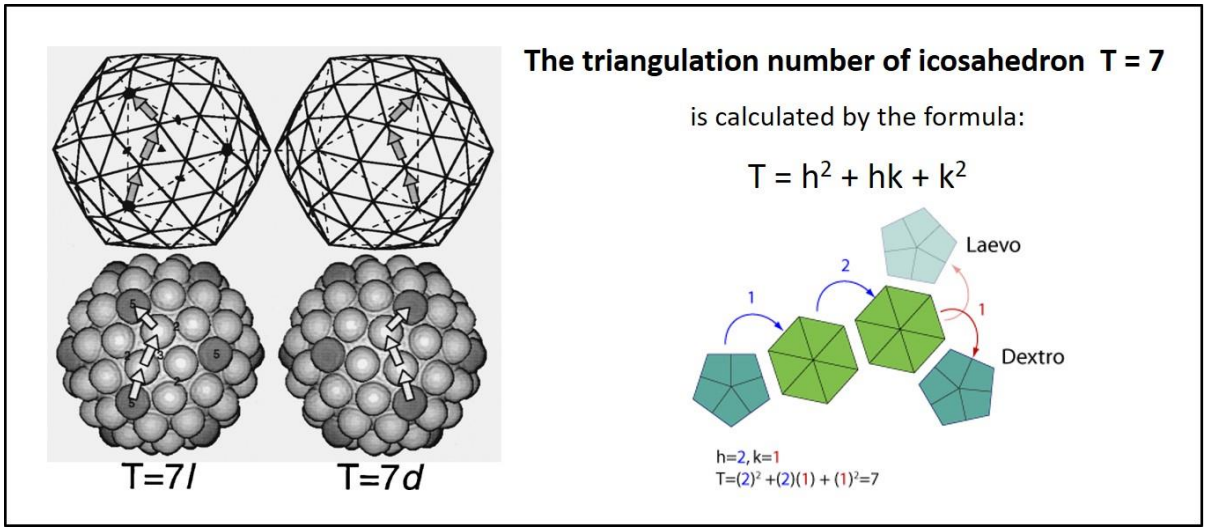

Figure 1.6.2: Calculation of the triangulation number [44]. There are two icosahedral lattices with a triangulation number of seven: left T = 7 *laevo* and right T = 7 *dextro* handed enantiomorph. The particle is formed by sixty hexavalent and twelve pentavalent capsomeres. The calculation figure is adapted from the ViralZone website.

1.7 Capsid assembly

The major capsid proteins L1 are expressed and assembled into capsomeres in the cytoplasm of terminally differentiated keratinocytes. Subsequently, the assembled capsomeres pass through the nuclear pores and are translocated into nucleus due to the nuclear localization sequence (NLS) signal at C-terminus of L1 protein [48, 49]. The minor capsid proteins L2 normally associate with promyelocytic leukemia protein (PML) bodies and translocate into nucleus, thus assisting capsid assembly [50]. It is reported that L2 could facilitate the transport of L1 capsomeres to nucleus, and complement L1 nuclear translocation even NLS of L1 is defective [51]. The viral capsid assembly machinery eventually occurs in the nucleus based on the translocation of L1 and L2 proteins after packaging with the replicated PV genomes. Both L1 and L2 proteins are able to bind DNA without sequence specific interaction *in vitro*, suggesting that they might directly bind virus genomic DNA, thus enabling DNA encapsidation [52, 53]. The positively charged residues from C-terminal region of L1 (also overlapping with the NLS) and both N-terminus and C-terminus of L2 are the potential DNA-binding domains. However, even though eight residues from N-terminus or nine C-terminal amino acids of L2 are deleted, viral genome encapsidation

still remains, but resulting in non-infectious virions [54, 55]. L2 could also recruit E2 to PML bodies, suggesting a role of E2-mediated replication during DNA encapsidation process [56]. The participation of L2 in capsid assembly might influence the final structure of virions and additionally increase viral infectivity and virus nucleic acid encapsidation.

Depending on the L1 proteins self-assembly ability, VLPs, pseudoviruses (PsVs) and quasivirions (QV) are produced in different synthetic systems *in vitro*, which could mimic the structure of the native viral capsid (T = 7 icosahedral lattice). VLPs can be produced in different prokaryotic or eukaryotic systems such as mammalian cells, Sf9 cells, *E.coli*, or yeast by transfection of expression plasmids containing L1 alone or L1 with L2 together [41, 42, 57]. Since VLPs are found to be uniform in size and remain similar structures as the native virions, vaccines based on VLPs production are used to induce high titer of neutralizing antibodies to prevent HPV infection [58]. PsVs are produced by transfection of L1 and L2 codon-modified expression plasmids as well as a reporter plasmid containing GFP/Gaussia luciferase with a size of 5.9 kb. Since the expression of wild type L1 and L2 genes is restricted in cultured mammalian cells, L1 and L2 ORFs are codon modified [59]. The primary amino acid sequence is not changed but a significantly increased expression can be achieved by these codons changes. The plasmid containing SV40 origin of replication (ori) is used for generation of high copy number pseudogenomes, which can be packaged in the capsids. 293T or 293TT cells that express high levels of SV40 large T antigen (LT) enable the replication of plasmids containing SV40 ori. After maturation, PsVs are isolated from cell debris in detergent and high salt solution, and then followed by Optiprep ultracentrifugation. The Optiprep gradient, which presents a combined velocity sedimentation and buoyant density, is much more efficient for virus purification than the classic CsCl purification [60]. QV production in 293T or 293TT is a similar technology to that of PsVs. The only difference between QV and PsVs production is that re-circularized HPV genomes rather than reporter plasmids are incorporated into particles. The PsVs and QV production can be used in multiple aspects including particles structure, capsid assembly, neutralization capacity and virus entry [61].

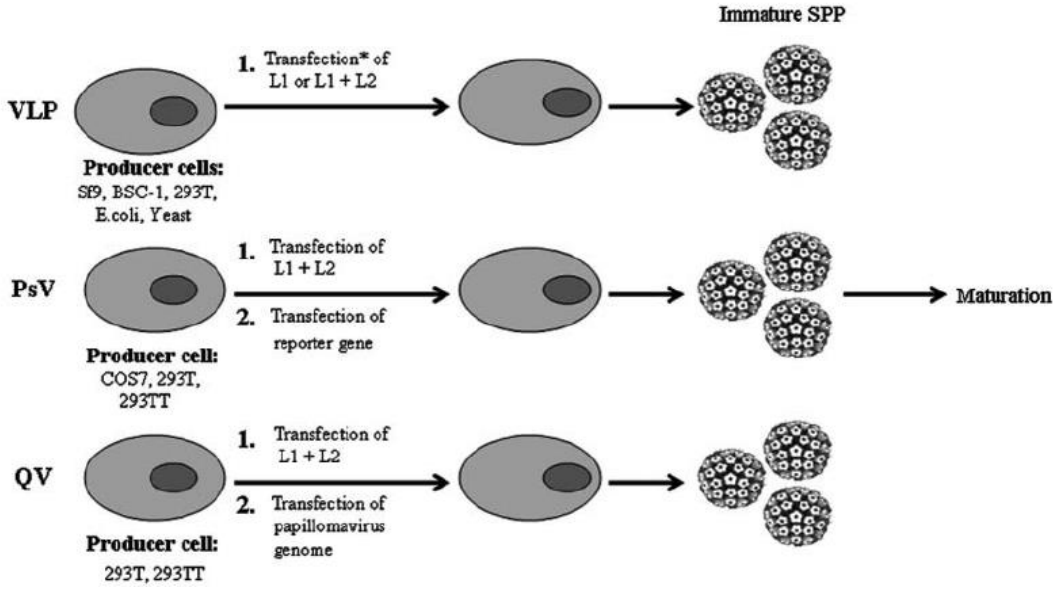

Figure 1.7: Schematic overview of VLP, PsVs and QV production [61]. The synthetic papillomavirus particles (SPP) are produced by transfection of plasmids expressing capsid proteins L1 alone, or together with L2. The difference of three particles production is the presence or absence of incorporated DNA. PsVs contain reporter plasmids with GFP/Gaussia luciferase and QV contain full length papillomavirus genomes.

VLPs can be disassembled into capsomeres in the presence of reducing agents, such as dithiothreitol (DTT), with low ionic strength and high pH (pH = 8.2) [62] [63]. This is caused by the insufficient formation of disulfide bonds network within pentamers under the reducing condition. However, instead of particles disassembly, DTT treatment to BPV purified intact particles leads to a conformational change (expansion of 10% in diameter), and finally results in virions disruption by the entry of proteases and nucleases to the interior [64]. Therefore, for virus particles production, there are several methods to stabilize the intact structure, such as high ionic strength (> 0.5 M sodium chloride), low pH and removal of reducing agents. The reassembly of VLPs can be achieved by simply dialyzing out the disassembly buffer.

1.8 The human papillomaviruses life cycle

HPVs infection as well as the viral gene expression is absolutely confined to the keratinocyte differentiation program, which presents in a differential spatial and temporal pattern [13]. The initial HPV infection occurs in keratinocytes in the basal layer of epithelium due to abrasion or micro-wounds during scarification or sexual intercourse [65]. The virus attachment to the host cells mainly depends on the binding of heparin sulfate proteoglycans (HPSGs) on the cell surface with C-terminus of L1 protein, thus leading to the conformational change of L1 and

subsequently exposure of N-terminal domain of L2 [65-67]. The L2 additional epitopes are then exposed by furin protein convertase cleavage at amino acid 12, which is important for the internalization of virus capsids into cells and transport of virus genomes to nucleus [66, 68]. After virus binding and entry, the viral genomes are established in the nucleus as low-copy episomes (20-100 per cell) and replicated in synchrony with the expression of the early genes E1 and E2 [69-71]. The infected cells undergo differentiation and the cellular DNA synthesis machinery enables viruses to maintain the productive phase of the viral life cycle. After cell division, the infected daughter cell migrates away from the basal layer and enters the spinous layer. The expression of E6 and E7 pushes differentiating infected cells into S phase, resulting in the immortalization of the host cells and facilitating the following steps for tumorigenesis [72, 73]. A dramatically amplification of viral DNA (many thousands of viral copies per cell) and gene expression is achieved in this stage, along with activation of the late viral promoter [74, 75]. Finally, L1 and L2 proteins in the late phase assemble into infectious particles encapsidated with synthesized viral genomic DNA, which are then released from the uppermost layers (*Stratum granulosum*) [76].

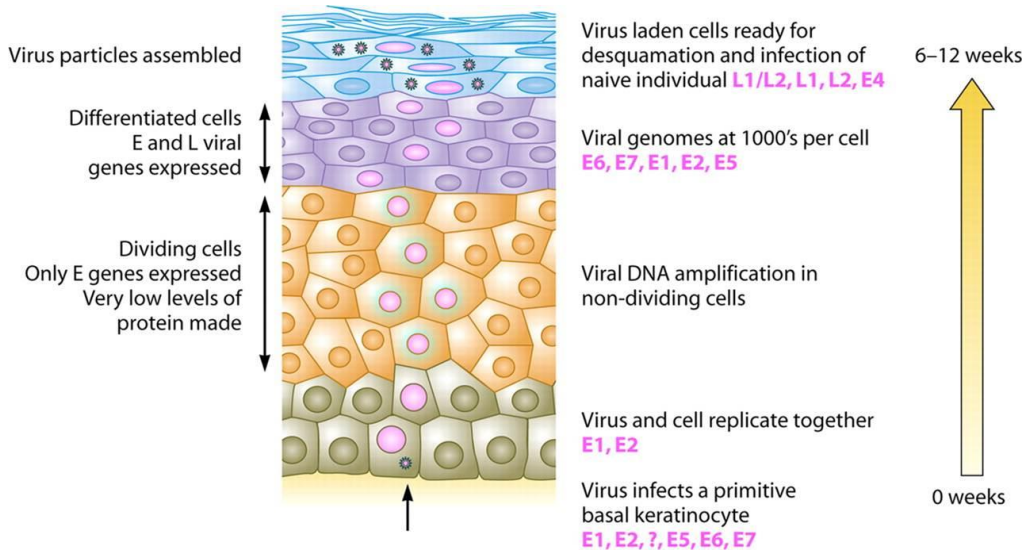

Figure 1.8: The PV life cycle in the infected epithelial tissue [13]. The HPV infectious life cycle is tightly restricted to the infected epithelium differentiation and divided into early and late phase. The virus infects keratinocyte in the basal layer through micro-wounds. The expression of E1 and E2 proteins mediates the replication of the viral genome, which coincides with the cell division. During the program of differentiation, the early genes E6 and E7 expression is strictly controlled, unless the infected cells terminate division and start differentiating into mature status. This leads to a highly amplification of viral gene expression and genome cope numbers. Finally, L1 and L2 proteins in the top layer assemble into infectious particles with replicated viral genome, which are then released from the tissue through desquamation process.

1.9 The humoral immune response against papillomaviruses

The humoral immune responses against papillomaviruses antigens are used to monitor the course of infection. There are different antibodies responses, which mainly are against early proteins E2, E4, E6 and E7 as well as the viral capsid proteins L1 and L2. E2 seroresponses are more abundant in CIN1-2 lesions and decrease within the higher grade CIN as well as cervical cancer population. Anti-E4 antibodies are more frequently present in the population with precancerous lesions than the healthy group or the one with cervical cancer. [77]. The humoral responses to E6 and E7 are found to correlate with cervical cancer and pre-cancer lesions [78, 79]. Compared to E6, there is a higher rate for a correlation of E7 antibodies responses with the late stage cervical cancer [80, 81]. However, some reports suggest that E7 seroresponses are associated with the early stage of cervical cancer such as CIN3 lesions [82].

The HPV serotype specific L1 responses are generally detected in individuals with long term viral infection and HPV-carrying high grade CIN [83, 84]. However, these responses are developed very slow and finally detectable around 8 and 9 months after the first HPV positive DNA detection. Two L1 peptides located on the L1 surface exposed regions are strongly positive in the cervical cancer patients' sera [85]. VLPs are used to measure the neutralizing antibodies responses as well as some conformational epitopes. The antibodies against VLPs are increased with the grade of cervical lesions [77]. Based on previous results, L1 positivity against MnPV is a potential serological marker for tumor development, whereas E2 seroreactivity can be used as an early marker for virus infection [86] .

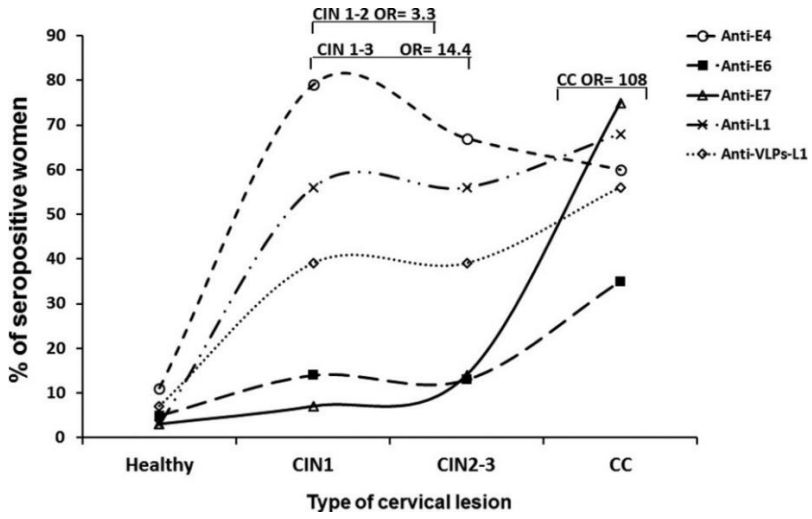

Figure 1.9: Anti-E4, E6, E7 and L1 antibodies responses in different populations with different CIN grade and cervical cancer [77]. CC: Cervical cancer

1.10 Animal models for papillomaviruses research

Various animal models are used to comprehensively understand HPV infection in human including virus life cycle, immune responses and process of lesion formation. The earliest models of PV study are cottontail rabbit papillomavirus (CRPV) and bovine papillomavirus type 1 (BPV1), but neither of them are the ideal models [87]. In 1933, CRPV was found as a transmissible agent for the prominent papillomas formation in cottontail rabbits and domestic rabbits at the cutaneous sites [88]. However, as CRPV natural host, cottontail rabbits are not easy to be kept in captivity since they are genetically diverse wild animals. Therefore, the use of DNA gun technologies allows experimental infection of CRPV to the domestic rabbits, thus investigating the individual roles of viral proteins during the process of tumorigenesis. In addition, CRPV is also used for the preclinical trials of prophylactic vaccines. However, compared to the high abundance of virus production in cottontail rabbit's lesions, there are few or no infectious virions in domestic rabbits leading to an incomplete virus life cycle [87].

Six BPVs can be divided into two groups according to the ability to induce fibropapillomas (BPV1 and 2) or papillomas (BPV 3, 4 and 6). BPV5 is the unique one that can induce both fibropapillomas and papillomas. BPV1 causes fibropapillomas of teats, udders and penis of cows. BPV2 induces fibromas and polyps of skin, squamous cell carcinoma of the gastrointestinal tract and bladder cancer. In cattle, BPV 1 and BPV 2 are the only papillomaviruses that can infect other hosts including horses, donkeys and mules. BPV4 intensifies the carcinogenic process at the upper gastrointestinal (GI) tract under the presence of immunosuppressant and chemical carcinogens in bracken fern fed cattle. BPV6 infection at teats and udders is not only a healthy burden but also an economic issue [89]. However, even though BPVs cause diverse lesions in their natural hosts, cows are inconvenient animal models to study the PV-associated diseases due to their size and cost [87].

Furthermore, canine oral papillomavirus (COPV/CPV1), which induces oral papillomas in dogs, is used for the preclinical vaccination study. Recently, COPV is replaced by the rabbi oral papillomavirus (ROPV) [90-92]. By using these models, it is shown that vaccination of VLPs can elicit neutralizing antibodies to protect individuals from PVs infection as well as experimentally induced tumors [93]. Another animal papillomavirus type named *Mus musculus* papillomavirus (MmuPV), which induces papillomas in the immunosuppressed mice, is the closest model for

studying β-PVs infection. Besides, MmuPV can also infect the mucosal genital tissues, which is also observed in beta and gamma HPVs infection. Therefore, MmuPV as a model to resemble β- and γ-PVs, can potentially provide information regarding the pathogenic mechanism [87].

The African multi-mammate mice *Mastomys coucha*, which belongs to the rodent family *Muridae*, is a promising model to investigate the principle of PV-associated skin tumorigenesis at DKFZ [94, 95]. They are naturally infected with *Mastomys natalensis* papillomavirus (MnPV) and *Mastomys coucha* papillomavirus 2 (McPV2), which infect epidermal and mucosal tissues, respectively [95, 96]. MnPV belongs to iota-papillomavirus family and McPV2 is classified to pi-papillomavirus family. The reason why the names of two viruses are different is due to the fact that these animals were considered as *Mastomys natalensis* by mistake for a long time, until a taxonomical re-classification as *Mastomys coucha* was achieved [94, 97-99]. Although both species have similar morphology, the chromosome set is totally different, which is 32 chromosomes for *Mastomys natalensis* and 36 chromosomes for *Mastomys coucha.* There is no evidence of DNA integration in the host genome for these two papillomaviruses. The viral genomes persist in the episomal status in *Mastomys*, which is analogous to cutaneous HPVs types [100]. MnPV and McPV2 are not transmitted *in utero* and natural infection occurs earlier than eight weeks after birth [101]. The infection of viruses elicits diverse immune responses against the viral proteins. A high incidence of naturally developing skin and anogenital lesions can be found in the majority of older animals, including papillomas, keratoacanthomas and condylomas [96] [102, 103].

The virus-free colony was established by hysterectomies on pregnant *Mastomys* under sterile conditions. The offspring were nursed by mice which were kept in specified pathogen-free (SPF) isolator system. The antibodies responses against MnPV and McPV2 together with the viral DNA is regularly tested to verify the pathogen free. The virus-free animals can be used as a control in the vaccination study or UV irradiation. Especially, experimental infection can be performed on these animals for certain purposes. By using *Mastomys* model, it is reported that immunization of VLPs can raise long-lasting neutralizing antibodies responses that completely prevent the appearance of skin tumors under immunocompetent and immunosuppressed conditions [100]. *Mastomys coucha* can also be a suitable model for non-melanoma skin cancer (NMSC) development along with MnPV infection and UV exposure, which reflects a similar situation in human [104]. Therefore, *Mastomys coucha* performs an ideal model to exhibit an analogous

tropism and pathogenicity as skin-associated HPV under different conditions, such as immunization, immunosuppression and UV irradiation.

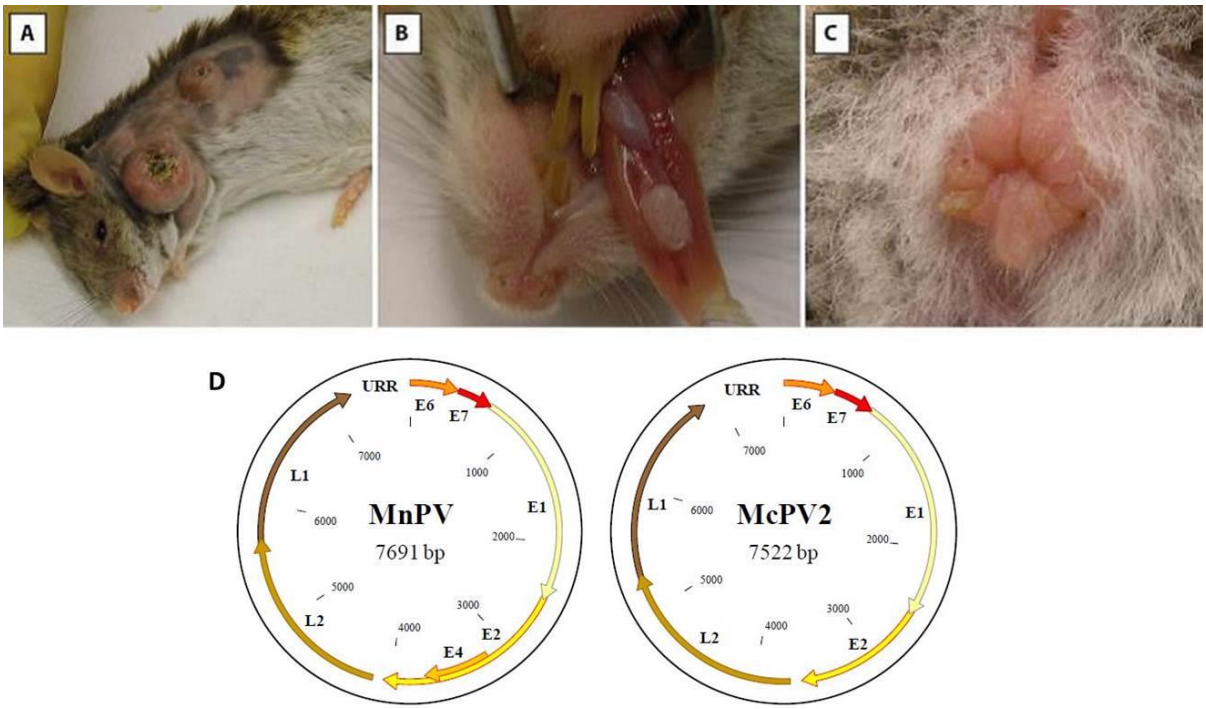

Figure 1.10: ***Mastomys coucha.*** The infection of MnPV leads to skin papillomas **(A)** in the older populations of *Mastomys*. The McPV2 infection leads to the mucosal tumors such as Oral papillomas **(B)** and condylomas **(C)**. **(D).** The MnPV and McPV2 genome. Both genomes are approximately 7,600 bp and lack E5 open reading frame.

1.11 Aim of the study

HPVs have developed a variety of strategies to evade clearance by innate and adaptive immunity [105, 106]. A common feature of high-risk HPV types is that the open reading frame of the major capsid protein L1 contains alternative translation initiation codons. A VLP-based vaccine derived from L1 protein is crucial for the prevention of virus infection, since VLPs can resemble the structures of native virions and are able to elicit neutralizing antibodies. Therefore, it is worthy investigating the capsid formation ability of different L1 isoforms and the role in virus infection, especially the immune escape mechanism. In this context, since three start codons of L1 protein are found in MnPV genome, which initiate L1LONG, L1MIDDLE and L1SHORT, respectively, *Mastomys* exhibits as an optimal model. The animals are naturally infected with MnPV, providing an analogous tropism and pathogenicity as wart-associated HPV. The major aims of this study are:

1) The capsid formation ability of different L1LONG, L1MIDDLE and L1SHORT proteins.
   - VLPs production by Baculovirus expression system
   - Production of pseudoviruses

2) The characterization of anti-L1LONG, L1MIDDLE and L1SHORT antibodies in the naturally MnPV-infected animals.
   - Follow up of anti-L1 antibodies at different time points

3) Neutralizing capacity of anti-L1LONG, L1MIDDLE and L1SHORT antibodies
   - Neutralizing assay

4) Epitope identification of anti-L1LONG, L1MIDDLE and L1SHORT antibodies
   - Denatured-VLP ELISA and Denatured-GST ELISA of anti-L1 antibodies at different time points
   - Epitope mapping

5) Interaction between L1LONG and L1SHORT proteins
   - Comparison of pseudovirus infectivity between “L1S + L2” and “L1L + L1S + L2” group
   - Colocalization of L1LONG, L1MIDDLE and L1SHORT proteins in the transfected HeLa cells.

2. Material

2.1 Chemicals and reagents

Acetic acid	Merck Calbiochem, Darmstadt
Acrylamide-Bis Solution (29:1), 30% w/v	Serva Feinbiochemica, Heidelberg
Agarose	Sigma-Aldrich, Steinheim
Ammonium persulfate	Sigma-Aldrich, Steinheim
Aqua ad iniectabilia	Braun, Melsungen
Bradford-Reagent	Bio-Rad Laboratories, München
10% Briji 58	Sigma-Aldrich, Steinheim
Bromphenol blue	Serva Feinbiochemica, Heidelberg
BSA Molecular Biology Grade (20 mg/ml)	New England BioLabs, Frankfurt/Main
Casein from bovine milk	Sigma-Aldrich, Steinheim
$CaCl_2$	Sigma-Aldrich, Steinheim
Chloroform	Merck Calbiochem, Darmstadt
Complete Protease Inhibitor Cocktail	Roche Diagnostics, Mannheim
CsCl	Roth, Karlsruhe
Dako Faramount Aqueous Mounting Medium	Dako Deutschland GmbH, Hamburg
DAPI	Sigma-Aldrich, Steinheim
DTT	Biomol, Hamburg
dNTPs Set PCR Grade	Thermo Fisher Scientific, Darmstadt
EB buffer	Qiagen, Hilden
ECL SuperSignal West Femto	Thermo Scientific, St. Leon-Rot
EDTA	Carl Roth GmbH, Karlsruhe
Enhanced Chemiluminescence Substrate (ECL)	PerkinElmer, USA
Ethanol, absolute	Merck Calbiochem, Darmstadt
Ethidium bromide, 1% solution	Sigma-Aldrich, Steinheim
Formaldehyde	Merck Calbiochem, Darmstadt
Gaussia-Juice BIG KIT	jpk GmbH, Kleinblittersdorf
Glucose	Roth, Karlsruhe
Glycerol	AppliChem, Darmstadt
Glycine	Gerbu, Gaibach
H_2O_2	Merck Calbiochem, Darmstadt
HEPES Eurobio	Les Ulis Cedex, France
IsoFlo 100% v/v inhalation gas, liquid	Toetis Österreich GmbH, Wien
KCl	Merck Calbiochem, Darmstadt
KH_2PO_4	Carl Roth GmbH, Karlsruhe
L-Glutathione reduced	Sigma-Aldrich, Steinheim
Methanol	Sigma-Aldrich, Steinheim
$MgCl_2$	Merck Calbiochem, Darmstadt
$MgSO_4$	Sigma-Aldrich, Steinheim
Milk powder	Carl Roth GmbH, Karlsruhe
NaCl	Carl Roth GmbH, Karlsruhe
Na_2CO_3	Carl Roth GmbH, Karlsruhe
$NaHCO_3$	Carl Roth GmbH, Karlsruhe
NaH_2PO_4	Carl Roth GmbH, Karlsruhe

NaOH	Carl Roth GmbH, Karlsruhe
OptiPrep™ Density Gradient Medium	Sigma-Aldrich, Steinheim
Phenol	Carl Roth GmbH, Karlsruhe
Phenol Red Solution	Sigma-Aldrich, Steinheim
PMSF	Roche Diagnostics, Mannheim
Protease Inhibitor Cocktail Complete, EDTA-free	Roche Diagnostics, Mannheim
SDS	Carl Roth GmbH, Karlsruhe
Sucrose	Merck Calbiochem, Darmstadt
TEMED	Sigma-Aldrich, Steinheim
TMB	Sigma-Aldrich, Steinheim
Triton® X-100	Serva Feinbiochemica, Heidelberg
Trizma® base (Tris)	Sigma-Aldrich, Steinheim
Tween® 20	Gerbu, Gaibach
2-mercaptoethanol	Carl Roth GmbH, Karlsruhe
2-Propanol	Merck Calbiochem, Darmstadt
6X DNA Loading Dye	Thermo Fisher Scientific, Darmstadt

2.2 Reagents for Bacteria Cultivation

Ampicillin	Sigma-Aldrich, Steinheim
Bacto™ Agar	Becton Dickinson, Heidelberg
Bacto™ Tryptone	Carl Roth GmbH, Karlsruhe
Bluogal	Invitrogen, Karlsruhe
Chloramphenicol	Sigma-Aldrich, Steinheim
Gentamycin	Sigma-Aldrich, Steinheim
IPTG	AppliChem, Darmstadt
Kanamycin	Sigma-Aldrich, Steinheim
LB Medium	Carl Roth GmbH, Karlsruhe
Tetracycline	Sigma-Aldrich, Steinheim
X-gal	Sigma-Aldrich, Steinheim
Yeast extract	Gerbu, Gaibach

2.3 Reagents for cell culture

Dulbecco's Modified Eagle's Medium (DMEM)	Sigma-Aldrich, Steinheim
Dulbecco's Phosphate Buffered Saline (D-PBS)	Invitrogen, Karlsruhe
Dulbecco's Phosphate Buffered Saline (D-PBS) (+$CaCl_2$ +$MgCl_2$)	Thermo Fisher Scientific, Darmstadt
Dimethylsulfoxid (DMSO)	Carl Roth GmbH, Karlsruhe
EX-CELL™ 405 serum-free insect cell medium	Sigma-Aldrich, Steinheim
Fetal Bovine Serum (FCS)	Linaris GmbH, Wertheim
Grace's Insect Medium, supplemented	Sigma-Aldrich, Steinheim
Hygromycin B	Sigma-Aldrich, Steinheim
Opti-MEM serum-free medium	Invitrogen, Karlsruhe
Penicillin/Streptomycin (10,000 U/ml)	Thermo Fisher Scientific, Darmstadt
TNM-FH Insect Medium	Sigma-Aldrich, Steinheim
Trypan blue	Biochrom, Berlin

Turbofect *in vitro* Transfection Reagent	Thermo Fisher Scientific, Darmstadt
0.25% Trypsin/EDTA	Invitrogen, Karlsruhe
Pluronic F-68	Sigma-Aldrich, Steinheim

2.4 Kits

AllPrep DNA/RNA Mini Kit	Qiagen (Hilden, Germany)
Axygen™ AxyPrep™ Plasmid Miniprep Kit	Fisher Scientific GmbH, Schwerte
CloneJET PCR Cloning Kit	Thermo Fisher Scientific, Darmstadt
High Pure PCR Product Purification Kit	Roche Diagnostics, Mannheim
TURBO DNA-freeTM Kit	Thermo Fisher Scientific, Darmstadt
QIAamp DNA Mini Kit	Qiagen, Hilden
QIAGEN® Plasmid Midi Kit	Qiagen, Hilden
QIAGEN® Plasmid Maxi Kit	Qiagen, Hilden
QIAquick® Gel Extraction Kit	Qiagen, Hilden
RNeasy® Mini Kit	Qiagen, Hilden

2.5 DNA and protein size markers

GeneRuler™ 1 kB DNA Ladder	Thermo Fisher Scientific, Darmstadt
PageRuler™ Plus Prestained Protein Ladder	Thermo Fisher Scientific, Darmstadt

2.6 Universal enzymes

Benzonase	Merck Calbiochem, Darmstadt
DreamTaq™ Green DNA Polymerase	Thermo Fisher Scientific, Darmstadt
Dream Taq™ Green PCR Master Mix (2X)	Thermo Fisher Scientific, Darmstadt
Phusion® High-Fidelity DNA Polymerase	New England BioLabs, Frankfurt/Main
RevertAid Reverse Transcriptase	Thermo Fisher Scientific, Darmstadt
RNase A/T1 Mix	Thermo Fisher Scientific, Darmstadt
T4 DNA Ligase	New England BioLabs, Frankfurt/Main

2.7 Restriction enzymes

AgeI	New England BioLabs, Frankfurt/Main
BamHI-HF	New England BioLabs, Frankfurt/Main
DpnI	New England BioLabs, Frankfurt/Main
DraIII	New England BioLabs, Frankfurt/Main
EcoRI-HF	New England BioLabs, Frankfurt/Main
HinDIII-HF	New England BioLabs, Frankfurt/Main
NheI-HF	New England BioLabs, Frankfurt/Main
SalI	New England BioLabs, Frankfurt/Main
SacII	New England BioLabs, Frankfurt/Main
SphI	New England BioLabs, Frankfurt/Main
XbaI	New England BioLabs, Frankfurt/Main
XmaI	New England BioLabs, Frankfurt/Main

2.8 Consumables

Amersham™ Hybond™ P 0.45 PVDF	Th. Geyer, Renningen
Capillary tips (200 µl)	Biozym, Hessisch Oldendorf
Cell culture dishes (6, 10, 15 cm)	TPP, Trasadingen, Switzerland
Cell culture flasks (25, 75 cm2)	TPP, Trasadingen, Switzerland
Cell culture flasks 175 cm2	Greiner Bio-One GmbH, Frickenhausen
Cell culture plates (6 well)	BD Falcon, Heidelberg
Cell culture plates (12, 24, 96 well)	Greiner Bio-One GmbH, Frickenhausen
Cell scraper	Corning Sigma, München
Centrifuge Tubes (14 x 89 mm)	Beckman Coulter.Inc, USA
Cover slides Menzel-Gläser	Thermo Fisher Scientific, Darmstadt
Facial tissues	WEPA Professional GmbH, Arnsberg
Gloves (Microflex® XCEED)	MICRFLEX, USA
GSTrap™ FF	GE Healthcare Bio-Science, Sweden
Incidin® Foam	Ecolab Deutschland, Monheim am Rhein
Luer-Lock Syringe (50 ml)	Terumo Detuschland, Eschborn
Millex-HV filter unitt, PVDF	Merck Millipore, Darmstadt
Minisart Syringe Filter	Sartorius, Göttingen
Multiplate™ PCR Plates 96-well, clear	Bio-Rad, München
Needles, sterile (18G, 20G, 25G, 27G)	Braun, Melsungen
Nunc® Cryo Tubes	Sigma-Aldrich, Steinheim
Nunc™ F96 MicroWell™ White Polystyrene Plate	Thermo Fisher Scientific, Darmstadt
Objektträger Superfrost® Plus	Carl Roth GmbH, Karlsruhe
Optical Adhesive Covers MicroAmp	ABiosystems, Foster City, USA
PCR SingleCap 8er Soft Strips	Biozym, Hessisch Oldendorf
Phase Lock Gel Light	5PRIME GmbH, Hilden
Pipette Tips (10, 200, 1000 µl)	Steinbrenner, Gießen
Pipette Tips RAININ (200 µl)	Steinbrenner, Gießen
Polysorb Nunc-Immuno plates	Thermo Fisher Scientific, Darmstadt
Protein LoBind Tube 1.5ml	Eppendorf, Hamburg
Precision Wipes	Kimberly-Clark Professional, Reigate, UK
Scalpels, disposable	Feather Safety Razor, Osaka, Japan
Special autoclavable bags	Nerbe plus GmbH, Winsen/Luhe
Syringes, single use 1 ml	Th. Geyer GmbH, Renningen
Reaction Tubes (0.5, 1.5 and 2.0 ml)	Eppendorf, Hamurg
X-ray films Super RX	X-ray films Super RX

2.9 Laboratory equipment

Analytical scale ABJ-120-4NM	Kern & Sohn GmbH, Balingen
Autoradiography Cassettes	Kodak, Stuttgart
Bacterial shaker G25	Infors, Bottmingen, CH
Centrifuge Heraeus Pico 17	Thermo Fisher Scientific, Darmstadt
Centrifuge Heraeus Fresco 17	Thermo Fisher Scientific, Darmstadt
Centrifuge Megafuge 1.0R	Heraeus, Hanau

Centrifuge Sprout	Biozym, Hessisch Oldendorf
Centrifuge Rotina 380R	M&S Laborgeräte, Wiesloch
Confocal Olympus FluoView FV1000	Olympus, Hamburg
Developing machine CURIX 60	AGFA, Cologne
Easy-Cast™ Electrophoresis System	Thermo Fisher Scientific, Darmstadt
EVOS® XL Core Imaging System	Thermo Fisher Scientific, Darmstadt
Freezer profi line	Liebherr, Ludwigshafen
Freezer VIP™ Series -86°C	Sanyo, USA
Fridge Premium	Liebherr, Ludwigshafen
Gel documentation system GELSTICK	INTAS Science Imaging Instruments
Impulse Sealer	Tew Electric Heating Equipment, Taiwan
Incubator C200	LaBoTect, Göttingen
Kern EMB 1200-1 Tischwaage 1200 g	KERN & SOHN GmbH, Balingen
Liquid nitrogen tank CHRONOS Biosafe	Messer, Griesheim
Magnetic stirrer MR3000	Heidolph Instruments, Schwabach
Microscope Dialux 22	Ernst Leitz Wetzlar GmBH, Wetzlar
Microscope Olympus CK2	Olympus, Hamburg
Microwave	DéLonghi GmbH, Seligenstadt
Mini-PROTEAN® 3 Cell	Bio-Rad, München
Mini PROTEAN® Trans Blot	Bio-Rad, München
Moser ChroMini Pro Trimmer	Wahl GmbH, Unterkirnach
Moser Trimmer 1556	Wahl GmbH, Unterkirnach
Multichannel Pipette RAININ (50-200 µl)	Eppendorf, Hamburg
MyCycler thermal cycler	Bio-Rad, München
Neubauer hemocytometer	Bender&Hobein, Bruchsal
Overhead shaker REAX2	Heidolph Instruments, Schwabach
Peltier Thermal Cycler PTC-200	MJ Research, St. Bruno, Canada
pH-meter 761 Calimatic	Knick, Berlin
Pipette Boy Acu	Integra Biosciences GmbH, Fernwald
Pipettes Research (2, 10, 20, 100, 200, 1000 µl)	Eppendorf, Hamburg
Plate Reader SPECTROstar Nano	BMG LABTECH Ortenberg
Power supply PowerPacTM HC/basic	Bio-Rad, München
Roller Mixer SRT9D	Stuart, USA
Spectrophotometer NanoDrop® ND-1000	NanoDrop, USA
STERI-CULT 200 Incubator	Forma Scientifc, Marietta, USA
SterilGARD Hood	Baker Company, Sanford, USA
Thermal Cycler C1000TM	Bio-Rad, München
Thermomixer compact/pico	Eppendorf, Hamburg
UV table N90	Benda Konrad, Wiesloch

2.10 Buffers and Solutions

Ammonium persulfate (APS)	10% (w/v) in water
Ampicillin	100 mg/ml
Buffer L	40 mM Tris 200 mM NaCl 1 mM EDTA pH 8.2 2 mM DTT
Blocking buffer (Immunofluorescence)	1% BSA 0.02% Tween 20 in PBS, filtered
Casein blocking buffer	0.2 % (w/v) casein in PBS-T
Cesium chloride solution	57.5 % CsCl (w/v) in VLP extraction buffer
Chloramphenicol stock solution	34 mg/ml
Coating buffer (ELISA)	50 mM carbonate buffer pH 9.6: 1 part 50 mM Na_2CO_3 4 parts 50 mM $NaHCO_3$
DMEM Cryo Medium	10% DMSO 20% FCS 70% DMEM
DPBS/0.8M NaCl (50 ml)	42 ml DPBS (+$MgCl_2$ + $CaCl_2$) 8 ml 5M NaCl
2 x HBS	15 ml 0.5M HEPES 14 ml 5M NaCl 0.75 ml 0.5M Na_2HPO_4 add to 250 ml ddH_2O adjust the pH exactly to 7.13
27% Iodiaxanol (4 ml)	1.8 ml Optiprep™ Density Gradient Medium 2.2 ml DPBS/0.8M NaCl
33% Iodiaxanol (4 ml)	2.2 ml Optiprep™ Density Gradient Medium 1.8 ml DPBS/0.8M NaCl
39% Iodiaxanol (4 ml)	2.6 ml Optiprep™ Density Gradient Medium 1.3 ml DPBS/0.8M NaCl 80 µl Phenol red solution
Kanamycin	50 mg/ml
PBS (10 x)	1.24 M NaCl 0.22 M Na_2HPO4 0.1 M KH_2PO4 adjust the pH exactly to 7.2
PBST (1 x)	1X PBS, pH 7.2 0.1% (v/v) Tween 20
Permeabilisation buffer	1% BSA

(Immunofluorescence)	0.02% Tween 20 0.2% Triton X-100 in PBS, filtered
Pseudovirus lysis buffer	1 ml DPBS (+$MgCl_2$ + $CaCl_2$) 58.3 µl 10% Briji58 6.7 µl RNAse A/T cocktail
RIPA Buffer	20 mM Tris pH 7.5 150 mM NaCl 1 mM Na_2EDTA 1 mM EGTA 1% NP-40 1% sodium deoxycholate
SDS Loading Dye (5 x)	1% (w/v) SDS 0.03% (w/v) bromophenol blue 12.5% (v/v) 2-mercaptoethanol 5 mM EDTA, pH 8.0 47.3% (v/v) glycerol 0.3 M Tris, pH 6.8 2.5 mM NaF
SDS PAGE Running Buffer (10 x)	10% SDS 0.25 M Tris 1.9 M Glycine
Substrate buffer (ELISA)	100 mM sodium acetate adjust to pH 6 with acetic acid
Sucrose solution	30 % sucrose (w/v) in VLP extraction buffer
TAE Buffer (50 x)	2 M Tris 0.25 M NaAc 0.05 M EDTA, pH 8.0 adjust to pH 7.8 with acetic acid
TBS (10 x)	Tris 0.5 M NaCl 1.5 M adjust to pH 7.5
TBST (1 x)	1X TBS, pH 7.5 0.1% (v/v) Tween 20
TMB stock solution	10 mg/ml TMB in DMSO
Transfection buffer (for Sf9 cells)	25 mM Hepes 125 mM $CaCl_2$ 140 mM NaCl adjust to pH 7.0, 7.1, 7.2
VLP extraction buffer	5 mM $MgCl_2$ 5 mM $CaCl_2$ 150 mM NaCl 0.01 % Triton X 100 20 mM HEPES pH 7.4 2.5 mM PMSF (freshly added)

2.11 Bacteria

DH10MultiBac^{Cre} Electrocompetent *E. coli*	Kindly provided by Prof. Dr. M. Müller, DKFZ
E. coli BL21	Kindly provided by Prof. Dr. M. Müller, DKFZ
E. coli Rosetta	Kindly provided by Prof. Dr. M. Müller, DKFZ
TOP10 Chemically Competent *E. coli*	Invitrogen, Karlsruhe

2.12 Cell lines

Cell line	Properties	Medium
HEK 293TT	Human embryonic kidney cells, transformed with E1A/B of adenovirus 5, stably expressing two gene copies of SV40 large T-antigen	DMEM supplemented with 10% Fetal calf serum, 1%Penicillin/Streptomycin and 1% L-glutamine, 125 µg/ml Hygromycin B
HeLaT	HPV18 human cervical carcinoma cell line stably expressing one copy of SV40 T-antigen under control of a CMV promotor	DMEM supplemented with 10% Fetal calf serum, 1%Penicillin/Streptomycin and 1% L-glutamine, 125 µg/ml Hygromycin B
HeLa	HPV18 human cervical carcinoma cell line	DMEM supplemented with 10% Fetal calf serum, 1%Penicillin/Streptomycin and 1% L-glutamine
SF9	Insect cell line, clonal isolated from *Spodoptera frugiperda* Sf21 cells	TNM-FH insect medium supplemented with 10% Fetal calf serum, 1% Penicillin/Streptomycin and 1% L-glutamine
TN-High-Five	Insect cell line, ovarian cells of the cabbage looper *Trichoplusia ni*	EX-CELL™ 405 serum-free medium supplemented with 1% Penicillin/Streptomycin and 1% L-glutamine

2.13 Oligonucleotides

All primers were synthesized by Sigma-Aldrich, Germany.

Primers for construction of pseudovirus pGEM-IRES expression plasmids		linker	T_{an} [°C]
MnPV L1$_{LONG}$: start codon at 5701 bp - Codon optimized			
For: L1L-NheI-Forward	5'- CTA GCT AGC GCC ACC **ATG** AGC TAT ATT G - 3'	*NheI*	60°C
Rev: L1L-SalI-Reverse	5'- ACG CGT CGA CTC ACT TCT TGC GTC TCT T - 3'	*SalI*	
MnPV L1$_{MIDDLE}$: start codon at 5722 bp - Codon optimized			
For: L1middle-NheI-Forward	5'- CTA GCT AGC GCC ACC **ATG** GGT AGG ACC ATC - 3'	*NheI*	60°C
Rev: L1L-SalI-Reverse	5'- ACG CGT CGA CTC ACT TCT TGC GTC TCT T - 3'	*SalI*	
MnPV L2: start codon at 4248 bp - Codon optimized			
For: L2-NheI-Forward	5'- CTA GCT AGC **ATG** AGC CGC CGC CGC AAG C - 3'	*NheI*	62°C
Rev: MnL2 hum-BamHI-R*	5'- GGA TCC TCA TGC GGC GAG CAC CCC G - 3'	*BamHI*	

*kindly provided by Dr. Kai Schäfer, DKFZ Heidelberg

Primers for site-directed mutagenesis of pseudovirus expression plasmids		linker	T_{an} [°C]
Mutation on 2nd ATG of L1$_{LONG}$: From Methionine (ATG) to Alanine (GCG) - Codon optimized			
For: L1L-1.5thM-NheI-Forward-1	5'-GCT AGC GCC ACC **ATG** AGC TAT ATT GGC GCC ATT GCG GGT AGG ACC ATC AT- 3'	*NheI*	62°C
Rev: L1L-SalI-Reverse	5'- ACG CGT CGA CTC ACT TCT TGC GTC TCT T - 3'	*SalI*	
Mutation on 3rd ATG of L1$_{LONG}$: From Methionine (ATG) to Alanine (GCG) - Codon optimized			
For: L1-L-Forward1	5'-GCT GGG ATA TCC ATC TTC CAG GCG GCC TAT TG - 3'		60°C
Rev: L1-L-Reverse1	5'- CA ATA GGC CGC CTG GAA GAT GGA TAT CCC AGC - 3'		

Primers for construction of pPK-CMV E3-MnPVL1 and L2 expression plasmids		linker	T_{an} [°C]
MnPV L1$_{LONG}$: start codon at 5701 bp - Codon optimized with HA tag			
For: pCMV-L1L- EcoRI	5'- CCG GAA TTC GCC ACC **ATG** AGC TAT ATT GGC GCC ATT GCG -3'	*EcoRI*	60°C
Rev: pCMV-L1L-BamHI-1	5'- CGC GGA TCC CTT CTT GCG TCT CTT TG - 3'	*BamHI*	

MnPV L1MIDDLE: start codon at 5722 bp - Codon optimized with HA tag

For: pCMV-L1mid- EcoRI	5'- CCG GAA TTC GCC ACC **ATG** GGT AGG ACC ATC -3'	*EcoRI*	60°C
Rev: pCMV-L1L-BamHI-1	5'- CGC GGA TCC CTT CTT GCG TCT CTT TG - 3'	*BamHI*	

MnPV L1SHORT: start codon at 5794 bp - Codon optimized with HA tag

For: pCMV-L1S- EcoRI	5'- CCG GAA TTC GCC ACC **ATG** GCC TAT TGG CTC C -3'	*EcoRI*	60°C
Rev: pCMV-L1L-BamHI-1	5'- CGC GGA TCC CTT CTT GCG TCT CTT TG - 3'	*BamHI*	

MnPV L1LONG: start codon at 5701 bp - Codon optimized without HA tag

For: pCMV-L1L- EcoRI	5'- CCG GAA TTC GCC ACC **ATG** AGC TAT ATT GGC GCC ATT GCG -3'	*EcoRI*	60°C
Rev: pCMV-L1L-BamHI	5'- CGC GGA TCC TCA CTT CTT GCG TCT CTT - 3'	*BamHI*	

MnPV L1MIDDLE: start codon at 5722 bp - Codon optimized without HA tag

For: pCMV-L1mid- EcoRI	5'- CCG GAA TTC GCC ACC **ATG** GGT AGG ACC ATC -3'	*EcoRI*	60°C
Rev: pCMV-L1L-BamHI	5'- CGC GGA TCC TCA CTT CTT GCG TCT CTT - 3'	*BamHI*	

MnPV L1SHORT: start codon at 5794 bp - Codon optimized without HA tag

For: : pCMV-L1S- EcoRI	5'- CCG GAA TTC GCC ACC **ATG** GCC TAT TGG CTC C-3'	*EcoRI*	60°C
Rev: pCMV-L1L-BamHI	5'- CGC GGA TCC TCA CTT CTT GCG TCT CTT - 3'	*BamHI*	

MnPV L2: start codon at 4248 bp - Codon optimized without HA tag

For: : L2-EcoRI-Forward	5'- CCG GAA TTC GCC ACC **ATG** AGC CGC CGC CGC AAG C - 3'	*EcoRI*	60°C
Rev: L2-BamHI-Reverse	5'- CGC GGA TCC TCA TGC GGC GAG CAC CCC G - 3'	*BamHI*	

Primers for construction of pGEM-MnPV L1LONG 3rd mutation plasmids **linker** **Tan [°C]**

MnPV L1LONG: start codon at 5701 bp

For: MnPVL1long-Forward	5'- **ATG** TCA TAT ATA GGG GCT ATA -3'	T/A	58°C
Rev: MnPVL1long-Reverse	5'- CTA TTT TTT TCT CCG CTT GGT GGA -3'	T/A	

Mutation on 3rd ATG of L1LONG: From Methionine (ATG) to Alanine (GCG)

For: OF	5'- CTC TTC GCT ATT ACG CCA GC -3'	*SacII*	58°C
Rev: IR	5'- CCA GTA CGC CGC CTG AAA AAT AGA TAT GCC TGC GC -3'		
For: IF	5'- CT ATT TTT CAG GCG GCG TAC TGG CTG CCT AAT AAC -3'	*AgeI*	58°C
Rev: OR	5'- ATA CAC CAT GCA AGC CGT TGC -3'		

Primers for construction of pFBDM-MnPV L1 expression plasmids **linker** **Tan [°C]**

MCSI: MnPV L1LONG: start codon at 5701 bp

For: MnPVL1-2ndM-EcoRI	5'- CCG GAA TTC **ATG** TCA TAT ATA GGG GCT ATA GCG GGA CGG ACT ATT - 3'	*EcoRI*	60°C
Rev: MnPVL1-HinDIII	5'- CCC AAG CTT CTA TTT TTT TCT CCG CTT GGT GGA - 3'	*HinDIII*	

MCSII: MnPV L1LONG: start codon at 5701 bp

For: MnPVL1-2ndM-SmaI	5'- TCC CCC GGG **ATG** TCA TAT ATA GGG GCT ATA GCG GGA CGG ACT ATT - 3'	*XmaI*	60°C
Rev: MnPVL1-SphI	5'- A GCA TGC CTA TTT TTT TCT CCG CTT GGT GGA - 3'	*SphI*	

MCSI: MnPV L1MIDDLE: start codon at 5722 bp

For: MnPVL1mid-EcoRI	5'- CCG GAA TTC **ATG** GGA CGG ACT ATT ATC TAC ACC - 3'	*EcoRI*	60°C
Rev: MnPVL1-HinDIII	5'- CCC AAG CTT CTA TTT TTT TCT CCG CTT GGT GGA - 3'	*HinDIII*	

MCSII: MnPV L1MIDDLE: start codon at 5722 bp

For: MnPVL1mid-SmaI	5'- TCC CCC GGG **ATG** GGA CGG ACT ATT ATC TAC ACC - 3'	*XmaI*	60°C
Rev: MnPVL1-SphI	5'- A GCA TGC CTA TTT TTT TCT CCG CTT GGT GGA - 3'	*SphI*	

MCSI: MnPV L1SHORT: start codon at 5794 bp

For: MnPVL1S-EcoRI	5'- CCG GAA TTC **ATG** GCG TAC TGG CTG CCT AAT AAC - 3'	*EcoRI*	60°C
Rev: MnPVL1-HinDIII	5'- CCC AAG CTT CTA TTT TTT TCT CCG CTT GGT GGA - 3'	*HinDIII*	

MCSII: MnPV L1SHORT: start codon at 5794 bp

For: MnPVL1S-XmaI	5'- TCC CCC GGG **ATG** GCG TAC TGG CTG CCT AAT AAC - 3'	*XmaI*	60°C
Rev: MnPVL1-SphI	5'- A GCA TGC CTA TTT TTT TCT CCG CTT GGT GGA - 3'	*SphI*	

Detection of Inserts in MultiBac multiple cloning sites*			T_M [°C]
MCSI	For: TS#32 (MCS1-100bp)	5' - AAT GAT AAC CAT CTC GC - 3'	55
	Rev: TS#33 (MCS1 +100bp)	5' - TAT GTT TCA GGT TCA GG - 3'	55
MCSII	For: TS#30 (MCS2 -50bp)	5' - GTC ATA GCG CGG GTT CC - 3'	61
	Rev: TS#31 (MCS2 +100bp)	5' - CGG ACC TTT AAT TCA ACC - 3'	61

*kindly provided by Dr. Kai Schäfer, DKFZ Heidelberg

Primers for construction of pGEX-MnPV L1 expression plasmids		linker	T_{an} [°C]
MnPV L1MIDDLE: start codon at 5722 bp			
For: MnPV-L1middle-XmaI	5' -TCC CCC CGG GCC **ATG** GGA CGG ACT ATT ATC TAC ACC - 3'	*XmaI*	60°C
Rev: MnPV-L1-SalI-1	5' - ACG CGT CGA CTT TTT TTC TCC GCT TGG TGG - 3'	*SalI*	
MnPV L1NT-41aa: start - stop: 5701bp to 5823bp			
For: MnPV-L1NT-XmaI	5' -TCC CCC CGG GCC **ATG** TCA TAT ATA GGG GCT ATA - 3'	*XmaI*	60°C
Rev: MnPV-L1NT-SalI-41	5' -ACG CGT CGA CCT TCT GGT TAT TAG GCA GCC - 3'	*SalI*	

Primers for construction of pJET-MnPV URR genome plasmid (Gibson Assembly)		Size	T_{an} [°C]
Fragment1: Use pJET-MnPV URR 1.8 as the template			
For: FYY-15	5' - TTT TCA GCA AGA TTA TAG TCG ACA GCA CGC TG - 3'	2957bp	60°C
Rev: FYY-16	5' - GTC TCC TCC CCA TCC TCA TAC ATG CAC ATC AGT TCC TC - 3'		
Fragment2: Use pUC19-MnPV L2 as the template			
For: FYY-17	5' - TGT GCA TGT ATG AGG ATG GGG AGG AGA CAC TG - 3'	1681bp	60°C
Rev: FYY-18	5' - TTC TCC TTC TAG ACA TGC TAA TAT TAG TAG GTT AGT ACT GTG TAA AGG - 3'		
Fragment3: Use pUC19-MnPV L2 as the template			
For: FYY-19	5' - TAA TAT TAG CAT GTC TAG AAG GAG AAA GCG ACA TAC - 3'	2468bp	60°C
Rev: FYY-20	5' - AGC ATC AGA TGA CAC TAG TGA CCC TGA CGG AG - 3'		

Fragment4: Use pJET-MnPV URR 1.8 as the template

For: FYY-21	5' - CAG GGT CAC TAG TGT CAT CTG ATG CTG TAC TG - 3'	3685bp	60°C
Rev: FYY-22	5' - GCT GTC GAC TAT AAT CTT GCT GAA AAA CTC GAG - 3'		

Primers for construction of pUC19-MnPV URR mutation genome plasmids		linker	T_{an} [°C]

Mutation on 1st and 2nd ATG of L1: From Methionine (ATG) to Alanine (GCG)

For: PUC-L1-1F	5' - AGA GTA TAG AAC TCA GCA CC - 3'	*DraIII*	60°C
Rev: PUC-L1Lmid-1R	5' - GC TAT AGC CCC TAT ATA TGA CGC GGG GAC GAG CAC TGT CCC TA - 3'		
For: PUC-L1Lmid-2F	5' - TCA TAT ATA GGG GCT ATA GCG GGA CGG ACT ATT ATC TAC AC - 3'	*DraIII*	60°C
Rev: PUC-L1-2R	5' - CCA TGT CAC CAT CCT CAA TC - 3'		

Mutation on 3rd ATG of L1: From Methionine (ATG) to Alanine (GCG)

For: PUC-L1-1F	5' - AGA GTA TAG AAC TCA GCA CC - 3'	*DraIII*	60°C
Rev: PUC-L1S-1R	5' - CCA GTA CGC CGC CTG AAA AAT AGA TAT GCC TG - 3'		
For: PUC-L1S-2F	5' - CT ATT TTT CAG GCG GCG TAC TGG CTG CCT AAT AAC - 3'	*DraIII*	60°C
Rev: PUC-L1-2R	5' - CCA GTC ACC ATC CTC AAT C - 3'		

Primers for construction of pUC19-MnPV URR L1NT genome plasmids		Size	T_{an} [°C]

Fragment1: Use pUC19-MnPV URR L1Lmid M as the template

For: F1-F	5' - CTA CTG CTT GAC GGG CTA AGA GTG ATC TGT CCG CG - 3'	2343bp	62°C
Rev: F1-R	5' - GTT AAT GAG TAC CTC TTT GCT TCC TCT TTG AAC CGC - 3'		

Fragment2: Use pUC19-MnPV URR L1Lmid M as the template

For: F2-F	5' - AGG AAG CAA AGA GGT ACT CAT TAA CAG GAA CTT GG - 3'	2660bp	62°C
Rev: F2-R	5' - GCA GCC AGT ACG CCA TGG GGA CGA GCA CTG TCC C - 3'		

Fragment3: Use pUC19-MnPV URR L1Lmid M as the template

For: F3-F	5' - CTC GTC CCC ATG GCG TAC TGG CTG CCT AAT AAC C - 3'	2633bp	62°C
Rev: F3-R	5' - GTA GAA AAG ATC AAA GGA TCT TCT TGA GAT C - 3'		

Fragment4: Use pUC19-MnPV URR L1Lmid M as the template

For: F4-F	5' - CAA GAA GAT CCT TTG ATC TTT TCT ACG GGG TCT G - 3'	2756bp	62°C
Rev: F4-R	5' - GAT CAC TCT TAG CCC GTC AAG CAG TAG ATG TTC - 3'		

Start codons are in black. Stop codons are in red. Mutated start codons are in green. T_{an}= Annealing temperature; T_M = Melting temperature.

2.14 Antibodies

Antibody	Source	Application
Alexa Fluor 488 donkey anti-rat IgG (H+L)	Invitrogen; Cat.#: A21208	IF: 1: 500
Alexa Fluor 594 goat anti-mouse IgG2a (γ2a)	Invitrogen; Cat.#: A21135	IF: 1: 2,000
Anti-actin (human) mouse monoclonal	MP Biomedical; Cat.#: 69100	WB: 1: 10,000
Anti-HA (3F10) rat monoclonal	Roche; Cat.#: 11867423001	WB:1: 1,000; IF: 1: 1000
Goat anti-Mouse IgG (H+L) HRP	Promega; Cat.#: W402B	ELISA: 1: 10,000; WB: 1: 10,000
Goat anti-Rat IgG (H+L) HRP	JacksonImmunoResearch, Cat.#: 112-035-143	WB: 1: 10,000
Mouse monoclonal anti-MnPV VLP (2E2; 2D6; 2D11; 5E5; 3H8)	Selfmade from Laura Katharina Schmitt, DKFZ	ELISA: 1: 20; IF: 1: 300
Mouse monoclonal anti-SV40tag KT3	Selfmade from Dr. Tim Waterboer, DKFZ	ELISA: 1: 300; WB: 1: 1000
Serum mix	Sera of five MnPV infected tumor bearing animals	ELISA: 1: 1000; WB: 1: 500

3. Methods

3.1 Animals experiments

3.1.1 Animals following-up experiments

Mastomys coucha from MnPV naturally infected breeding colony were maintained at 22-24°C with 55% relative humidity, mouse breeding diet and water ad libitum. For the follow-up experiment, animals were monitored for the duration of their life until they had to be sacrificed due to tumor development, eye inflammation or decrepitude. The blood was taken from the submandibular vein at intervals of 2 weeks at the early age and 8 weeks at the late age. *Mastomys coucha* at DKFZ are housed and handled in accordance with German and European statutes. All the animal experiments were undertaken with the approval of the responsible Animal Ethics Committee for the use and care of live animals (Regional Council of Karlsruhe, Germany). The Cyclosporine A (CsA) treatment and UV irradiation experiment was done in collaboration with Dr. Julita Mikulec and Dr. Daniel Hasche. Animals were fed with the immunosuppressant CsA with a concentration (125 mg/kg) starting from the age at 15 weeks. UV irradiation was performed with a dose of 450 mJ/ cm^2 three times per week also starting from the age at 15 weeks.

3.1.2 Serum

Blood was taken from submandibular vein with a 25G needle when the animals were under Isoflurane anesthetized status. The blood droplets were collected in 1.5 ml Eppi™ tubes and incubated at room temperature for 1 hour until it was completely clotted. The serum was carefully collected after centrifugation at 8000 rpm.

3.2 Cloning and analysis of plasmids

3.2.1 Cloning polymerase chain reaction (PCR)

The polymerase chain reaction was performed to amplify the DNA sequences of respective inserts for plasmid construction. Specific primers were designed for amplification process, containing respective enzyme restriction sites at the 5' end and a Kozak sequence in the upstream of start codon in some cases. All PCRs were performed by Phusion High-Fidelity DNA polymerase (NEB) according to the manufacturer's instructions:

Component	50 µl Reaction
Nuclease - free water	to 50 µl
5 x Phusion HF buffer	10 µl
10 mM dNTPs	1 µl
10 µM Forward Primer	2.5 µl
10 µM Reverse Primer	2.5 µl
Template DNA	variable
DMSO (optional)	(1.5 µl)
Phusion DNA Polymerase	0.5 µl

Thermocycling conditions for a routine PCR:

Step	Temperature	Time	
Initial Denaturation	98 °C	30 s	
Denaturation	98 °C	5-10 s	25-35 cycles
Annealing	56-62°C	10-30 s	
Elongation	72 °C	15-30 s/kb	
Final Extension	72 °C	5-10 min	

3.2.2 Restriction enzyme digestion and ligation

Prior to the restriction enzyme digestion, PCR product of insert was purified by QIAquick Gel Extraction Kit according to the manufacturer's protocols. The cutting of purified PCR products and vector backbone were performed using restriction enzyme for 1-4 hours according to NEB protocol:

Component	Reaction
Restriction Enzyme 1	10 units - 20 units
Restriction Enzyme 2	10 units - 20 units
DNA	1 - 10 µg
10 x NEBuffer	5 µl
Total Reaction Volume	50 - 100 µl

DNA fragments were separated by agarose gel electrophoresis (1-1.2% agarose in 1 x TAE buffer) and visualized by UV light after ethidium bromide staining. DNA fragments were linked in a molecular ration of 1: 5 (vector to insert) by T4 DNA ligase (Thermo Fisher Scientific) overnight at 22°C.

Component	Reaction
Linear vector DNA	20 - 100 ng
Insert DNA	5: 1 molar ration over vector
10 x T4 DNA Ligase Buffer	2 µl
T4 DNA Ligase	1 Weiss U
Nuclease - free water	to 20 µl

3.2.3 Transformation of competent bacteria

1-5 µl containing 1pg-100 ng of plasmid DNA was added to NEB DH5α or TOP10 competent cells. The mixture was incubated for 30 min on ice and followed by a heat shock at 42°C for 30s. The bacteria were then put on ice for 5 min and shaken in 250 µl SOC medium at 37°C for one hour. 50-100 µl of transformed cells were plated on agar plates with respective antibiotics and incubated overnight at 37°C.

3.2.4 Plasmids preparation and sequencing

A single colony was picked from selective agar plate and incubated in 3 - 4 ml LB medium for 8 hours at 37°C. Plasmid DNA was isolated by using Axygen™ Plasmid Miniprep Kit according to standard protocol and sent for sequencing. Large amounts of plasmid DNA were prepared by QIAGEN Plasmid Midi Kit and glycerol stocks were made for long term storage at -80°C.

3.2.5 Construction of pseudovirus pGEM-IRES expression plasmids

For production of MnPV pseudoviruses, plasmids exclusively encoding L1 variants and L2 gene were used. The MnPV $L1_{LONG}$, $L1_{MIDDLE}$ $L1_{SHORT}$ and L2 coding sequences derived from codon-optimized MnPV sequences were synthesized by GenScript Company from Dr. Kai Schäfer (DKFZ, Heidelberg). The inserts were amplified by PCR and subcloned into pGEM-IRES expression backbone, which was kindly provided by Prof. Dr. Martin Müller. The second and third ATG of $L1_{LONG}$ expression plasmid was mutated to GCG in order to guarantee unique $L1_{LONG}$ expression. The second ATG mutation was introduced by using PCR with a forward primer containing the GCG, whereas the third ATG was mutated by Phusion site-directed mutagenesis method. Similarly, the second methionine of $L1_{MIDDLE}$ expression plasmid was mutated to alanine for exclusive expression of $L1_{MIDDLE}$.

3.2.6 Construction of pPK-CMV-E3 expression plasmids

The humanized MnPV $L1_{LONG}$ (2^{nd} and 3^{rd} ATG mutation to GCG), $L1_{MIDDLE}$ (3^{rd} ATG mutation to GCG), $L1_{SHORT}$ and L2 coding sequence with or without stop codon, were PCR-amplified from pGEM-IRES expression plasmids and subcloned into pPK-CMV-E3 vector with *EcoRI* and *BamHI* sites.

3.2.7 Construction of pGEX-4T-3 plasmids

Native MnPV L1MIDDLE gene and N-terminal 1 - 41 amino acids of L1LONG ORF were PCR-amplified from GST-MnPV-L1LONG plasmid [107]. The inserts were subcloned into pGEX-4T-3 vector backbone, which contains an N-terminal GST-tag and a C-terminal SV40 tag, with *XmaI* and *SalI* sites.

3.2.8 Construction of pFBDM plasmids and Multibac plasmids

To ensure only L1LONG and L1MIDDLE gene expressed in the Multibac expression system, the 2nd ATG of L1LONG was mutated by PCR-amplification with a forward primer containing the mutated nucleotides GCG. The 3rd ATG of L1LONG was mutated to GCG by overlapping-PCR method in pGEM-MnPV L1LONG plasmid. Two copies of MnPV native L1LONG (2nd and 3rd ATG mutation to GCG), L1MIDDLE (3rd ATG mutation to GCG) and L1SHORT genes were inserted into pFBDM vector with two multiple cloning sites MCSI (*EcoRI/HinDIII*) and MCSII (*XmaI/SphI*). These two copies genes are flanked by polyhedrin or p10 promoters, respectively, which present two expression cassettes in a head to head arrangement. Since pFBDM plasmids contain the sequences used for Tn7 transposition (Tn7L and Tn7R), the recombinant MultiBac bacmids were generated by transforming pFBDM plasmids into electrocompetent DH10MultiBacCre *E. coli*. Following electroporation (1.8 kV pulse), competent cells are shaken at 37°C for 8 hours and plated on agar containing kanamycin (50 μg/ml), gentamycin (7 μg/ml), ampicillin (100 μg/ml), tetracycline (10 μg/ml), BluoGal (100 μg/ml) and IPTG (40 μg/ml). White colonies were picked after 18-24h incubation at 37°C. Recombinant MultiBac bacmids were then isolated by QIAGEN® Plasmid Mini Kit followed by ethanol precipitation.

3.2.9 Construction of pUC19-MnPV genome plasmids - Gibson assembly

MnPV genome was amplified by a pair of primers containing a *SalI* restriction site into the MnPV upstream regulatory region. This sequence was inserted in to pJET1.2/blunt vector by Dr. Daniel Hasche (named pJET-MnPV URR 1.8 plasmid). However, this plasmid contains three mutations and the LB culture needs to be incubated at 22°C for two days for plasmid isolation. Therefore, the wildtype MnPV genome without any mutations was inserted into pJET1.2/blunt vector by Gibson assembly method. Briefly, Gibson assembly master mix allows for successful assembly of multiple DNA fragments. This is due to three different enzymatic activities:

exonuclease creates single-stranded 3' overhangs; DNA polymerase fills in gaps within each annealed fragment and DNA ligase seals nicks. For construction of pJET-MnPV URR genome plasmid, two fragments were PCR-amplified from pJET-MnPV URR 1.8 vector and two fragments were PCR-amplified from pUC19-MnPV L2 to remove the mutations (from Dr. Kai Schäfer, DKFZ Heidelberg). The four fragments with a ratio of 2: 2: 2: 1 (fragment 1-4) were mixed with Gibson Assembly Master mix which was kindly provided by Dr. Guochao Wei as follows:

Component	Reaction
Total Amount of Fragments	0.2 - 1 pmols
Gibson Assembly Master mix	10 µl
Deionized H_2O	10 - x µl
Total volume	20 µl

The DNA mixture was incubated at 50°C for one hour and transformed in NEB DH5α competent cells. The successful pJET-MnPV URR genome plasmid was verified by sequencing the whole plasmid.

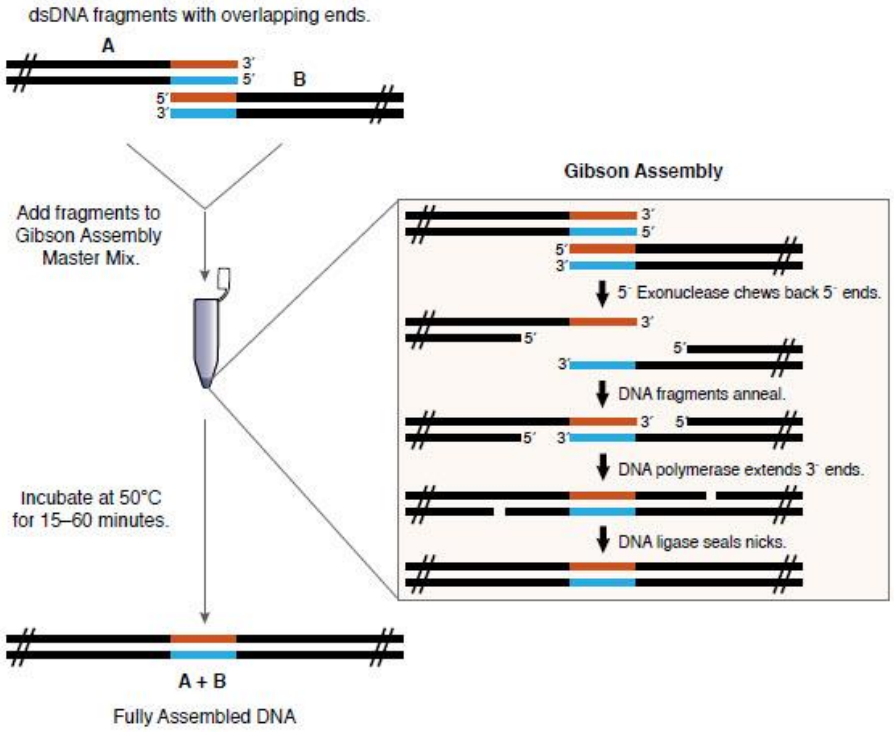

Figure 3.2.9: The overview of Gibson Assembly method (adapted from Gibson Assembly Master Mix protocol from NEB)

To construct pUC19-MnPV wt plasmid, the wildtype MnPV genome starting from the URR was cut by *SalI* enzyme from pJET-MnPV URR genome plasmid and inserted to pUC19 vector. The pUC19 MnPV L1LMid mutation plasmid was constructed by introducing mutations

on 1st and 2nd ATG to GCG by overlapping PCR method using the primers in Chapter 2.13. The pUC19 MnPV L1S mutation plasmid was constructed by introducing the mutation on 3rd ATG to GCG by overlapping PCR method using the primers in Chapter 2.13. To completely avoid the expression of $L1_{LONG}$ and $L1_{MIDDLE}$, pUC19 MnPV L1ΔNT plasmid, which lacks the 31 amino acids of N terminal L1 ORF, was constructed by Gibson assembly method described above using primers in Chapter 2.13.

3.3 Cell culture

3.3.1 Maintenance conditions of mammalian cells

All mammalian cells were grown in Dulbecco's Modified Eagle's Medium supplemented with 10% fetal calf serum (FCS), 1% Penicillin/Streptomycin and 1% L-glutamine. Hygromycin B (125 µg/ml) was added to the culture of human cervical carcinoma cell lines HeLaT as well as human embryonic kidney cells 293TT. All cell lines were maintained in the cell incubator at 37°C, 5% CO_2 and 95% humidity. Possible contamination with *Mycoplasma* was checked by PCR from time to time.

For the passaging of HeLa, HeLaT and 293TT cells, cells were washed once with 1 x DPBS prior to the addition of 1-2 ml of 0.25% trypsin-EDTA for detachment. Trypsin was inactivated by supplemented DMEM medium. Cell pellets were collected by the centrifugation at 1000 rpm for 5 minutes. For maintenance culture, cells were transferred into culture flasks at a ratio of 1:5 (293TT) or 1:15 (HeLa and HeLaT).

For cryoconservation, cell pellet of approximately 2 x 10^6 cells was resuspended in 1 ml of DMEM Cryo Medium into cryotube, which was then wrapped in several layers of tissue papers and transferred to -80°C. For longer storage, cells were transferred to liquid nitrogen after one day.

For reactivation of cells, frozen cells were thawed at 37°C and quickly added supplemented DMEM medium. The residual DMSO was removed by the centrifugation and cells were then seeded to culturing flasks in fresh culture medium.

3.3.2 Maintenance conditions of insect cells

Insect cell lines for VLP production were kindly provided by Prof. Dr. Martin Müller and kept at 27°C. Sf9 cells for recombinant baculovirus production were maintained in TNM-FH insect medium supplemented with 10% FCS, 1% Penicillin/Streptomycin, 1% L-glutamine and 0.1% Pluronic F-68. TN-High-Five cells for baculovirus expression were cultivated in EX-CELL™ 405 serum-free medium supplemented with 1% Penicillin/Streptomycin and 1% L-glutamine.

For adherent culture, cells were detached by cell scraper and passaged at a ratio of 1:3. For suspension culture, 50ml of culture at 1 x 10^6 viable cells/ml insect cells were seeded with 200ml supplemented medium in the spinner flask and cultivated with constant shaking speed of 125-150 rpm at 27°C. Cell densities were measured by using a standard trypan blue dye exclusion procedure. After two or three days, when cell densities reached at 1 x 10^6 viable cells/ml, cells were seeded to the culture flasks according to different amount requirements.

For cryoconservation, cell pellet of approximately 1 x 10^7 cells was resuspended in 1 ml of Cryo Medium (10% FCS, 10% DMSO and 80% TNM-FH supplemented insect medium for Sf9; 10%DMSO and 90% EX-CELL™ 405 supplemented serum-free medium for High-five) into cryotube, which was then wrapped in several layers of tissue papers and transferred to -80°C. For longer storage, cells were transferred to liquid nitrogen after one day.

3.3.3 Transfection of expression plasmids

Mammalian cells were seeded in Petri dishes or Plates one day prior to transfection. Cells with confluency of 80% were transfected by using TurboFect transfection reagent according to the standard protocol. The ratio of DNA amount and TurboFect transfection reagent was used as 1:2.

3.3.4 Immunofluorescence staining

First, HeLa cells were grown on coverslips in supplemented DMEM medium to approximately 60% confluence. Then, cells were transfected with respective expression L1 plasmids for 48 hours or infected with respective PsVs ($L1_{LONG\text{-}HA}$ +$L1_{SHORT}$ +L2, $L1_{MIDDLE\text{-}HA}$ +$L1_{SHORT}$ +L2 or $L1_{SHORT}$ +L2) for 30 min. Subsequently, after washing, the cells were fixed in 4% paraformaldehyde (PFA) for 30 min at room temperature and washed once again in 1 x PBS. Cells

were then permeabilized and blocked in the permeabilization buffer for one hour. The primary antibodies were diluted in blocking buffer and applied to the cells for one hour. After washing in 1 x PBS three times, cells were incubated with specific fluorescein-conjugated second antibodies (1: 500) and DAPI (1: 10,000) protected from light for one hour. The stained cells were then washed several times in 1 x PBS and mounted on glass slides with a drop of Dako Faramount Aqueous Mounting Medium. L1 proteins with HA tag were detected by anti-HA antibody and donkey anti-rat Alexa Fluor 488. $L1_{SHORT}$ protein without HA-tag was detected by mAbs mixture (mAbs 2E2, mAbs 2D11 and mAbs 3H8) and goat anti-mouse IgG2a (γ2a) Alexa Fluor 594. For each individual experiment, images were analyzed under confocal microscope with the same laser power settings.

3.4 Pseudoviruses production and purification

3.4.1 Plating and transfection of 293TT cells

293TT cells (3 x 10^5 cells/ml) were resuspended and seeded in a 10-cm dish plate with 10 ml supplemented DMEM one day ahead of transfection. For a normal preparation of pseudoviruses production, ten 10-cm dishes were used. Transfection was performed until cells reached 70% - 80% confluency by Calcium phosphate transfection. Two tubes were prepared for each transfection: one for the DNA/$CaCl_2$/ddH_2O mixture, one for the 2 x HBS buffer. 5 μg of each capsid expression plasmid and Gaussia/GFP plasmid were mixed with 75 μl 2.5M $CaCl_2$ in ddH_2O (750 μl in total). The DNA/$CaCl_2$/ddH_2O mixture was pipetted to 2 x HBS buffer (750 μl) drop by drop. Then, transfection reagent (1.5 ml) was added to each 10-cm dish after the incubation for 30 min at room temperature. The cells were incubated for 48h at 37°C, 5% CO_2 and 95% humidity without changing medium.

3.4.2 Pseudoviruses maturation

For pseudoviruses production, transfected 293TT cells from 10 dishes were detached by pipetting medium up and down several times and were harvested in a 50 ml Falcon tube. Cell pellet was resuspended in 1ml DPBS containing $CaCl_2$ and $MgCl_2$ in a 1.5ml Lo-Bind protein tube after centrifugation at 1900 rpm for 5 minutes. After another centrifugation at 5000 rpm for 5 min at 4°C, pellet was estimated and resuspended in an equal volume of pseudovirus lysis buffer (compared to pellet). Cells were lysed for 24 hours on an end-over-end rotator at 37°C.

3.4.3 Pseudoviruses purification

Three-step gradient with Iodixanol of 27%, 33% and 39% diluted in 0.8M NaCl/DPBS was made and used for pseudoviruses separation. 39% layer was colored with phenol red to make a distinction between 39% and 33%. The gradient had to be left overnight at 4°C to soften the edges. For the following day, cell lysate was treated with 5M NaCl (17 µl per 100 µl of total volume in tube, including pellet and lysis buffer). After centrifugation, the supernatant was collected in a new Lo-Bind protein tube and incubated with 2 µl Benzonase for 1 hour at 37°C. After incubation, the supernatant was carefully loaded on the top of the Optiprep gradient and balanced with DPBS/0.8M NaCl. The pseudoviruses were purified by ultracentrifugation through the gradient at 37,000 rpm for 5 hours at 16°C with TH641 rotor. The pseudoviruses fractions of each 500 µl were collected in Lo-Bind protein tubes by a 0.90 x 40 mm needle puncture on the gradient tube, which is one centimeter below the 39% interface line. Fractions were labeled and stored at -80°C.

3.4.4 Infection assay

HeLaT cells (50 µl, 2.5 x 10^5 cells/ml) were seeded in 96-well plates 2-5 hours prior to the pseudoviruses infection. Pseudoviruses were diluted in 1: 200 and added to the adherent HeLaT cells, which were then incubated for 48 hours at 37°C, 5% CO_2 and 95% humidity. Gaussia luciferase signal in 10 µl of cell medium was measured 15 min after addition of 100 µl mixture of Gaussia glow juice and coelenterazine substrate in a microplate luminometer Synergy2 reader.

3.4.5 Pseudovirus-based neutralization assay

To evaluate the neutralizing capacity of serum from animals, a pseudovirus based neutralization assay was carried out. Briefly, 1: 3 serial dilutions from each diluted animal serum (1: 60) were made in 96 well plates in duplicate. 40 µl of pseudoviruses with proper dilution were mixed with the serial diluted sera at room temperature for 15 min. Next, 50 µl of a density of 2.5x10^5 cells/ml HeLaT cells were seeded to the pseudoviruses-serum mixture and followed by two days incubation at 37°C, 5% CO_2 and 95% humidity. The amount of secreted Gaussia luciferase was determined as described in Chapter 3.4.4.

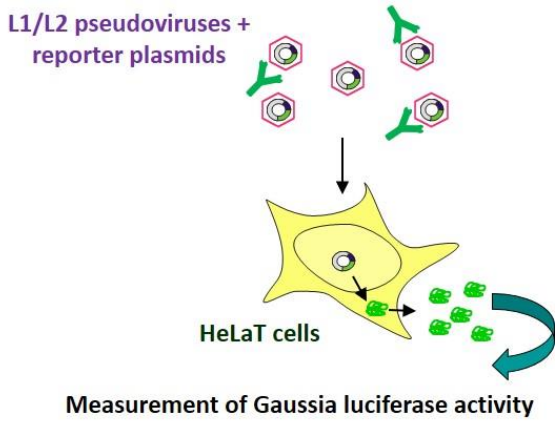

Figure 3.4.5: The overview of neutralization assay [108]. Prior to the infection, pseudoviruses are incubated with the antibody or serum from animals. The neutralizing capacity is determined by measurement of Gaussia luciferase.

3.5 VLP production

3.5.1 Generation of recombinant baculoviruses

The generation of recombinant baculoviruses was performed as previously described [100] with some modifications. Briefly, recombinant baculoviruses were produced by transfecting Sf9 cells with recombinant MultiBac bacmids via calcium phosphate precipitation method. At the time of transfection, the optimal confluency for adherent Sf9 cells is 75% in 25 cm^2 flask. After washing, cells were replaced with 1 ml Grace's Insect Medium supplemented with 1% L-glutamine. The MultiBac bacmid DNA (1 µg) was diluted in 1 ml transfection buffer and followed by dropwise adding to Sf9 cells. After incubation at 27°C for 5 hours, the cells were washed twice and then maintained in 10 ml TNM-FH supplemented medium for 6 days. The supernatant was used for generation of a high-titer baculovirus stock. Sf9 cells with the density of 2 x 10^6 were seeded in a T25 flask and infected with 1 ml supernatant for virus amplification in next 6 days. This step was repeated by passaging increasing supernatant for at least two weeks (3 ml supernatant for 1 x 10^7 Sf9 cells in a 75 cm^2 flask and 5 ml supernatant for 2.5 x 10^7 Sf9 cells in a 175 cm^2 flask).

3.5.2 Recombinant Baculovirus expression test

Sf9 cells in a 25 cm^2 flask were infected by 1 ml supernatant from Passage 2 and incubated for 3 days at 27°C. Proteins were extracted and the expression of different L1 isoforms was analyzed by Coomassie blue staining and Western blot.

3.5.3 VLP production and purification

TN-High Five cells were cultivated to a density of 2.5 x 10^6/ml in 250 ml suspension culture, which were then pelleted and resuspended in 42 ml EX-CELL™ 405 serum-free medium and 8 ml high titer virus stock. The cells were shaken at a low speed for 1 hour at room temperature and then incubated within 250 ml final volume of medium for 3 days at 27°C. Cell pellets were harvested by centrifugation (3,000 rpm for 10 minutes at 4°C in Sorvall GS-3 rotor) and washed in pre-chilled PBS for two times. Dry pellets were resuspended in 10 ml VLP extraction buffer containing 200 µl 100 mM PMSF, and then followed by three times sonication. A two-step gradient consisting of 7 ml of 40% sucrose on top of 7 ml CsCl solution was prepared. Clear cell lysate was obtained by centrifugation (10,000 rpm for 10 min at 4°C in Sorvall F-28/50 rotor) and carefully loaded onto the top of the CsCl layer. After centrifugation (27,000 rpm for 3 hours at 10°C in SW-31Ti rotor), the interphase between sucrose and CsCl together with the complete CsCl layer was transferred into a Quickseal tube. The fractions were collected in 1 ml aliquot after a 16-hour centrifugation at 48,000 rpm at 20°C in a Beckman 70Ti rotor and analyzed by Coomassie blue dye and Western blot. Small aliquots from the fraction with the highest and lowest protein yield were dialyzed against H_2O on a membrane filter and sent for Electron microscopy.

3.6 Preparation and analysis of proteins

3.6.1 Quantification of proteins

Protein concentrations were measured by Bio-Rad Protein Assay. Briefly, 5 µl of 1: 10 diluted protein sample with 155 µl H_2O were mixed with 40 µl of Bio-Rad Protein Assay solution into 96-well plate. BSA serial solutions (0.25 mg/ml to 7.5 mg/ml) were used as the standard curve for calculation. The absorptions of protein samples and BSA standard were determined at 595 nm in a SPECTROstar Nano plate reader.

3.6.2 SDS-polyacrylamide gel electrophoresis

Denatured proteins were separated due to their electrophoretic mobility in discontinuous sodium dodecyl sulfate polyacrylamide gel electrophoresis (SDS-PAGE), which consists of a stacking gel and a separating gel. The SDS gels were made as follows:

Separating gel (10% / 12%)	Stacking gel (5%)
0.25 M Tris-HCl, pH 8.8	0.25 M Tris-HCl, pH 6.8
0.1 % SDS	0.1 % SDS
10% / 12% Acrylamide/Bisacrylamide 29:1	4% Acrylamide/Bisacrylamide 29:1
0.05% ammonium persulfate	0.05% ammonium persulfate
0.08% TEMED	0.08% TEMED

After denaturation at 95°C for 5 min, protein samples were supplemented with 5 x SDS loading dye. After brief centrifugation, 100-200 µg treated proteins were loaded to the gel along with PageRuler Prestained Protein Ladder. The current changed from 80V to 120V until the samples reached to the separating gel and stopped until the desired protein separation was achieved.

3.6.3 Coomassie blue staining

The protein bands were directly visualized in the gel by staining with colloidal Coomassie G-250 after gel electrophoresis. The gel was washed in water with agitation until the background became clear. For longer time storage, the gel was scanned and dried in a vacuum gel dryer for one hour at 80°C.

3.6.4 Immunoblotting

Proteins separated by gel electrophoresis were electrophoretically transferred to a PVDF membrane by a wet "sandwich" blotting, which was performed in Mini Trans-Blot® Electrophoretic Transfer Cell (Bio-Rad). The wet transfer was assembled according to the manufacturer's instructions and performed 400 mA for 60 min. After blotting, PVDF membrane was blocked with 5% milk powder in 1 x TBST at room temperature for 1 hour. The primary antibody was added in appropriate dilution with rocking agitation at 4°C overnight. The next day, the membrane was washed three times with 1 x TBST and incubated with the secondary antibody conjugated with HRP at a 1:10,000 dilution for 1 hour at room temperature, followed by further washing. Finally, the specifically bound antibodies were visualized by an HRP-catalyzed enhanced chemiluminescent reaction (ECL) and detected by exposure to X-ray film.

3.7 Production of Glutathione-S-Transferase (GST)-tag antigen

The pGEX-4T-3 plasmids with different MnPV late genes ($L1_{LONG}$, $L1_{MIDDLE}$, $L1_{SHORT}$, L1ΔNT-31aa and L1ΔNT-41aa) were transformed in *E. coli* BL21 Rosetta bacteria and cultivated in LB medium supplemented with 100 µl/ml ampicillin and 20 µg/ml chloramphenicol at 37°C overnight (pre-culture). The early gene E2 vector and empty vector (GST-SV40-tag) was transformed in *E. coli* BL21 and grown in LB medium containing 100 µl/ml ampicillin (pre-culture). 50 ml of pre-culture was diluted into 1L LB containing the respective antibiotics and grown at 37°C until OD_{600} reached approximately 0.4. The culture was further grown at 25°C until OD_{600} value reached 0.5-0.6 and then induced with 250 mM isopropyl β-D-1-thiogalactopyranoside (IPTG). After certain cultivation at 25°C (6 hours for L1ΔNT-31aa, L1ΔNT-41aa and GST-SV40-tag; 8 hours for $L1_{SHORT}$; 18 - 20 hour for $L1_{LONG}$, $L1_{MIDDLE}$ and E2), the pellets were collected by centrifugation for 20 min at 5000 rpm at 4°C in Sorvall GS-3 rotor. The pellets were resuspended in 10 ml lysis buffer (1 x PBS for E2 and GST-SV40-tag; buffer L for L1 antigens) containing 0.5 ml protease inhibitor cocktail complete and 2 mM DTT. However, for L1 antigens, 2 mM ATP and 5 mM $MgCl_2$ were added to lysis buffer to facilitate bacterial chaperone dissociation. The lysate was sonicated 4 times x 15s with 30s break on ice and then centrifuged at 14,000 rpm for 1 hour in a Sorvall F-28/50 rotor. For L1 antigens, the homogenized lysate was further incubated for 1 hour at room temperature with agitation prior to centrifugation. Finally, the supernatant was mixed with one volume of 100% glycerol and store at -20°C. The antigens were diluted in a 1: 3 serial dilution in Polysorb Nunc-Immuno plates and titrated by a normal GST-ELISA method. Proper dilution of the antigens used for GST-ELISA was determined by comparing the OD_{450} raw value with the old antigen.

3.8 Enzyme-linked immunosorbent assay (ELISA)

3.8.1 GST-capture ELISA

The GST-capture ELISA was modified by Schäfer et al for detecting the seroreactivity of *Mastomys* sera [86, 107]. Briefly, glutathione is chemically crosslinked to casein and used to capture the fusion protein which contains an N-terminal GST tag. The C terminal SV40 tag is used to identify the bond of the completely expressed fusion protein via the monoclonal mouse antibody KT3. 200 ng/well glutathione-casein was diluted in 50 mM carbonate buffer (pH=9.6) and coated to 96 well polysorp plates overnight at 4°C. The next day, after blocking with casein

blocking buffer (180 µl/well) for 1 hour at 37°C, the plate was then incubated respective GST-tag fusion protein antigen lysate for 1 hour at room temperature which was purified from bacterial. Prior to the serum coating, each *Mastomys* serum was blocked with a dilution of 1:50 in GST-SV40-tag casein blocking buffer for 1 hour at room temperature. The GST-SV40-tag fusion antigen bacterial lysate was diluted according to the antigen titration as described in chapter 3.7. This incubation is essential to get rid of the unspecific reaction between antibodies and bacterial proteins or GST/SV40 tags. Afterwards, ELISA plates were washed with 1 x PBST for four times and incubated with treated sera for 1 hour at room temperature. After washing, 100 µl/well HPR-conjugated goat anti-mouse IgG antibody was applied to 96 ELISA plates with a dilution of 1: 10,000 in casein blocking buffer. After washing, antibodies were quantified colorimetrically by incubating with 100 µl/well of substrate buffer for 8 minutes (0.1 mg/ml tetramethylbenzidine and 0.006 % H_2O_2 in 100 mM sodium acetate, pH=6). The enzyme reaction was stopped with 50 µl/well of 1 M sulphuric acid and absorption was measured at a wavelength of 450 nm. The reactivity of serum against each antigen was calculated by subtracting the background GST-SV40 tag value from the respective viral antigen. Each ELISA was repeated at least twice.

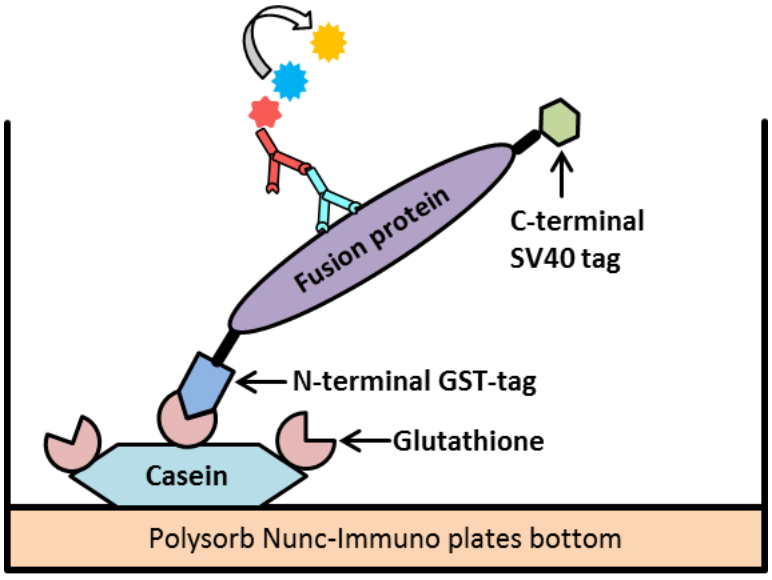

Figure 3.8.1: The reaction scheme of GST-capture ELISA. The fusion antigen, which displayed a GST-tag at the N-terminal and a SV40-tag at the C-terminal, was expressed in *E. coli* and captured by glutathione-casein via its N-terminal GST-tag. The antibodies in *Mastomys* sera were detected by second antibody (HRP-conjugated goat anti-mouse IgG).

3.8.2 VLP-ELISA

VLP-ELISA was used to detect antibodies which specifically bind to the intact surface of MnPV VLPs. 100 ng/well purified VLPs were coated in 96 Polysorb plates overnight at 4°C. The next day, the plates were blocked with casein blocking buffer (180 µl/well) for 1 hour at 37°C. *Mastomys* sera were diluted 1: 100 in casein blocking buffer and followed by adding 150 µl/well to first row of the ELISA plate. 100 µl/well of casein blocking buffer were added to the plates besides the first row. A 1: 3 serial dilution was made by transferring 50 µl from the previous row to the next row after mixing. After incubation of 1 hour at room temperature, the plates were washed with 1 x PBST for four times and incubated with 100 µl/well second anybody (HRP-conjugated goat anti-mouse IgG, 1:10,000 diluted in casein blocking buffer). After washing, antibodies were quantified colorimetrically by incubating with 100 µl/well of substrate buffer for 8 minutes (0.1 mg/ml tetramethylbenzidine and 0.006 % H_2O_2 in 100 mM sodium acetate pH=6). The enzyme reaction was stopped with 50 µl/well of 1 M sulphuric acid and the absorption was measured at a wavelength of 450 nm. Antibody titer represents the last reciprocal serum dilution above blank.

3.8.3 Denaturation assay

Denatured VLP-ELISA was performed to identify whether *Mastomys* sera could react with the linear epitopes of MnPV L1SHORT protein. Therefore, several denatured conditions were checked whether one can completely disrupt VLPs structure from conformational to linear form. For a final protocol, denatured VLPs were obtained by heating in coating buffer (50 mM carbonate buffer pH 9.6) and coated to ELISA plates overnight at 37°C. Further steps were carried out according to the general VLP-ELISA protocol. The five monoclonal antibodies against MnPV L1SHORT (mAb2E2, mAb2D6, mAb2D11, mAb5E5 and mAb3H8) and serum mix (sera from five tumor-bearing animals) were used as positive and negative controls for denaturation.

Denatured GST-ELISA was performed to identify whether *Mastomys* sera could react with the linear epitopes of MnPV L1LONG and L1SHORT proteins. The denatured GST fusion antigens were obtained by heating in coating buffer and were directly coated to the ELISA plates without casein-glutathione coating overnight at 37°C. Further steps were carried out according to the general GST-ELISA protocol. The five monoclonal antibodies against MnPV L1SHORT (mAb2E2, mAb2D6,

mAb2D11, mAb5E5 and mAb3H8) and serum mix (sera from five tumor-bearing MnPV positive animals) were used as positive and negative controls for denaturation.

3.9 Epitope mapping

For linear epitope mapping, $L1_{LONG}$ protein was translated into 15 amino acids (aa) peptides with 14 aa peptides overlap in microarray by PEPperPRINT Company. Each array contains two identical peptide replicates. For conformational epitope mapping, $L1_{LONG}$ protein was translated into 7 aa, 10 aa and 13 aa cyclic peptides with 6 aa, 9 aa and 12 aa overlap. Epitopes were identified by the antigen and antibody reaction after $L1_{LONG}$ and $L1_{SHORT}$ positive sera were applied to the microarray.

3.10 Mass spectrometry

The peak fraction of pseudoviruses sample ($L1_{LONG}$ + $L1_{SHORT}$ + L2) were handed over to Zentrum für Molekulare Biologie der Universität Heidelberg (ZMBH) for Mass spectrometry analysis. The samples were loaded to SDS-gel and stained with Coomassie blue. The target protein region was excised from the gel, trypsinized and the peptides were analyzed.

3.11 Electron microscopy

Micrographs were taken by Dr. Karsten Richter and Dr. Michelle Neßling (DKFZ, Heidelberg) with Zeiss EM912 or EM910 electron microscopy.

3.11.1 Negative staining

The particles structure of pseudoviruses production and virus like particles (VLPs) preparation from different L1 isoforms were visualized by negative staining in electron microscopy. Samples were applied on carbon coated grids and stained with 2% uranyl acetate.

3.11.2 Transmission electron microscopy

The infected Sf9 cells or transfected HeLa cells were seeded on Aklar-punches in 12 well plates and fixed for conventional Epon-embedding according to a standard protocol. Briefly, cells were fixed in chemical fixation solution (4% formaldehyde/2.5% glutaraldehyde/1 mM $MgCl_2$ /1 mM $CaCl_2$/100 mM cacodylate-buffer, pH=7.2), followed by post fixation in 1% osmium tetroxide, dehydration in 50%, 75%, 100% ethanol and

resin-embedding. Ultrathin sections were cut at 60 nm nominal thickness and post stained with uranyl and lead citrate.

3.12 Statistical analysis

Graphs Prism 5.0 was used for data analysis. The Gaussia luciferase signals of each fractions were shown in mean ± SEM. Time course of different virial immune responses were shown in scatter diagram with mean ± SEM. The significant difference of pseudovirus infectivity between "L1S + L2" and "L1L + L1S + L2" group was determined by t tests (and nonparametric tests).

4. Results

The aim of this study is to investigate the role of three isoforms of MnPV major capsid protein L1 in the immune evasion during the persistence of viral infection. Firstly, the capsid assembly ability of L1 proteins was tested (**Chapter 4.1**). Secondly, L1 seroreactivity was characterized in the naturally infected animals (**Chapter 4.2**) to study the time course of seroconversion, neutralizing capacity and epitope recognition. Moreover, detailed analysis of the interaction among different L1 isoforms was investigated (**Chapter 4.3**).

4.1 Capsid formation of L1LONG, L1MIDDLE and L1SHORT

The open reading frame (ORF) of MnPV major capsid protein L1 contains three alternative translation initiation sites, which are located at nucleotide positions (nt) 5701, 5722 and 5794 in MnPV genome, potentially leading to the expression of L1LONG, L1MIDDLE and L1SHORT (**Fig. 4.1.1**). To test the capsid formation ability of these L1 isoforms, virus like particles (VLPs) and pseudoviruses (PsVs) were produced in insect cells and 293TT cells, respectively.

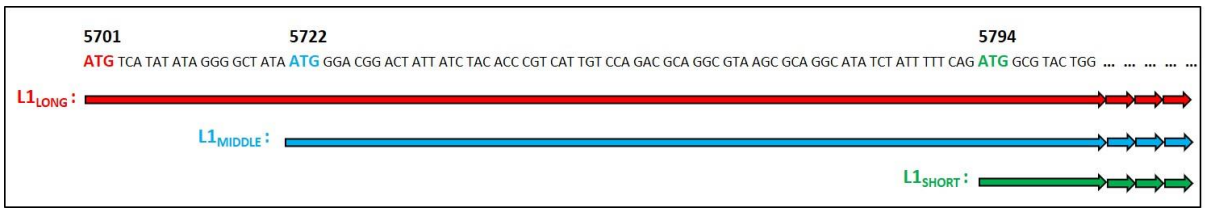

Figure 4.1.1: MnPV L1 potential open reading frames. L1LONG, L1MIDDLE and L1SHORT start at the ATGs at nucleotide positions 5701, 5722 and 5794 in MnPV genome, respectively

4.1.1 VLP production

The MultiBac baculovirus expression system was used to produce VLPs due to the efficient expression of multiple genes from independent cassettes [109-116]. The recombinant baculoviruses were produced by transfecting Sf9 cells with recombinant MultiBac bacmids. Then, cells were passaged once and examined under microscope to check the morphology. The infected cells showed typical morphology of baculoviruses infection, which were opaque, notably bigger in size and more granular than non-transfected cells (**Fig. 4.1.2 A**). The expression of three L1 isoforms was verified by Coomassie blue staining and Western blot before the infection of TN-High Five cells with the high titer virus stock. As expected, all L1 proteins were expressed and migrated at the predicted sizes (55-60 kDa) in SDS-PAGE gel (**Fig. 4.1.2 B**). These results indicate

successful recombinant baculoviruses generation along with L1 proteins expression in the infected Sf9 cells.

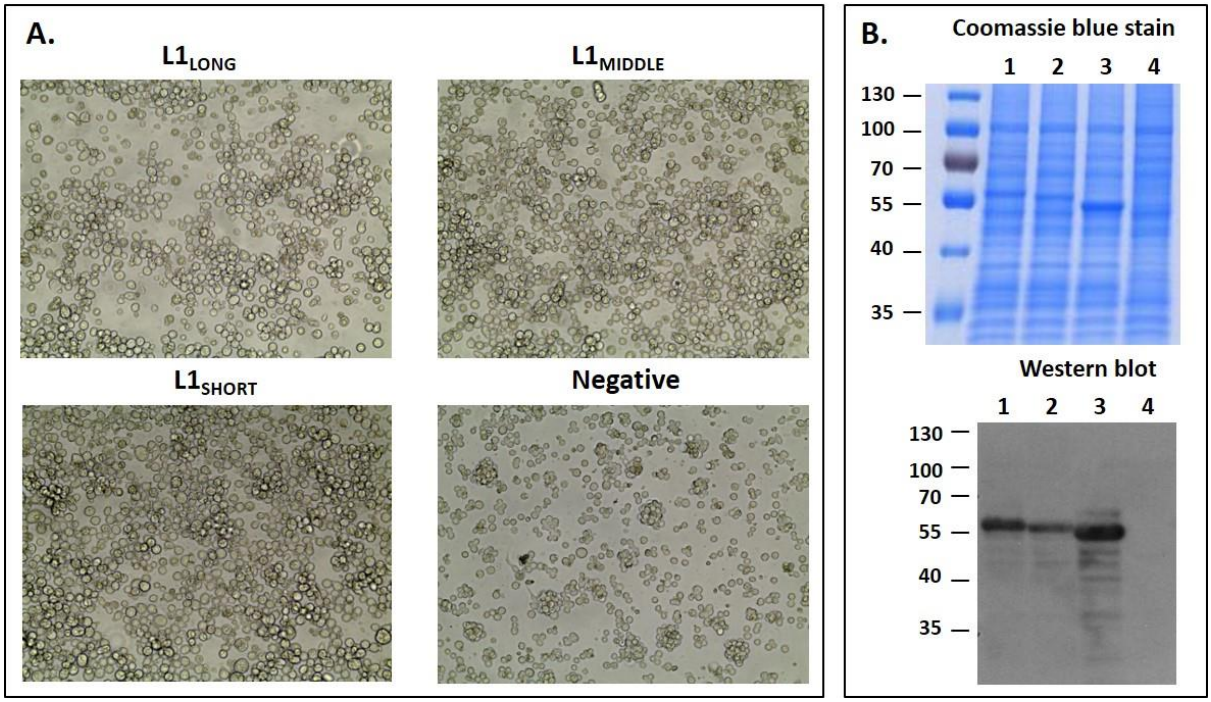

Figure 4.1.2: MultiBac baculovirus expression system. (A). The infected cells (L1LONG, L1MIDDLE and L1SHORT) showed typical morphology of baculoviruses infection, which was different from non-transfected cells (negative). **(B).** The expression of L1LONG, L1MIDDLE and L1SHORT. Proteins were extracted from the recombinant baculovirus infected Sf9 cells (Passage 2) and analyzed by Coomassie blue staining and Western blot. A pool of sera from five MnPV infected tumor-bearing animals (Serum mix) was used as the first antibody for immunoblots. 1. L1LONG; 2. L1MIDDLE; 3. L1SHORT; 4. Non-transfected.

VLPs were extracted by a two-step density gradient of sucrose and CsCl after ultracentrifugation. The quality of the CsCl gradient was monitored by measuring refractive index of each fraction at room temperature. A continuous rise of CsCl density was obtained, ranging from 1.317-1.527 g/cm^3 (**Fig. 4.1.3 A)**. Peak L1LONG bands were detected at approximately 1.419 to 1.407 g/cm^3 density in fraction six and seven (**Fig. 4.1.3 B**). Fraction five and six (CsCl density 1.427 to 1.415 g/cm^3) contained the most L1MIDDLE (**Fig. 4.1.3 C**). For L1SHORT, the strongest bands were in fraction two, three and five, corresponding to a CsCl density of 1.503, 1.474 and 1.446 g/cm^3 (**Fig. 4.1.3 D**).

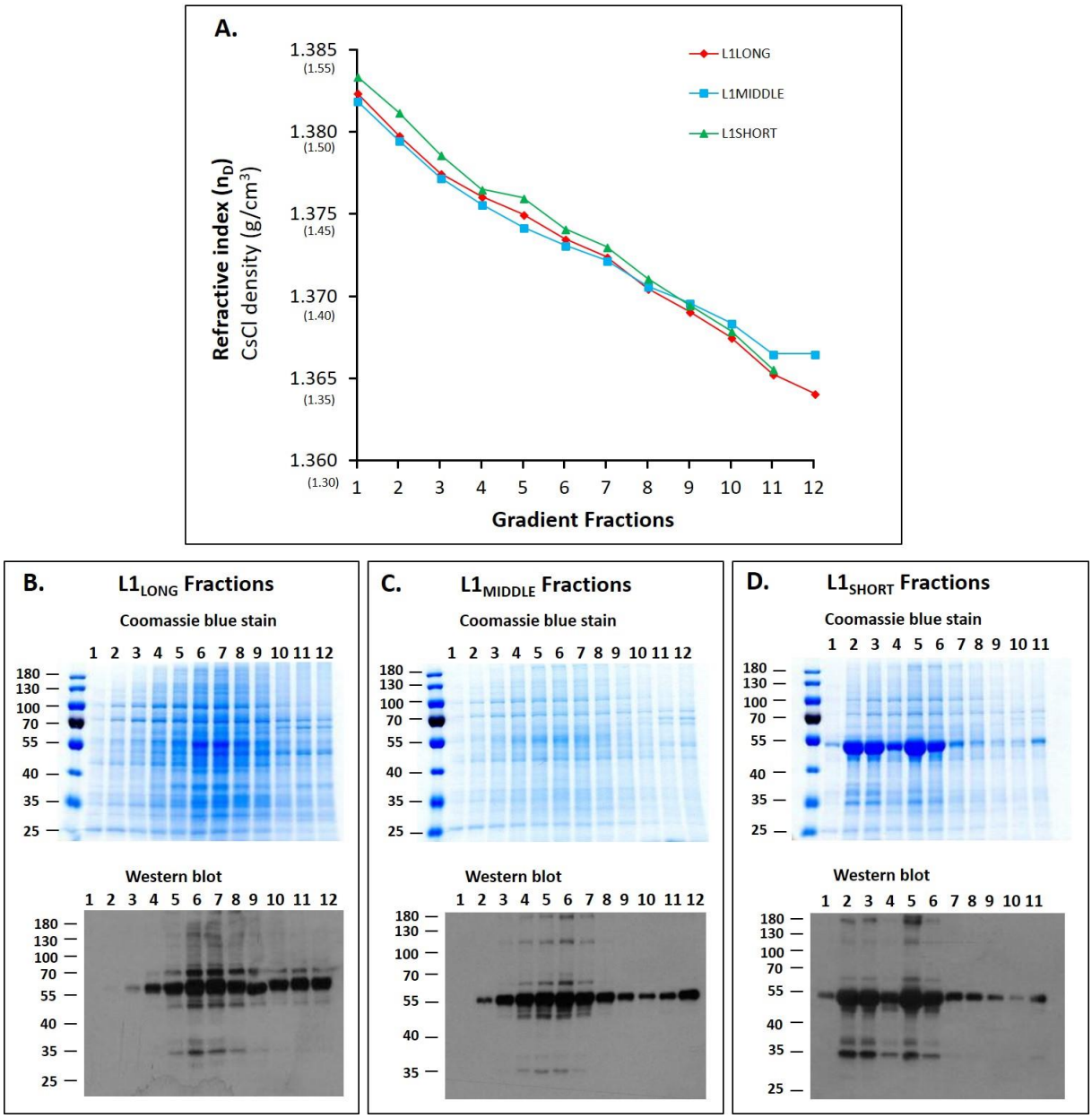

Figure 4.1.3: Expression of L1LONG, L1MIDDLE and L1SHORT in each fraction. (A). Refractive index of each fraction. The CsCl density of each fraction was determined by refractometer at room temperature. L1LONG **(B)**, L1MIDDLE **(C)**, and L1SHORT **(D)** fractions were analyzed by Coomassie blue staining (upper panels) and Western blot (lower panels) using serum mix as primary antibody, which was a pool of sera from five MnPV infected tumor-bearing animals.

VLPs formation of three L1 proteins was determined by electron microscope (EM). For L1LONG and L1MIDDLE, EM analysis revealed that no individual and uniformly shaped VLPs were visualized in fraction 6. However, plentiful irregularly shaped particles with size of 20-50 nm were found in the top gradient with lowest density (fraction 11). It was difficult to identify substructures such as normal capsomeres, indicating L1LONG and L1MIDDLE were not able to form

correct VLPs under the chosen production condition (**Fig. 4.1.4 A and B**). For L1SHORT, highly concentrated and spherically shaped particles with size of 45-50 nm or 60 nm were found in fraction 2 or 5 respectively, where capsomeres could be clearly observed. The VLPs in fraction 5 were more homogeneous. In fraction 11, particles with notable capsomeres were also detected (**Fig. 4.1.4 C**). These results provide strong evidences for the efficient VLPs formation of L1SHORT.

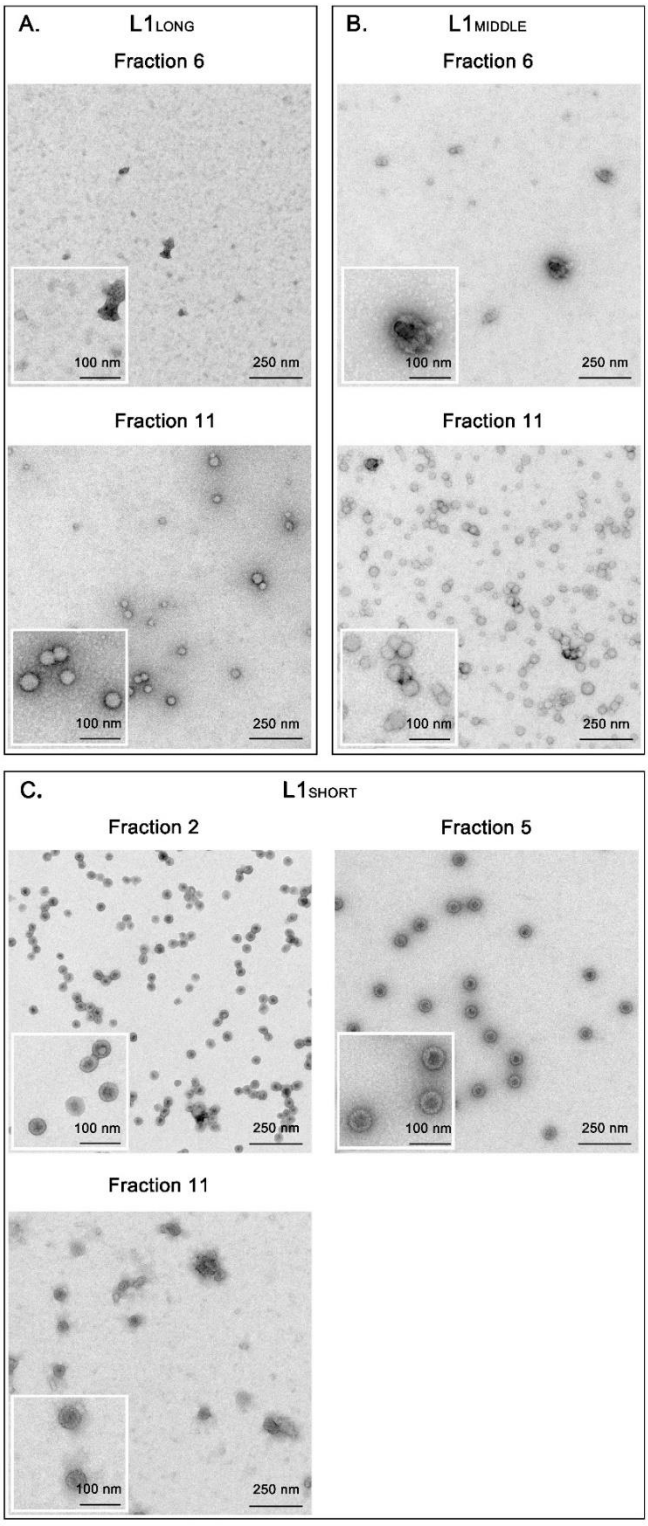

Figure 4.1.4: EM analysis of VLPs formation capacity of L1LONG, L1MIDDLE and L1SHORT. Peak fractions as well as the respective fractions with lowest density of L1LONG **(A)** L1MIDDLE **(B)** and L1SHORT **(C)** were analyzed by electron microscope.

To exclude the possibility that the lack of particles in L1LONG and L1MIDDLE fractions is due to loss of fragile or poorly formed particles during extraction procedures, VLPs formation was further examined in the SF9 cells without purification process. The cells were infected with high-titer recombinant baculoviruses at Passage 3 and fixed for EM analysis. The typical "rod" shape baculoviruses with approximate 32 nm diameter and 180 nm to 360 nm length were clearly seen in the nucleus of all the observed cells. There were abundant baculoviruses with multiple nucleocapsids wrapped in the envelope, which possessed a typical bilayer membrane structure. However, there were still some nucleocapsids without envelope (**Fig. 4.1.5**). Since the genes of interest were inserted into the engineered MultiBac baculoviral genome, the recombinant L1 proteins can be produced along with the baculoviruses in the host cell machineries. Although plenty of baculoviruses were found in the nucleus of Sf9 cells, indicating successful expression of L1LONG and L1MIDDLE, there were no VLPs observed (**Fig. 4.1.5 A and B**). On the contrary, high-level production of spherically shaped particles with size of approximate 50nm in diameter were discovered in the nucleus of L1SHORT expressing cells (**Fig. 4.1.5 C**).

In conclusion, this chapter suggested that L1LONG and L1MIDDLE derived from the first and second ATG hardly induced VLPs formation under the chosen condition. This was not due to the purification process, since no particles were found in the Sf9 cells. In contrast, L1SHORT starting from the third ATG strongly induced VLPs.

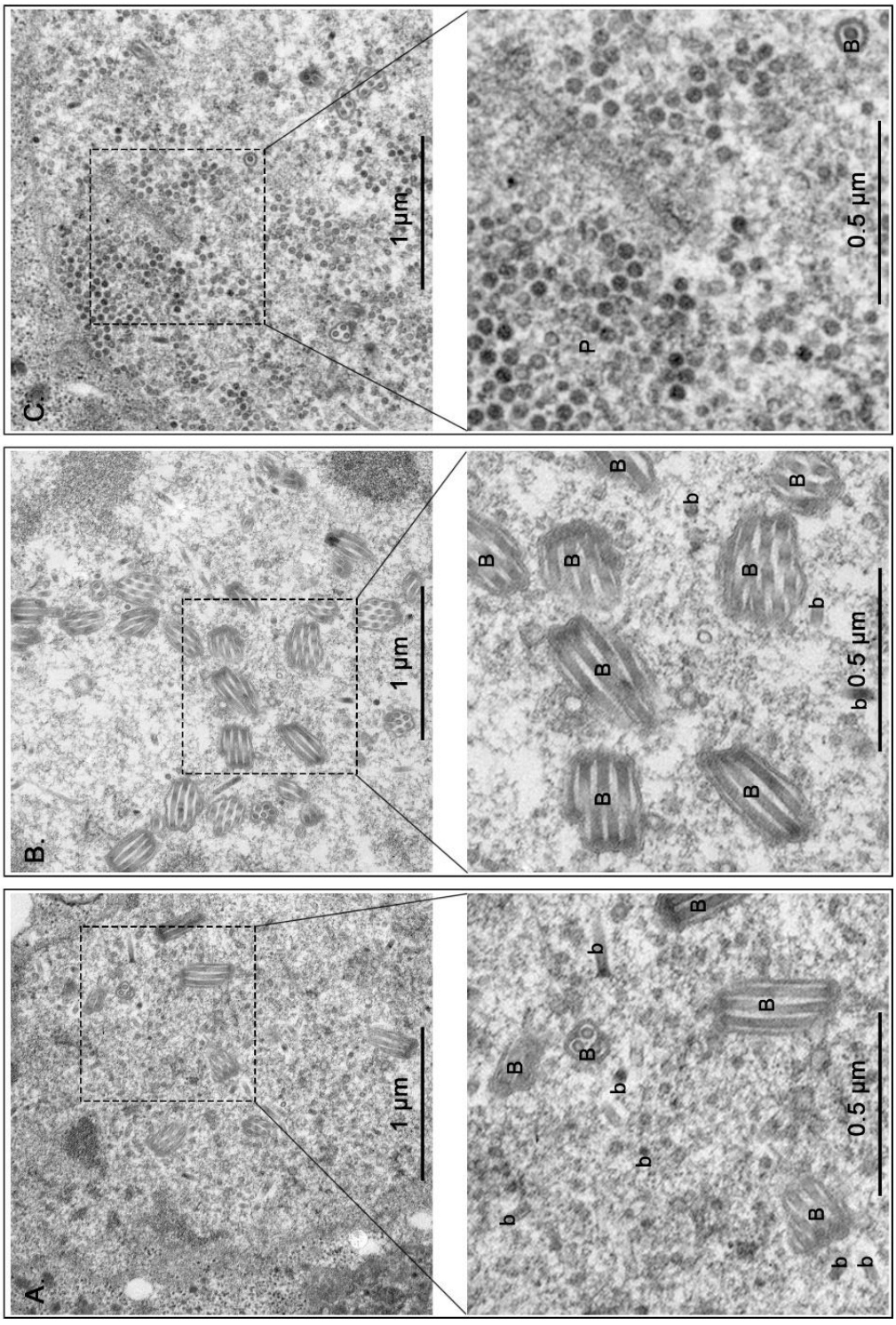

Figure 4.1.5: EM analysis of the VLPs formation of L1LONG, L1MIDDLE and L1SHORT in the Sf9 cells. Sf9 cells infected with respective recombinant baculoviruses derived from L1LONG **(A)** L1MIDDLE **(B)** and L1SHORT **(C)** were analyzed by EM. The box area indicates the lower pane image with higher magnification. The capital letter B represents single or multiple baculovirus nucleocapsids wrapped in the envelope. The lowercase letter b indicates the non-enveloped baculovirus nucleocapsid. The capital letter P represents the MnPV VLPs.

4.1.2 Pseudoviruses production

The minor capsid protein L2 plays an essential role for the virus particles formation and stabilization. It forms homotypic interactions with neighbor L2 as well as heterotypic binding with L1 molecules [117]. It is reported that including both L1 and L2 into particles production may facilitate increased particles yield, capsid stability, infectivity and DNA encapsidation [46, 53, 118-121]. In order to investigate whether L2 can influence the capsid formation ability of different L1 isoforms, different pseudoviruses (PsVs) were produced. PsVs were produced in 293TT cells by co-transfection of L1 and L2 codon-modified pGEM-IRES expression plasmids together with a reporter plasmid containing GFP/Gaussia luciferase and SV40 origin of replication. The expression of three L1 isoforms was identified by immunoblotting, using sera mixed from naturally infected tumor-bearing animals as primary antibody. As expected, all L1 proteins were detected at target size of 55, 58 and 60 kDa. (**Fig. 4.1.6 A**). PsVs were then purified by ultracentrifugation through an Optiprep (iodixanol) step gradient. The quality and quantity of PsVs were assessed by measuring the luciferase signals after infecting HeLaT cells for 48h. In the combinations where only $L1_{LONG}$ and L2 or $L1_{MIDDLE}$ and L2 were expressed, no luciferase signals were detectable in any fraction. Moreover, no PsV-like particles were observed in these fractions under electron microscope, which excludes the possibility that $L1_{LONG}$ and $L1_{MIDDLE}$ with L2 can form non-infectious particles. (**Fig. 4.1.6 B, C and E**). However, the detected luciferase signals and EM analysis revealed that $L1_{SHORT}$ with the help of minor capsid protein L2 can efficiently form infectious PsVs (**Fig. 4.1.6 D and E**).

In order to investigate the capsid formation ability of different L1 isoforms in various systems, PsVs were produced by using L1 codon-modified pPK-CMV-E3 expression plasmids. This vector contains a C-terminal HA-tag which facilitates the detection of the target protein by anti-HA antibodies. In addition, there was another set of plasmids with stop codon between the gene of interest and C-terminal HA-tag. The expression of pPK-L1 expression plasmids with or without HA-tag was detected by anti-HA antibodies or serum mix. Three L1 proteins migrated at the predicted sizes, but the expression of $L1_{SHORT}$ was much more efficient than that of $L1_{LONG}$ and $L1_{MIDDLE}$ (**Fig. 4.1.7 A**). PsVs was then produced by transfecting 293TT cells with pPK expression plasmids without HA-tag. PsVs formation capacity of L1 isoforms was consistent with the results from above pGEM-IRES expression system. $L1_{LONG}$ and $L1_{MIDDLE}$ hardly formed PsVs, since no

Gaussia signal and no particle was detected (**Fig. 4.1.7 B and C**). Both infection assay and EM analysis suggested that L1SHORT strongly induced PsVs (**Fig. 4.1.7 D**).

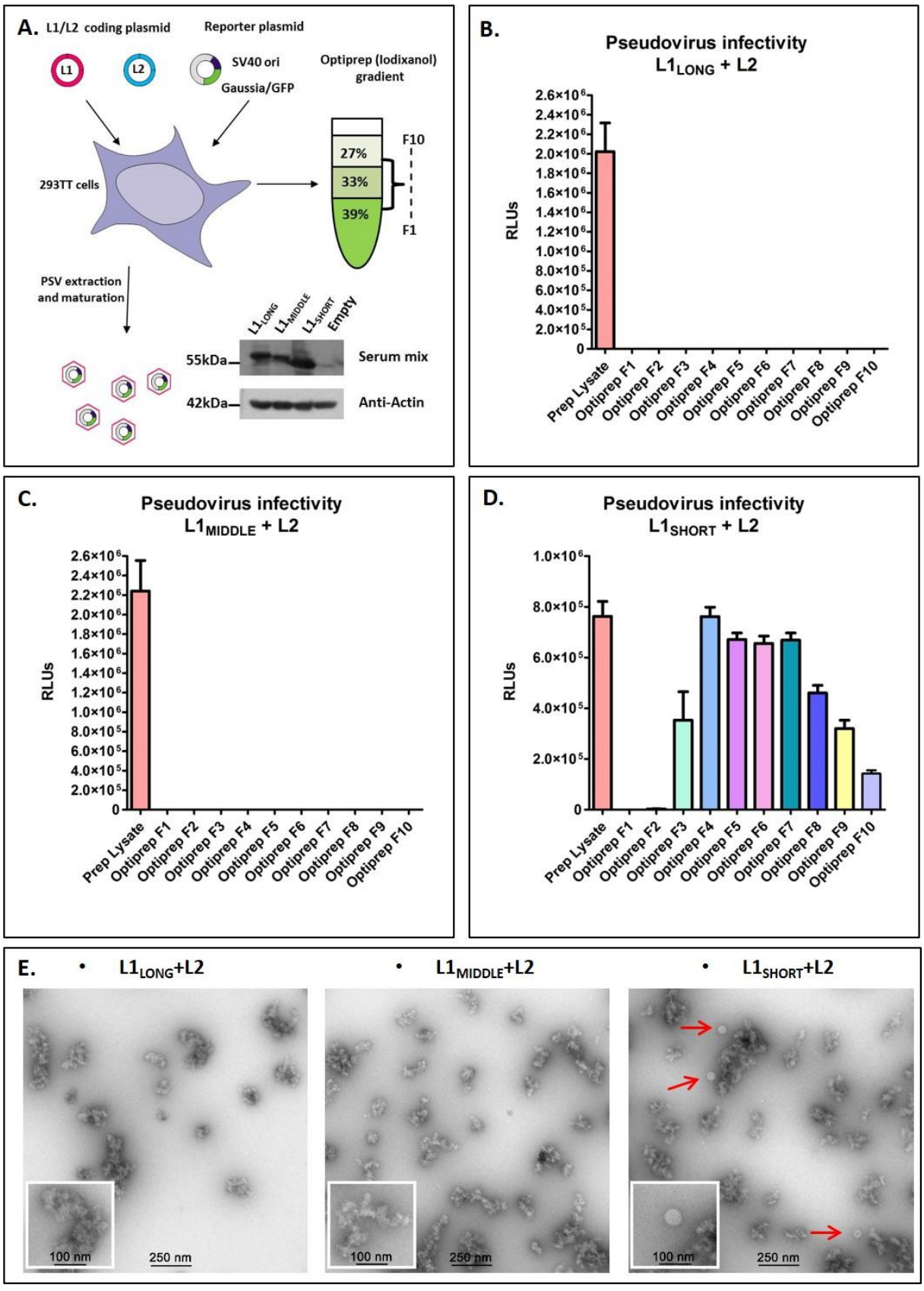

Figure 4.1.6: PsVs production via pGEM-IRES expression plasmids. (A). Overview of PsVs production. PsVs production is based on the transfection of capsid genes L1 and L2 (codon modified) expression plasmids together with a reporter plasmid in 293TT cells. PsVs were harvested by ultracentrifugation through Optiprep gradient. The expression of L1 isoforms in 293TT cells was checked by serum mix, which was a pool of sera from five MnPV infected tumor-bearing animals. The PsVs infectivity from each combination $L1_{LONG}$ + L2 **(B)**, $L1_{MIDDLE}$ +L2 **(C)** and $L1_{SHORT}$ +L2 **(D)** was determined by infection of HeLaT cells for 48h, after which the Gaussia signal was measured. The experimental data were shown in mean ± SEM from three independent experiments. **(E)**. PsVs formation of $L1_{LONG}$, $L1_{MIDDLE}$ and $L1_{SHORT}$ was checked by EM. The red arrow refers to PsVs.

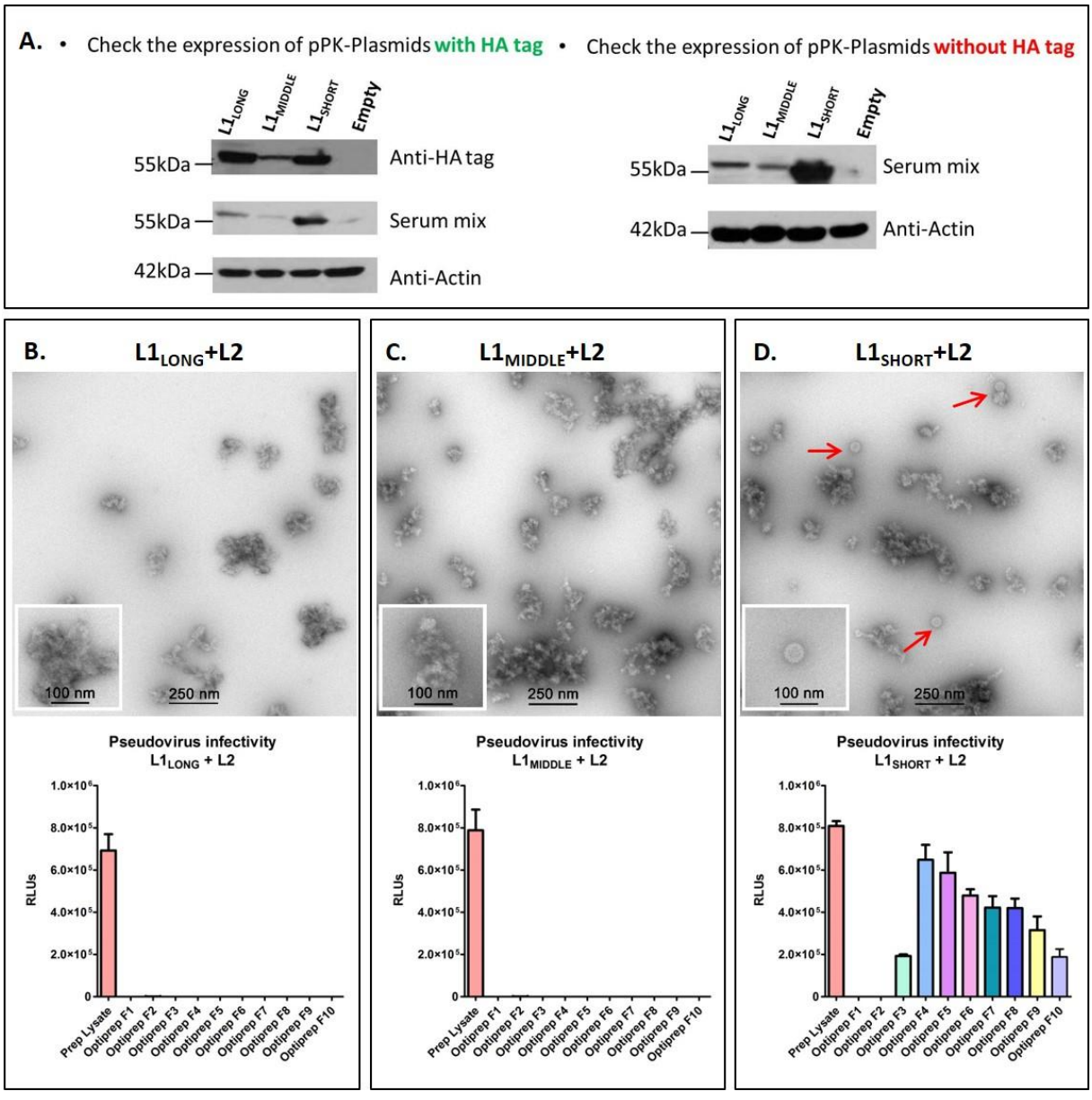

Figure 4.1.7: PsVs production via pPK-expression plasmids. (A). The expression of pPK-L1 expression plasmids in HeLa cells was checked by Western blot. The serum mix was a pool of sera from five MnPV infected tumor-bearing animals. Capsid formation and pseudovirus infectivity of $L1_{LONG}$ **(B)**, $L1_{MIDDLE}$ **(C)** and $L1_{SHORT}$ **(D)** was checked by the EM and measurement of Gaussia signals as described before. The red arrow refers to PsVs.

To observe particles formation capacity of L1 isoforms in HeLa cells, cells were transfected with pPK-L1 expression plasmids without HA-tag and fixed for EM analysis. No particle formation was observed in $L1_{LONG}$ and $L1_{MIDDLE}$ expressing cells (data not shown). However, plenty of particles were found in the nucleus of $L1_{SHORT}$ transfected cells and a few particles were discovered in the cytoplasm as well (**Fig. 4.1.8 A**). The darker particles might contain DNA inside and the lighter one might be empty (**Fig. 4.1.8 D**). One intriguing finding is that cells containing particles exhibited components of distinct structures. For example, apart from the spherically shaped particles, arrays of tubes (T) with similar diameter were exclusive in $L1_{SHORT}$-transfected cells (**Fig. 4.1.8 A and B**). Fiber-arrays (F) and crystalline arrangements (C) were less frequently but regularly found in particles-containing cells (**Fig. 4.1.8 C and D**). In the meantime, cells which harbored particles also showed chromatin condensed (Ch) and their nuclei were in pyknotic disintegration. Besides, mitochondria were inconspicuous and degraded severely to form potential mitophagy (A), which might indicate cells were under stress when producing PsVs (**Fig. 4.1.8 A**).

Altogether, capsid formation of different L1 isoforms was further confirmed by using both pGEM-IRES and pPK expression plasmids during the PsVs production. In line with the previous results, only $L1_{SHORT}$ possessed the ability to form infectious viral capsids. The $L1_{SHORT}$ expressing cells displayed not only PsVs but also tubes, fiber-arrays and crystalline structures, which were absent in non-particles-containing cells.

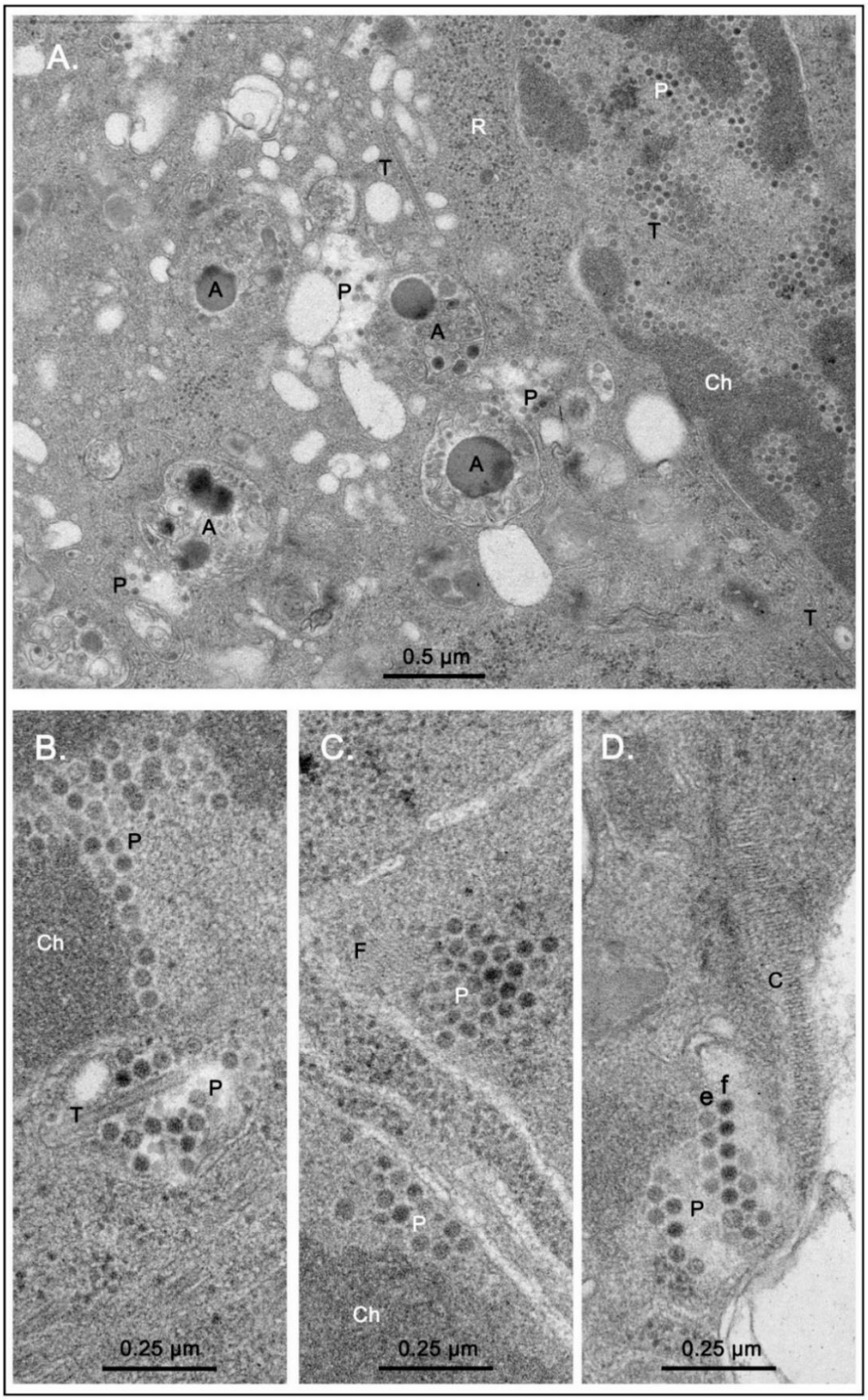

Figure 4.1.8: EM analysis of capsid formation of L1SHORT in transfected HeLa cells. (A). Overall view of L1SHORT transfected cells under EM. **(B)**. Particles and arrays of tubes with similar diameter were frequently found in L1SHORT-transfected cells. Fiber-arrays **(C)** and crystalline arrangements **(D)** were less frequent but regularly found in particles-containing HeLa cells. P: Particles; T: Tubes; Ch: Compact chromatin; R: Ribosomes; A: Potential mitophagy; F: Fiber-array; C: Crystalline arrangements; e: Empty particles; f: Full particles

4.2 Characterization of anti-L1 antibodies in the naturally infected animals

4.2.1 Time course of seroreactivity against early and late viral proteins

To investigate the humoral response to cutaneous *Mastomys* papillomavirus infections, especially for the L1 isoforms, a case study was performed by following 60 naturally infected animals for the duration of their life. Antibody reactions against capsid proteins L1 (long, middle, short, N-terminal peptides) and E2 were examined by glutathione S-transferase (GST)-capture ELISA and VLP-ELISA. Sera were collected from animals at different ages (682 sera in total). Previously, E2 was identified as an early marker for virus infection, as the responses can already be seen at an age of four weeks [86, 122]. The first analysis at 8 weeks after birth revealed E2 reactivity against virus (mean OD_{450} = 0.257) and the antibodies responses increased from 36 weeks (mean OD_{450} = 0.347) to 76 weeks (mean OD_{450} = 0.462) in the late infection stage (**Fig. 4.2.1**).

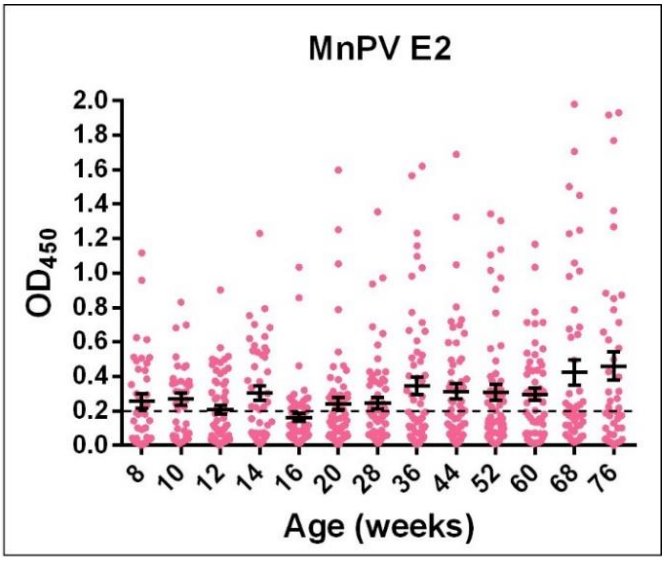

Figure 4.2.1: Seroreactivity against early viral protein E2. Antibody responses against E2 were measured by GST-ELISA and illustrated as scatter diagram using a cut-off of OD_{450} = 0.2. The OD_{450} represents the optical density at a wavelength of 450 nm. In total 682 sera were analyzed and for each time point the mean ± SEM is shown.

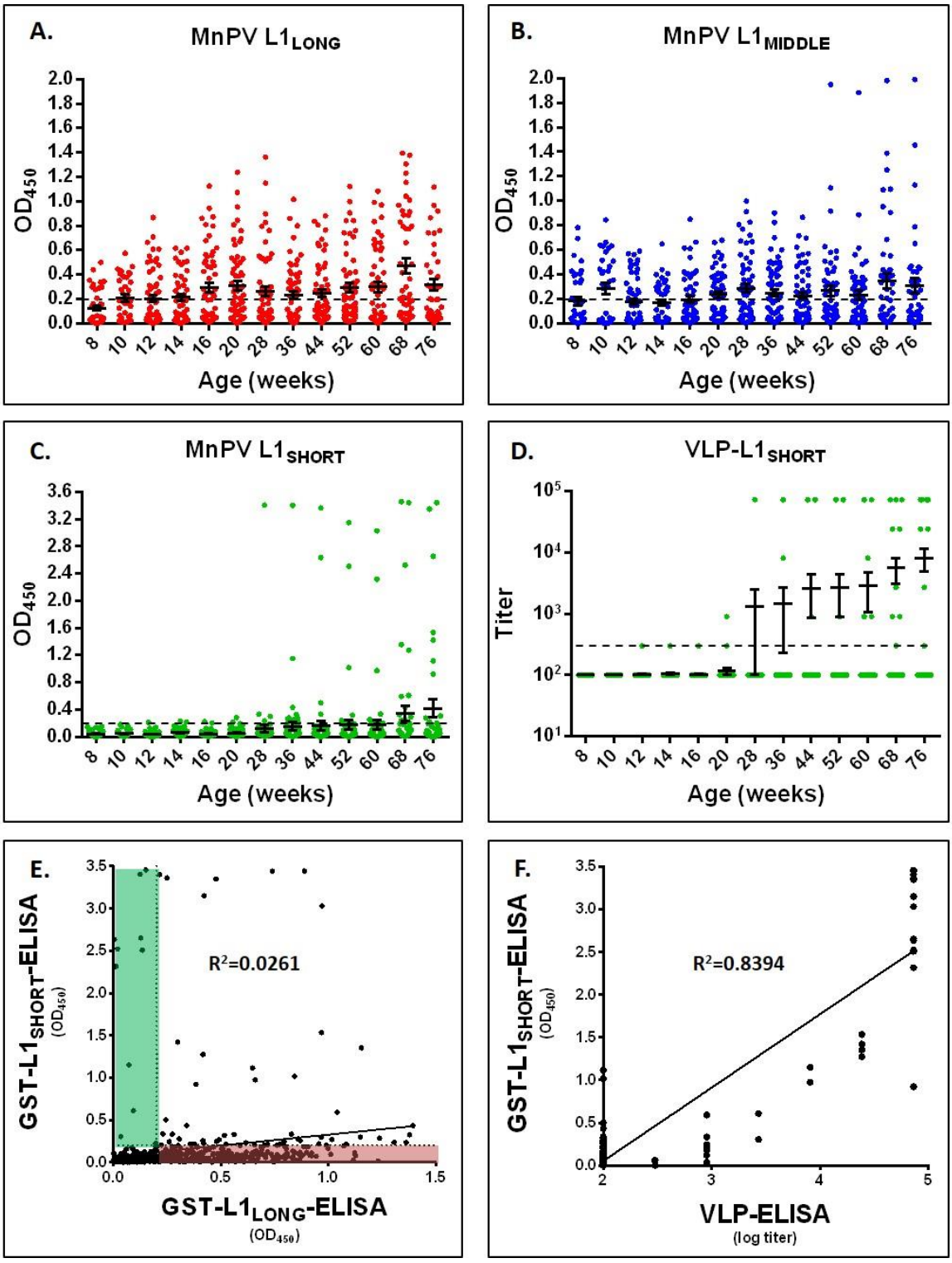

Figure 4.2.2: Seroreactivity against late viral protein L1 isoforms. Antibody responses against GST-L1LONG **(A)**, L1MIDDLE **(B)** and L1SHORT **(C)** fusion proteins were measured by GST-ELISA and illustrated as scatter diagram using a cut-off of OD_{450} = 0.2. The OD_{450} represents the optical density at a wavelength of 450 nm. **(D)**. The immune responses against VLPs were measured by VLP-ELISA and illustrated as scatter diagram using a cut-off of titer = 300. In total 682 sera were analyzed and for each time point the mean ± SEM is shown. **(E)**. Correlation of GST-L1LONG ELISA with GST-L1SHORT ELISA (n= 682 sera). Each point indicates a serum measured by both methods **(F)**. Correlation of GST-L1SHORT ELISA with VLP-ELISA (n= 682 sera). The regression line represents a linear regression fit.

The MnPV L1LONG seroreactivity of naturally infected *Mastomys* was detectable at 8 weeks (mean OD_{450} = 0.126) and increased in the late infection stage (mean OD_{450} = 0.474 at 68 weeks). The mean value of the animals at 76 weeks was lower than those at 68 weeks, which was mainly caused by the death of some infected animals. The number of animals which showed L1LONG responses was 8 of 60 at 8 weeks and increased to 39 of 60 by the end of the study, which indicates a propagation of virus infection within the colony (**Fig. 4.2.2 A**). Moreover, it is noteworthy that GST-L1MIDDLE antigen reacted with both positive sera for L1LONG and L1SHORT (**Fig. 4.2.2 B**). Furthermore, serological responses against GST-L1SHORT antigen as well as VLPs derived from L1SHORT were detectable after 28 weeks and remained high until 76 weeks. This result indicates that anti-L1LONG antibodies in the early infection (from 8 to 20 weeks) did not recognize the epitopes on the surface of both GST-L1SHORT antigen and intact VLPs (**Fig. 4.2.2 C and D**). Therefore, there was a complete lack of correlation to the GST-L1SHORT ELISA when the induction of the antibodies was detected by the established GST-L1LONG ELISA (**Fig. 4.2.2 E**). However, since only L1SHORT was able to form VLPs, there was a significant correlation between the GST-L1SHORT ELISA and VLP-ELISA ($P < 0.0001$, **Fig. 4.2.2 F**). This result confirms that the lack of reproducibility between GST-L1LONG and GST-L1SHORT ELISA was due to the different properties of L1 isoforms.

In summary, analysis of MnPV-infected animals during early infection revealed strong serological responses against the MnPV L1LONG protein. The majority of these animals did not develop anti-L1SHORT antibodies in their whole life, whereas only few animals (8 of 60) elicited L1SHORT responses during the late phase of infection.

4.2.2 Time course of individual seroreactivity against L1LONG and L1SHORT proteins

To better understand L1LONG and L1SHORT seroconversion, the time course of individual seroreactivity among 8 animals showing L1SHORT responses was analyzed. Two major immune responses patterns were found among these animals. **Pattern 1:** Antibody responses against L1LONG and/or E2 occurred in the early time and L1SHORT seroreactivity showed during late infection (four animals in total, **Fig. 4.2.3 A**). Anti-E2 antibodies of three animals (220A, 220D and 230C, **see Fig. 4.2.3 A, lower panel**) were slightly positive at the beginning and roughly fluctuated around cut-off line, whereas immune responses against L1LONG appeared before 20 weeks and L1SHORT seroresponses only arose after 44 weeks. Besides, one animal (221C, **see Fig. 4.2.3 A, lower panel**)

harbored very high E2 responses at 20 weeks and was positive for L1SHORT responses after 68 weeks, but it didn't develop anti-L1LONG antibodies in the whole observation period. **Pattern 2:** Anti-L1SHORT antibodies were detectable without any immune responses against E2 and L1LONG at the early time points (four animals in total, **Fig. 4.2.3 B**). Interestingly, E2 responses were negative in three animals (220B, 220C and 221A, **see Fig. 4.2.3 B, lower panel**) in the whole-time frame, which indicates a lack of strong virus replication after virus infection. After the development of L1SHORT responses at 20 weeks, 225A animal was positive both for L1LONG and E2 starting from 44 weeks.

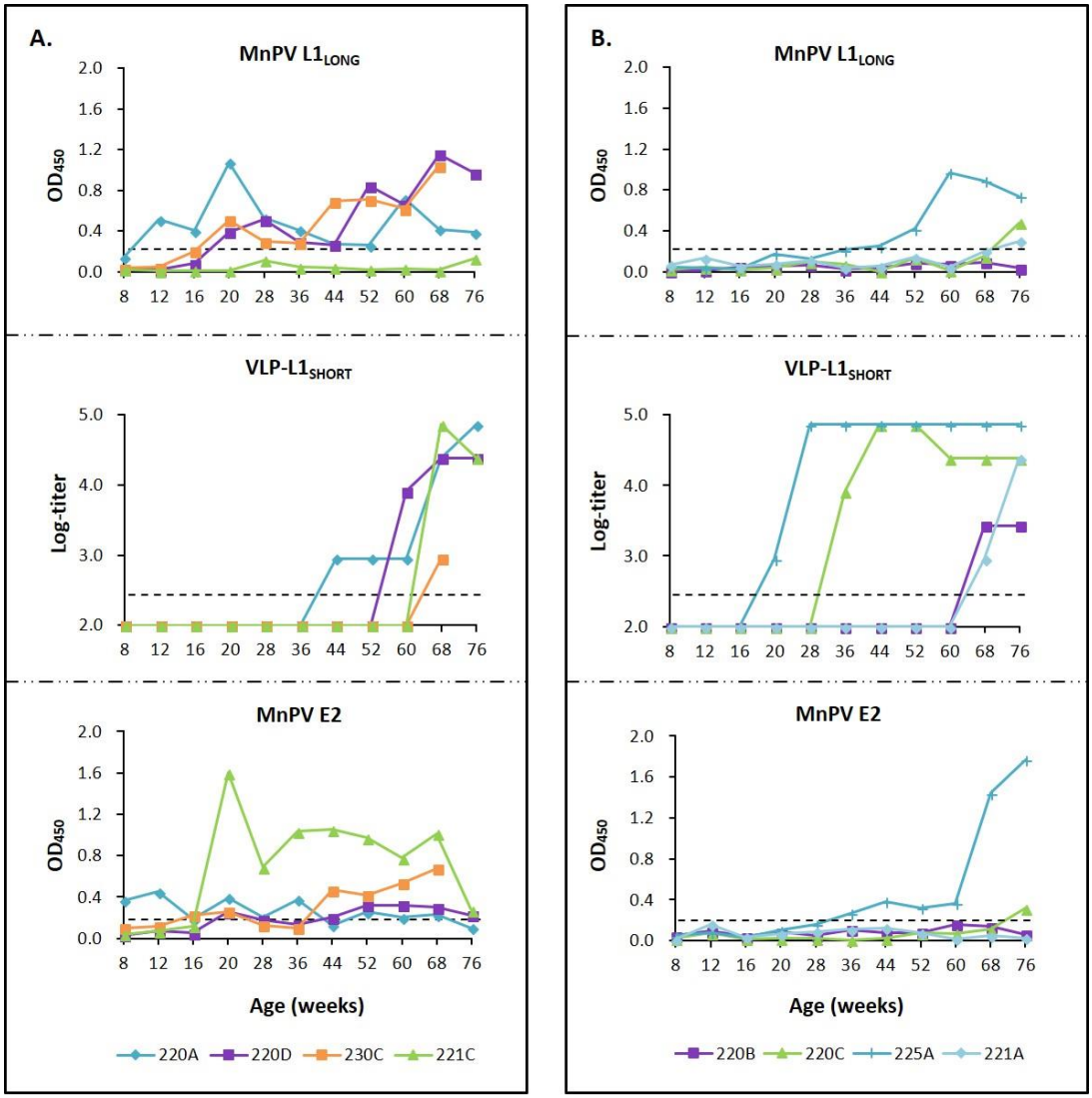

Figure 4.2.3: Time course of the individual seroreactivity against the viral E2, L1LONG and L1SHORT proteins in naturally infected colony. (A). Pattern 1: Seroresponses against L1LONG and/or E2 were firstly developed and then L1SHORT seroreactivity appeared later. **(B).** Pattern 2: L1SHORT seroreactivity was detectable without any immune responses against E2 and L1LONG at the early time points. Antibody responses against L1LONG and E2 were measured by GST-ELISA. The immune responses against L1SHORT were measured by VLP-ELISA. 8 developed anti-L1SHORT antibodies animals in the whole infection stage were shown (n=88 sera).

In order to study the influence of ultraviolet (UV)/immunosuppression on the L1 seroconversion, individual seroreactivity of four cohorts with different treatments was investigated (**Table 1**). This experiment was done in collaboration with Dr. Julita Mikulec and Dr. Daniel Hasche. Animals were fed with a normal diet or the immunosuppressant cyclosporine A (CsA) with a concentration (125 mg/kg) starting from the age at 15 weeks. UV irradiation was performed with a dose of 450 mJ/ cm^2 three times per week. Immune responses against the viral proteins E2, $L1_{LONG}$ and $L1_{SHORT}$ were followed up from 8 to 68 weeks. 8 animals from the Group A (CsA + UV) were negative for $L1_{SHORT}$ responses until 20 weeks of age. 6 of 8 animals had E2 and $L1_{LONG}$ responses in the early time, while another two animals (247.4 and 247.5, **see Fig. 4.2.4 A lower panel**) did not show any responses against E2 and $L1_{LONG}$ in their whole life. 6 animals from Group B (CsA) developed anti-E2 and anti-$L1_{LONG}$ antibodies early, but $L1_{SHORT}$ antibodies only showed up after 28 weeks (**Fig. 4.2.4 B**). The appearance of anti-$L1_{SHORT}$ antibodies (36 weeks) in the Group C (UV) was later than Group A and Group B. Similarly, 8 $L1_{SHORT}$ positive animals from Group C exhibited strong E2 and $L1_{LONG}$ responses during the early phase of infection and developed $L1_{SHORT}$ antibodies later (**Fig. 4.2.4 C**). The three naturally infected animals from Group D without any treatment, did not developed $L1_{SHORT}$ responses till 44 weeks (**Fig. 4.2.4 D**).

Table 1. Overview of the CsA and UV study

Group	n	Male	Female	Treatment
Group A	10	5	5	CsA + UV
Group B	10	5	5	CsA without UV
Group C	9	7	2	Normal diet +UV
Group D	8	3	5	Normal diet without UV

n = number of animals; CsA = Cyclosporine A.

In conclusion, in the majority of animals, anti-$L1_{LONG}$ antibodies had arisen early and anti-$L1_{SHORT}$ antibodies appeared only in late stage of infection. Compare to the naturally infected colony without treatment, the groups with CsA diet and/or UV irradiation showed more and earlier $L1_{SHORT}$ responses, which might indicate that the balance of the virus infection and surveillance of immune system had shifted to facilitate the virus propagation due to the suppressed immune system.

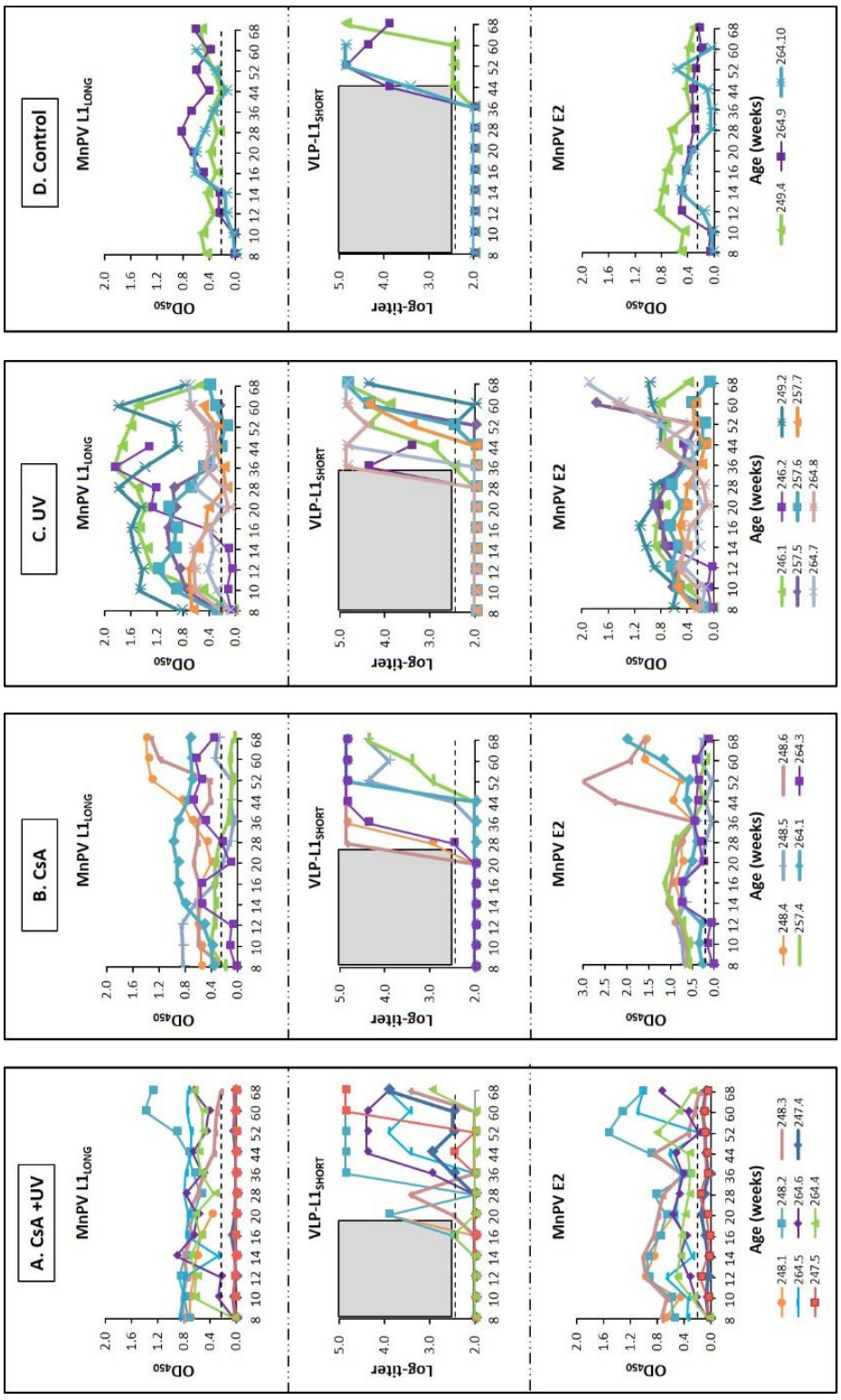

Figure 4.2.4: Time course of the individual seroreactivity against the viral E2, L1LONG and L1SHORT proteins in four naturally infected colonies with different treatments. Antibodies against E2 and L1LONG were measured by GST-ELISA. The immune responses against L1SHORT were detected by VLP-ELISA. **(A).** Animals were fed with cyclosporine A with a concentration (125 mg/kg) and irradiated with UV light with a dose of 450 mJ/ cm^2 three times per week. **(B).** Animals were fed with cyclosporine A without UV irradiation. **(C).** Animals were fed with normal diet and irradiated with UV light. **(D).** Animals were fed with normal diet without UV irradiation. Only the animals which were positive for viral proteins were shown. The boxed area indicates the time frame at which animals were negative for L1SHORT responses but positive for L1LONG responses.

4.2.3 Neutralizing capacity of anti-L1LONG and anti-L1SHORT antibodies

Given to the fact that L1LONG and L1SHORT responses appear at different time points, it is of importance to analyze whether anti-L1LONG and anti-L1SHORT antibodies have different neutralizing capacities. The pseudoviruses used for the neutralization assay were produced by co-expression of L1LONG, L1SHORT and L2 humanized genes in 293TT cells. Neutralization assay for all the positive L1LONG and L1SHORT sera among 60 naturally infected animals revealed that antibodies directed against the MnPV L1LONG protein during early infection were not neutralizing. However, anti-L1SHORT antibodies, which only appeared late, reacted with the surface epitopes of the intact viral capsids and were capable of neutralizing virus (**Fig. 4.2.5 A**). Therefore, a perfect correlation between VLP-ELISA and neutralization assay was revealed (**Fig. 4.2.5 B**). On the other hand, a lack of the correlation between the GST-L1LONG ELISA and neutralizing titer was observed (**Fig. 4.2.5 C**). Based on the above results, epitopes identification of anti-L1LONG and L1SHORT antibodies was tested to further elucidate the properties of L1LONG and L1SHORT proteins.

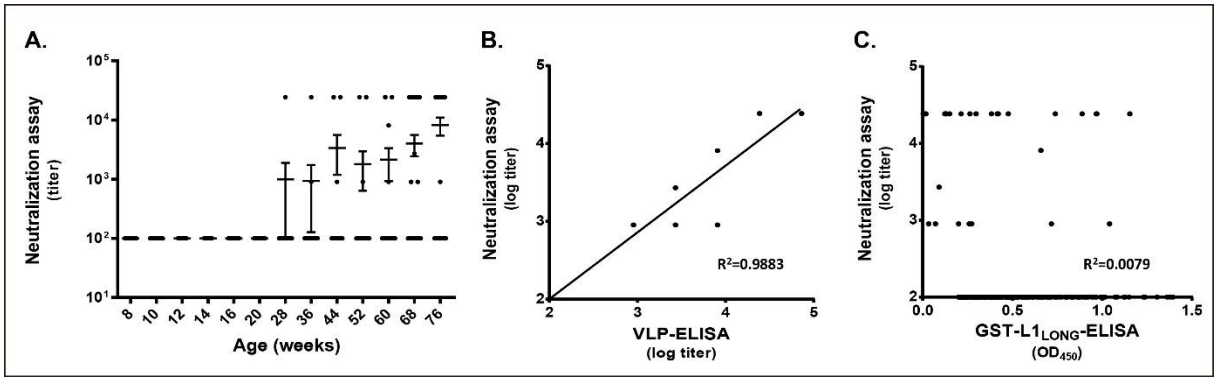

Figure 4.2.5: Neutralizing capacity of anti-L1LONG and anti-L1SHORT antibodies. (A). Neutralization assay for all positive L1LONG and L1SHORT sera among 60 naturally infected animals (n=294 sera). **(B).** Correlation of VLP-ELISA value and neutralizing titer of all positive L1LONG and L1SHORT sera (n=294 sera). **(C).** Correlation between GST-L1LONG ELISA value and neutralizing titer of all positive L1LONG and L1SHORT sera (n=294 sera).

4.2.4 Epitopes characterization of anti-L1LONG and anti-L1SHORT antibodies.

4.2.4.1 Detection of L1LONG N-terminal responses

The difference between L1LONG and L1SHORT ORF consists of 31 amino acids (aa) at the N-terminus. Therefore, to answer the question whether anti-L1LONG antibodies can actually bind to the epitopes at N-terminus (NT), immune responses against 31 aa were detected by GST-L1NT 31aa ELISA among 60 naturally infected animals (n= 682 sera). However, only weak or no detectable reactivity (under cut-off line) was observed (**Fig. 4.2.6 A**). Therefore, seroreactivity against extended peptide including 9 aa after the third methionine of L1LONG ORF was tested by

GST-L1NT 41aa ELISA among all the L1LONG positive animals (39 of 60 animals, n= 297 sera). Compared to the responses against 31 aa, there were significantly increased signals against 41 aa (**Fig. 4.2.6 B**). This result might explain why anti-L1LONG antibodies can react with GST-L1MIDDLE fusion protein (**see Fig. 4.2.2 A and B**), but not with GST- L1SHORT fusion protein and VLPs (**see Fig. 4.2.2 C, D and E**).

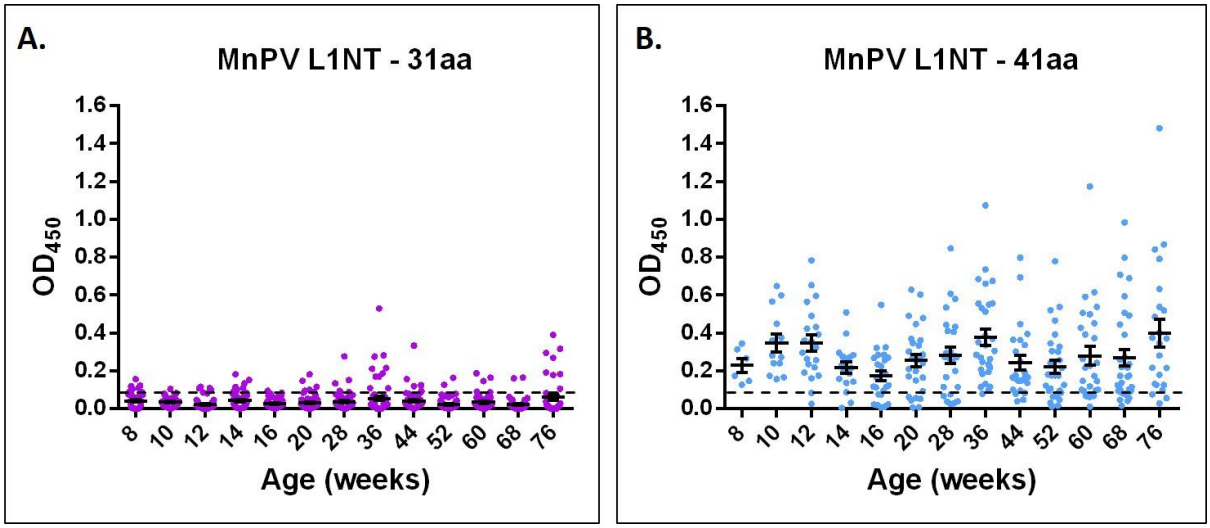

Figure 4.2.6: Seroreactivity against the N-terminal peptides of L1LONG. (A). Immune responses against 31aa at the L1LONG N-terminus were tested by GST-L1NT 31aa ELISA among 60 naturally infected animals (n=682 sera). **(B).** Immune responses against 41aa at the L1LONG N-terminus were measured by GST-L1NT 41aa ELISA among 39 L1LONG positive animals (n=297 sera). Cut off was determined as 0.08 by detection among the virus-free animals.

4.2.4.2 Denaturation assay

To determine the properties of epitopes (linear or conformational) recognized by anti-L1LONG and anti-L1SHORT antibodies, denaturation assays including VLP-ELISA and GST-L1 ELISA were performed. To optimize the VLPs denaturation condition, five monoclonal antibodies (mAb 2E2, mAb 2D11, mAb 3H8, mAb 2D6 and mAb 5E5) against the MnPV VLPs derived from L1SHORT were used as controls. Since mAb 2E2, mAb 2D11 and mAb 3H8 were known to recognize conformational epitopes [123], a very high signal against intact VLPs was shown in PBS. However, reactivities exhibited by mAb 2D6 and mAb 5E5 which were against linear epitopes were generally low under non-denatured condition **(in PBS, Table 2)**. Therefore, a successful denaturation would anticipate a completely reversed pattern, where mAb 2D6 and mAb 5E5 would have increased signals with a lack of reactivity of mAb 2E2, mAb 2D11 and mAb 3H8. Different reducing agents including increased pH and addition of SDS and urea were used to

disassemble VLPs structure into linear forms, yet all three conformation monoclonal antibodies still remained strongly reactive, indicating an incomplete denaturation. Finally, VLPs were diluted into denaturation buffers with additional heating at 95°C for 10 mins before coating to the immune plates. Here, a successful denaturation of VLPs into linear forms was achieved by heating VLPs which were diluted in 50 mM carbonate buffer, indicated by the respectively anticipated antibodies reactivities (**Red box, Table 2**).

Table 2. Testing condition of VLPs denaturation

	Without Heating						Heating		
Antibody	PBS	50mM Carbonate buffer pH=9.6	PBS-0.3M NaCl + 5% Mer	200mM Carbonate buffer pH=9.6	200mM Carbonate buffer + 2% Mer + 1.6% SDS pH=12	200mM Carbonate buffer + 2% Mer + 1.6% SDS + 8M Urea pH=12	50mM Carbonate buffer pH=9.6	200mM Carbonate buffer + 2% Mer + 1.6% SDS pH=12	200mM Carbonate buffer + 2% Mer + 1.6% SDS + 8M Urea pH=12
mAb 2E2	****	****	****	****	**	**	-	-	-
mAb 2D6	-	-	-	**	-	-	**	-	-
mAb 2D11	****	****	****	****	**	**	-	-	-
mAb 5E5	*	**	*	**	*	-	**	-	-
mAb 3H8	***	***	**	**	*	**	-	-	-

[1] **„****“ :** $OD_{450} > 2$; **„***“ :** $1 < OD_{450} < 2$; **„**“ :** $0.1 < OD_{450} < 1$; **„*“ :** $0.05 < OD_{450} < 0.1$; **„-“ :** OD_{450} = Blank.

[2] **Mer:** 2-Mercaptoethanol.

[3] **Red box:** The optimal condition for VLPs denaturation.

Furthermore, instead of coating the denatured VLPs at 4°C, increased signals of two linear antibodies were achieved after coating at 37°C overnight. Serum mix, which was a pool of sera mixed from five naturally infected tumor-bearing animals, also showed strong reactivity in the denaturation assay (**Fig. 4.2.7 A**). All $L1_{LONG}$ and $L1_{SHORT}$ positive sera from 60 naturally infected animals were tested in denatured-VLP ELISA (n= 306 sera). Interestingly, VLPs denaturation led to the reduction of reactivities of all positive sera, demonstrating that anti-$L1_{LONG}$ and anti-$L1_{SHORT}$ antibodies might be directed against conformational epitopes (**Fig. 4.2.7 B**).

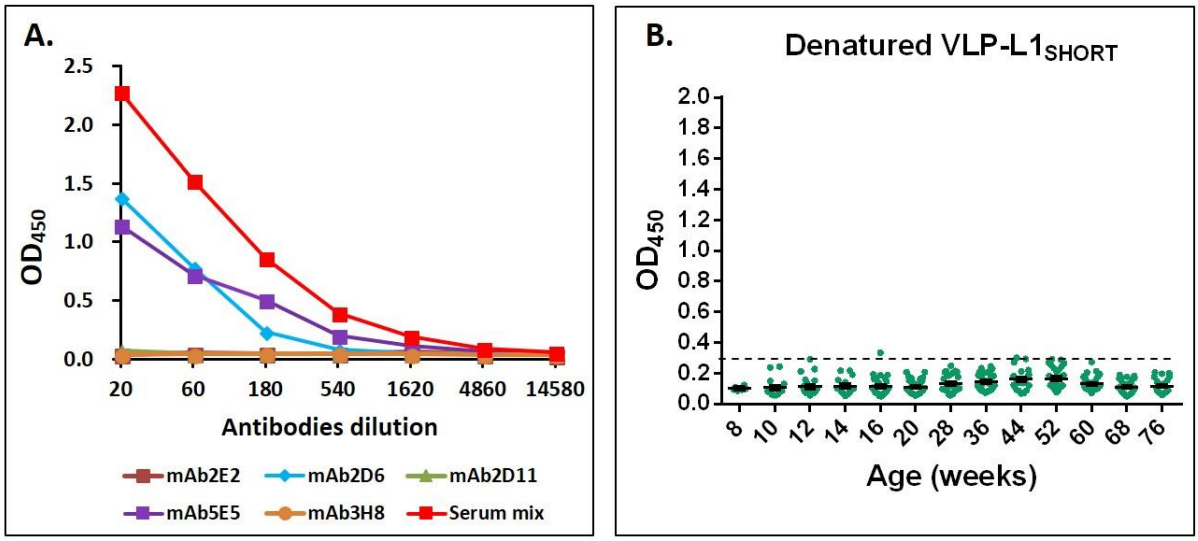

Figure 4.2.7: Denatured-VLP ELISA. (A). Five monoclonal antibodies and serum mix served as controls to evaluate the denaturation condition. VLPs were diluted in 50 mM carbonate buffer and then heated for 10 min at 95°C. Instead of coating at 4°C, the denatured VLPs were coated at 37°C overnight. **(B).** Responses to denatured VLPs are shown in OD_{450} value after the $L1_{LONG}$ and $L1_{SHORT}$ positive sera were diluted 1:20 (n=306 sera). Cut-off (0.3) was determined by the measurement of sera from virus-free animals.

Similar to the denatured-VLP ELISA, denatured-GST ELISA was performed by heating GST-$L1_{LONG}$ and GST-$L1_{SHORT}$ antigens at 95°C for 10 mins and the denaturation efficiency was assessed by the above-mentioned five monoclonal antibodies and serum mix. Under non-denatured condition, three monoclonal antibodies (mAb 2E2, mAb 2D11 and mAb 3H8) against conformation epitopes exhibited weak reactivities with GST-$L1_{LONG}$ fusion protein, but a strong binding with GST-$L1_{SHORT}$ antigen. Two antibodies (mAb 2E6 and mAb 5E5) recognized linear epitopes on both GST $L1_{LONG}$ and $L1_{SHORT}$ fusion proteins. After denaturation, only mAb 2E6 and mAb 5E5 remained positive reactivities with denatured GST-L1 fusion proteins **(Table 3)**. The $L1_{LONG}$ and $L1_{SHORT}$ positive sera from 40 of 60 naturally infected animals during the whole-time frame were tested by this denatured-GST ELISA (n= 142 sera). No seroreactivity of the GST-$L1_{LONG}$ and GST-$L1_{SHORT}$ positive sera was detectable, suggesting that anti-$L1_{LONG}$ and anti-$L1_{SHORT}$ antibodies were indeed directed against the conformational epitopes (**Fig. 4.2.8**).

Table 3. Optimization of the denatured-GST ELISA

	Non-denatured condition		Denatured condition	
Antibody	**GST-L1$_{LONG}$**	**GST-L1$_{SHORT}$**	**GST-L1$_{LONG}$**	**GST-L1$_{SHORT}$**
mAb 2E2	-	****	-	-
mAb 2D6	***	***	***	***
mAb 2D11	*	****	-	-
mAb 5E5	**	**	****	***
mAb 3H8	-	****	-	-
Serum mix	***	****	***	***

[1] **„****“ :** OD_{450} > 2; **„***“:** 1 <OD_{450} < 2; **„**“ :** 0.1 < OD_{450} < 1; **„*“ :** 0.05 < OD_{450} < 0.1; **„-“:** OD_{450} = Blank

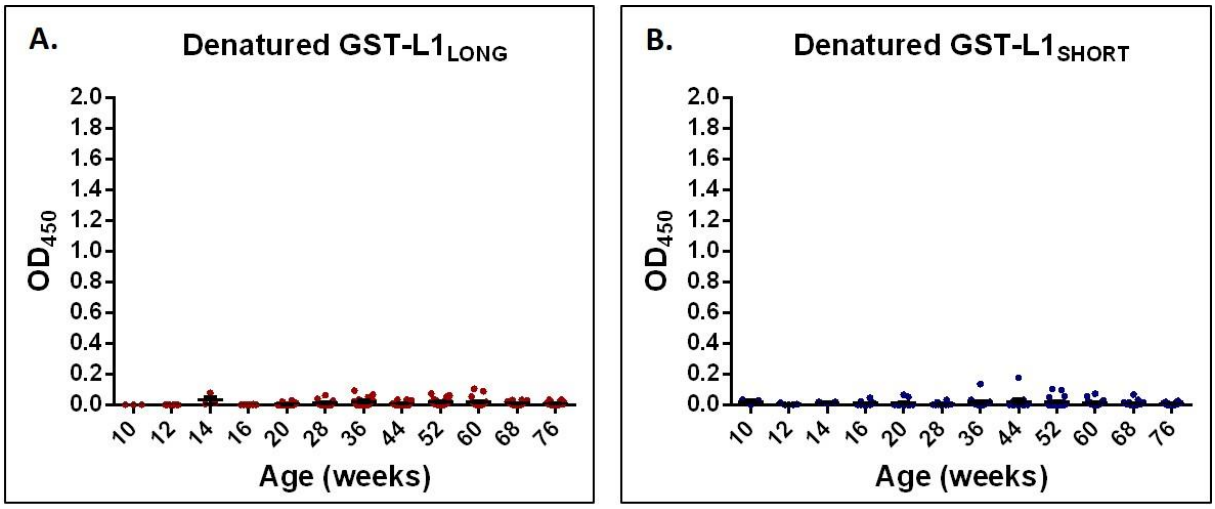

Figure 4.2.8: Denatured-GST ELISA. (A). Denatured GST-L1$_{LONG}$ ELISA **(B).** Denatured GST-L1$_{SHORT}$ ELISA. The structure of the GST- L1 antigens was disrupted by heating at 95°C for 10 minutes in the coating buffer. The heated antigens were directly applied to the immune plates and coated at 37°C overnight. L1$_{LONG}$ and L1$_{SHORT}$ positive sera from 40 of 60 naturally infected animals were measured (n= 142 sera).

In conclusion, by using denatured-VLP ELISA and denatured-GST L1 ELISA, anti-L1$_{LONG}$ and anti-L1$_{SHORT}$ antibodies from naturally infected *Mastomys* colony were proven to be directed against conformation epitopes of viral L1 proteins.

4.2.4.3 Epitope mapping of anti-L1LONG and anti-L1SHORT antibodies

In order to identify the epitopes recognized by anti-L1LONG and anti-L1SHORT antibodies, linear epitopes were mapped by synthetic 15-mer peptides of L1LONG ORF with a 14 aa overlap in microarray. Incubation of the synthetic peptides, microarray with serum samples as well as secondary antibodies gave rise to spot patterns indicating identified epitopes. Here, only three linear epitopes candidates (ITGHPLY, DYLGMSK and KRSLPASRN) were detected from serum mix (positive control), obtained from tumor-bearing animals (**Fig. 4.2.9 A and B**). No epitope was tested from L1LONG and L1SHORT positive sera by this assay (**Fig. 4.2.9 A**). Since anti-L1LONG and anti-L1SHORT antibodies were all thought to be directed against conformational epitopes (**see Chapter 4.2.4.2**), L1LONG ORF was translated into 7 aa, 10 aa and 13 aa cyclic peptides with maximum peptide overlaps of 6 aa, 9 aa and 12 aa. The cyclic peptides with stable thioether bonds were synthesized by thioether formation between a C-terminal cysteine side chain and the bromoacetylated N-terminus to mimic the conformational epitopes. However, again no epitope was successfully mapped (data not shown), which might be due to the limitation of this technique and complex situation of the conformation or discontinuous epitopes of anti-L1LONG and anti-L1SHORT antibodies.

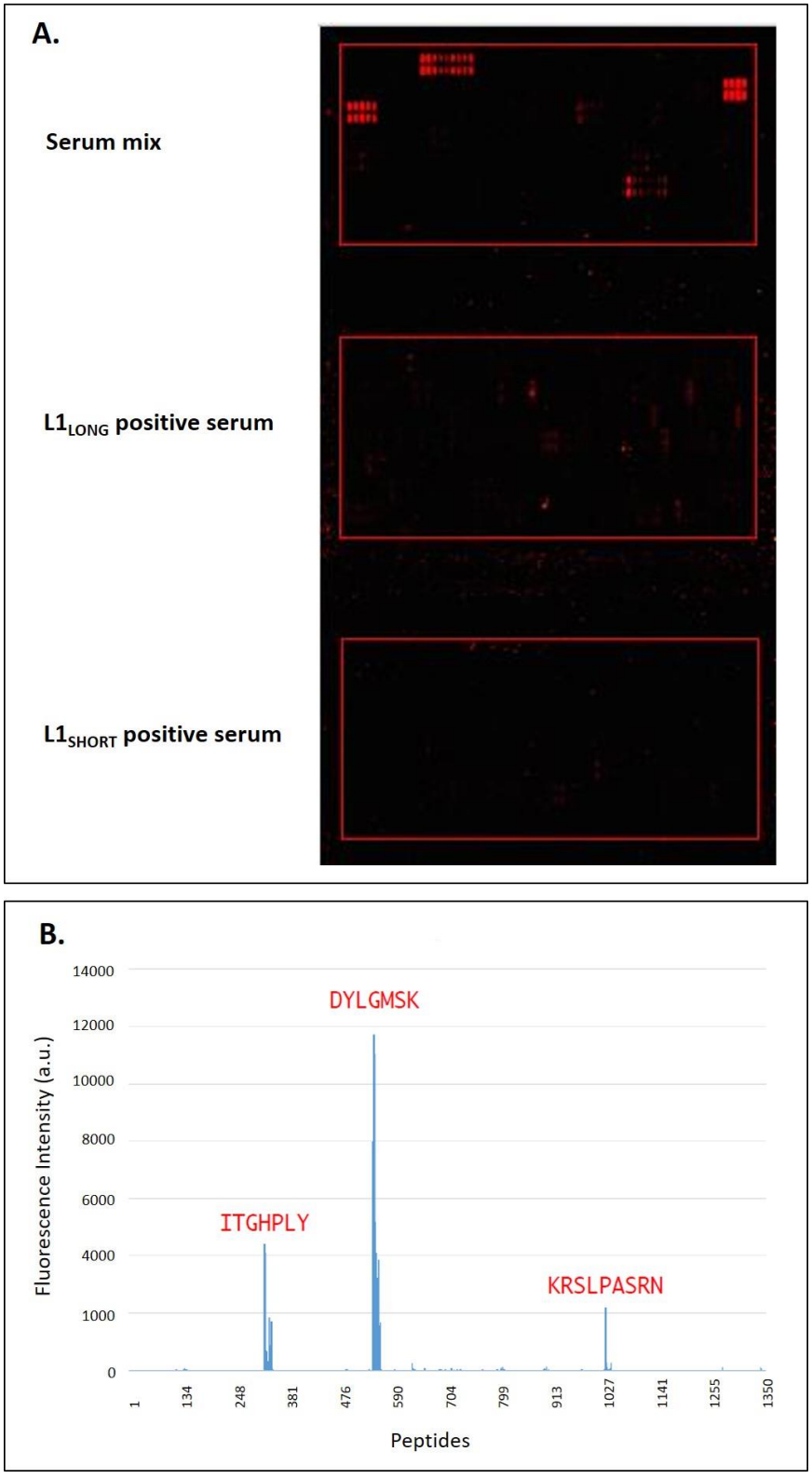

Figure 4.2.9: Epitope mapping of anti-L1 antibodies. (A). Identification of linear epitopes for anti-L1 antibodies. L1LONG ORF was translated into 15 aa peptides with 14 aa peptide overlap. Epitopes were identified by the antigen and antibody reaction after L1LONG and L1SHORT positive sera and serum mix were applied to the microarray. **(B).** The intensity plots with three linear epitopes candidates. The spot intensities of three linear epitopes identified from serum mix were shown.

4.3 The association of L1LONG, L1MIDDLE and L1SHORT proteins

4.3.1 Capsid formation of L1LONG and L1MIDDLE with the help of L1SHORT and L2

In order to investigate whether L1LONG protein is present in capsids of produced PsVs, mass spectrometric analysis was carried out. The quality and quantity of PsVs was examined by electron microscopy and infection assay prior to mass spectrometry (**Fig. 4.3.1 A**). The GST-L1 LONG antigen, which was expressed in the bacteria, was used as a reference to check the N-terminal peptides. The PsVs sample and GST-L1 LONG antigen were stained with Coomassie blue dye in SDS-PAGE gel. The target proteins were excised from the gel, trypsinized, and the peptides were analyzed (**Fig. 4.3.1 B**). Mass spectrometry analysis identified a long N-terminal peptide (HCPDAGVSAGISI FQMAYWLPNNQ) in the GST-L1LONG antigen lysate. Even though many peptides derived from the L1SHORT ORF were detected, no N-terminal peptide was found in PsVs sample by TOP-down proteomics. However, one peptide (TIIYTR) from the L1LONG N-terminus was detected by parallel reaction monitoring (PRM), a method which provides benefits in high resolution and high mass accuracy quantitative proteomics. (**Fig. 4.3.1 C**). This result suggests that L1LONG together with L1SHORT and L2 might be able to form the viral capsids or L1LONG protein might interfere with capsid formation in the presence of L1SHORT.

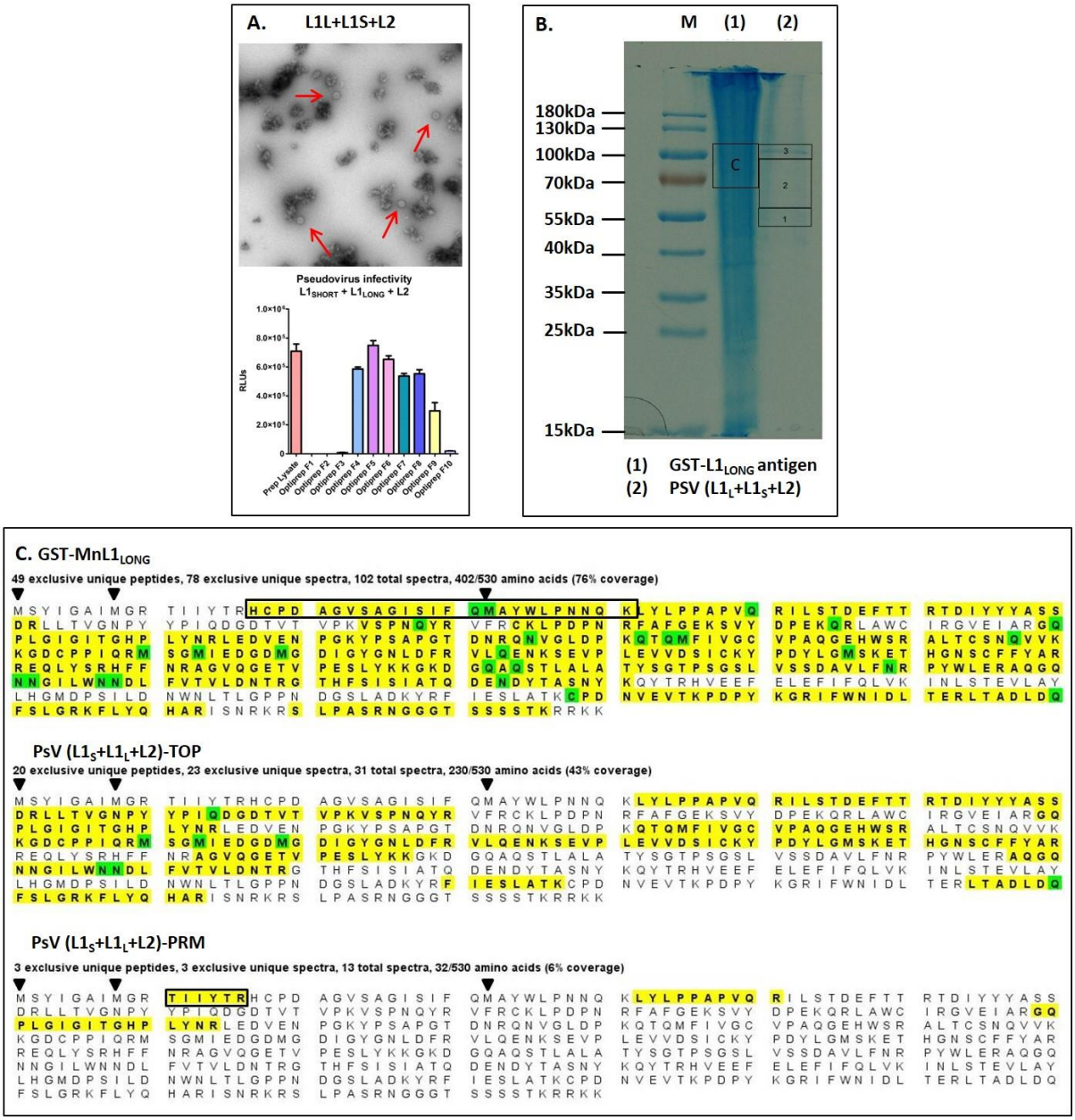

Figure 4.3.1: Mass spectrometry analysis of PsVs production. (A). The quality and quantity of PsVs was evaluated by EM and infection assay. PsVs were produced by co-transfection of L1LONG, L1SHORT and L2 expression plasmids in 293TT cells. The infectivity data were shown in mean ± SEM of one representative experiment, from which infectivity of each PsVs fraction was repeated four times. **(B).** GST-MnPV-L1LONG antigen and fraction 5 from representative PsVs production shown in (A) was stained by Coomassie blue dye. The boxed regions were cut for further trypsin digestion and Mass spectrometry. **(C)**. Peptides analysis of the GST-MnPV-L1LONG antigen and PsVs derived from L1LONG, L1SHORT and L2 combination. The inverted triangles represent methionine. The identified N-terminal peptides were marked in black squares. Identified peptides were marked in yellow. Peptides with residues modification (deamidation, oxidation and carbamidomethyl) were marked in green.

In order to determine whether both long and middle proteins can form capsids with the assistance of L1SHORT, the different proteins were analyzed by immunofluorescence staining of PsVs-infected HeLa cells. Since there was no antibody available to recognize N-terminal peptides of L1LONG, plasmids expressing L1LONG and L1MIDDLE fused to an HA-tag at the C-terminus (pPK-L1LONG-HA and pPK-L1MIDDLE-HA) were used for PsVs production. For the detection of L1SHORT protein (without HA-tag), a mixture of three monoclonal antibodies (mAbs) against conformational epitopes on MnPV VLPs (mAbs 2E2, mAbs 2D11 and mAbs 3H8) were used, according to a colocalization of HA and mAbs signals when L1SHORT-HA fusion protein was checked by immunofluorescence staining (**Fig. 4.3.2 A**). This result indicates that HA-tag at the C-terminus might do not change the capsid formation of L1 protein. Moreover, there was no cross reaction between the anti-HA antibody and mAbs mixture when L1SHORT (without HA-tag) and L1LONG-HA fusion proteins were detected in transfected cells (**Fig. 4.3.2 B and C**).

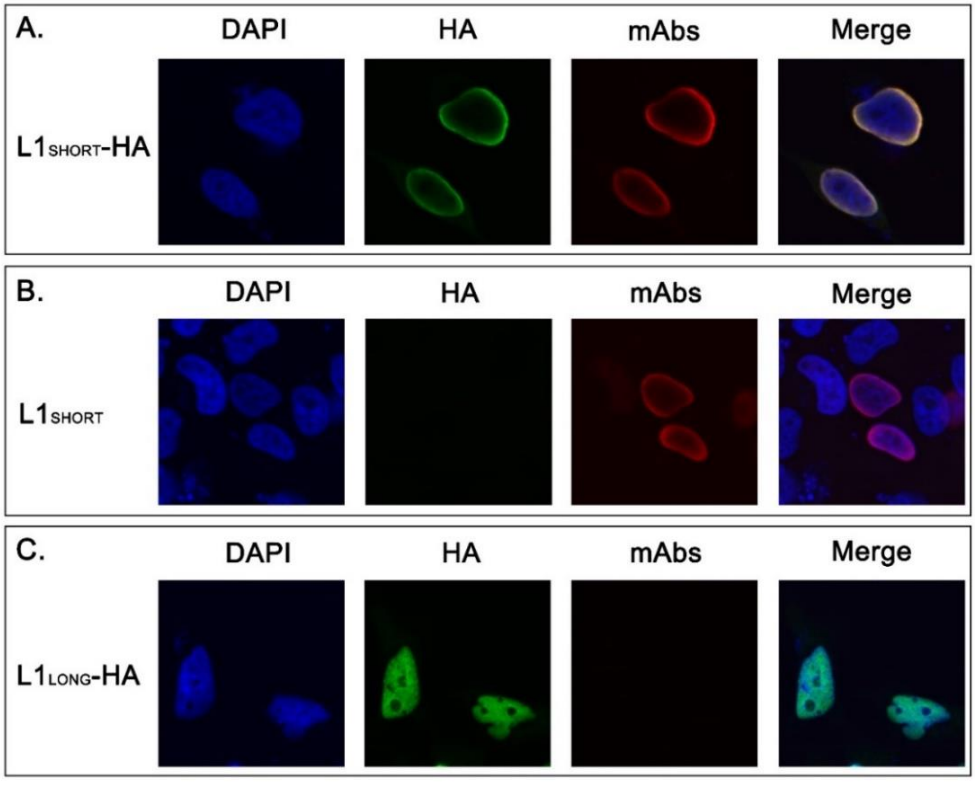

Figure 4.3.2: Detection of L1 proteins by anti-HA antibody and monoclonal antibodies mixture (mAbs 2E2, mAbs 2D11 and mAbs 3H8). HeLa cells were fixed and processed for the detection of DAPI (blue), HA (green) and mAbs (red) 48h after transfection of pPK-L1SHORT-HA plasmid **(A)**, pPK-L1SHORT plasmid **(B)** or pPK-L1LONG-HA plasmid **(C)**. The L1LONG-HA fusion protein was detected by anti-HA antibody and donkey anti-rat Alexa Fluor 488. The L1SHORT protein was detected by mAbs mixture and goat anti-mouse IgG2a (γ2a) Alexa Fluor 594.

HeLa cells were incubated with respective PsVs (L1LONG-HA +L1SHORT +L2, L1MIDDLE-HA +L1SHORT +L2 or L1SHORT +L2) for 30 min and fixed for indirect immunofluorescence staining with anti-HA antibody or mAbs mixture. L1SHORT was shown to be present in the PsVs capsids, indicated by the mAbs mixture staining on the surface of infected cells. However, no HA signal was observed, demonstrating that L1LONG-HA and L1MIDDLE-HA fusion protein did not take part in the capsid formation even with the help of L1SHORT and L2 proteins (**Fig. 4.3.3 A**). Meanwhile, since a reporter plasmid containing Gaussia/GFP was used for DNA encapsidation during the PsVs production, there might be a possibility that GFP is expressed in the cells after PsVs infection. To exclude the endogenous background fluorescence caused by the above reason, PsV-infected HeLa cells were fixed and then directly tested by confocal microscope with the same parameter settings (**Fig. 4.3.3 B**).

Taken together, in spite of adding L1SHORT and L2, L1LONG and L1MIDDLE still lack the ability to form capsids during PsVs production. Therefore, the detection of the N-terminal peptide of L1LONG in PsVs sample (**Fig. 4.3.1**) might suggest that L1LONG interferes with the capsid formation.

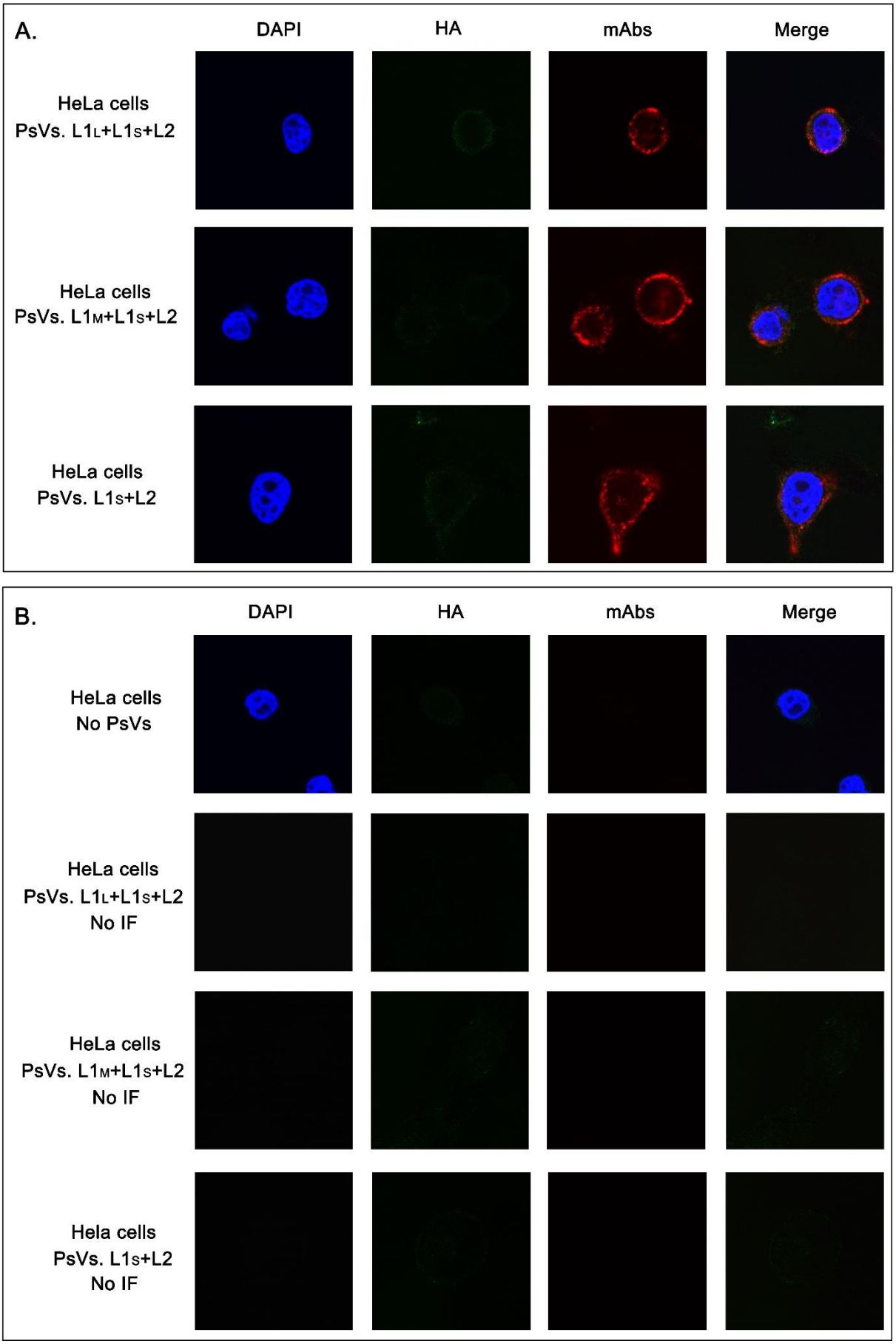
A.
DAPI
HA
mAbs
Merge
HeLa cells
PsVs. L1L+L1S+L2
HeLa cells
PsVs. L1M+L1S+L2
HeLa cells
PsVs. L1S+L2
B.
DAPI
HA
mAbs
Merge
HeLa cells
No PsVs
HeLa cells
PsVs. L1L+L1S+L2
No IF
HeLa cells
PsVs. L1M+L1S+L2
No IF
Hela cells
PsVs. L1S+L2
No IF

Figure 4.3.3: Detection of L1LONG, L1MIDDLE and L1SHORT protein in PsVs-infected HeLa cells. (A). Cells were infected with respective PsVs (L1LONG-HA +L1SHORT +L2, L1MIDDLE-HA +L1SHORT +L2 or L1SHORT +L2) for 30 min and fixed for further DAPI (blue), HA (green) and mAbs (red, mAbs 2E2, mAbs 2D11 and mAbs 3H8) staining. **(B).** Negative controls for the experiment in (A). Uninfected HeLa cells were fixed for immunofluorescence staining and then checked by confocal microscope. Additionally, PsVs-infected cells were fixed and directly examined under microscope to exclude background signals. The L1LONG and L1MIDDLE proteins with HA tag were detected with anti-HA antibody and donkey anti-rat Alexa Fluor 488. L1SHORT was detected with mAbs mixture and goat anti-mouse IgG2a (γ2a) Alexa Fluor 594.

4.3.2 Interference of L1LONG and L1MIDDLE proteins with capsid assembly

To investigate whether L1LONG protein could interfere with the capsid forming process, a competition assay was performed by the co-expression of L1LONG in the normal PsVs production (L1S + L2). PsVs infectivity was compared between these "L1S + L2" and "L1L + L1S + L2" groups. To ensure equal amounts of plasmids used in these two settings, pGEM-IRES vector without insert was co-transfected with expression plasmids in "L1S + L2" group. PsVs from both groups were produced and purified at the same time under the same condition to avoid an experimental bias. In comparison to the average of Gaussia signals of all the collected fractions, the PsVs infectivity of "L1S + L2" group was significantly higher than that of "L1L + L1S + L2" group ($p = 0.0014$), which indicates that less infectious particles were formed when L1LONG protein was expressed in the cells (**Fig. 4.3.4**).

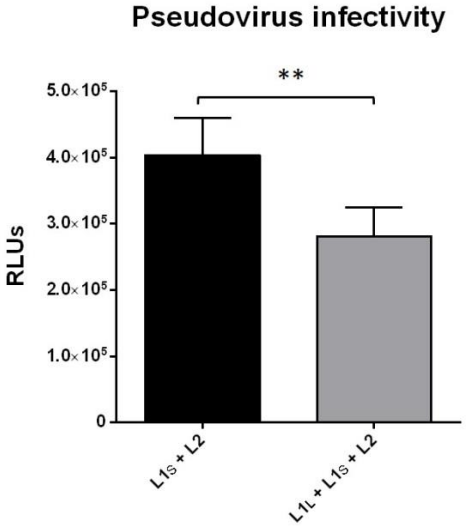

Figure 4.3.4: Comparation of PsVs infectivity between "L1S + L2" and "L1L + L1S + L2" group. 5 μg of each expression plasmid (L1LONG, L1SHORT and L2) was used for the PsVs production in "L1L + L1S + L2" group. 5 μg of pGEM-IRES vector without insert together with 5 μg of each expression plasmid (L1SHORT and L2) were used for PsVs production of "L1S + L2" group. The respective PsVs infectivity was determined by the average of Gaussia signals of all the collected fractions. The experimental data are shown in mean ± SEM from three independent experiments. $^{**}p < 0.01$, $p= 0.0014$.

To analyze the intracellular distributions of the different L1 isoforms, HeLa cells were transfected with different expression plasmids for 48h and processed for indirect immunofluorescence staining. The L1LONG-HA and L1MIDDLE-HA fusion proteins were detected by anti-HA antibody, whereas L1SHORT protein was detected by mAbs mixture as described before (**see Chapter 4.3.1**). The L1LONG-HA and L1MIDDLE-HA fusion proteins were found to be distributed in the nucleus. Due to the high expression levels, some cytoplasmic staining was also found (**Fig. 4.3.5 A and B**). However, the majority of the L1SHORT protein exhibited smooth nuclear rim staining in the cells (**Fig. 4.3.5 C**).

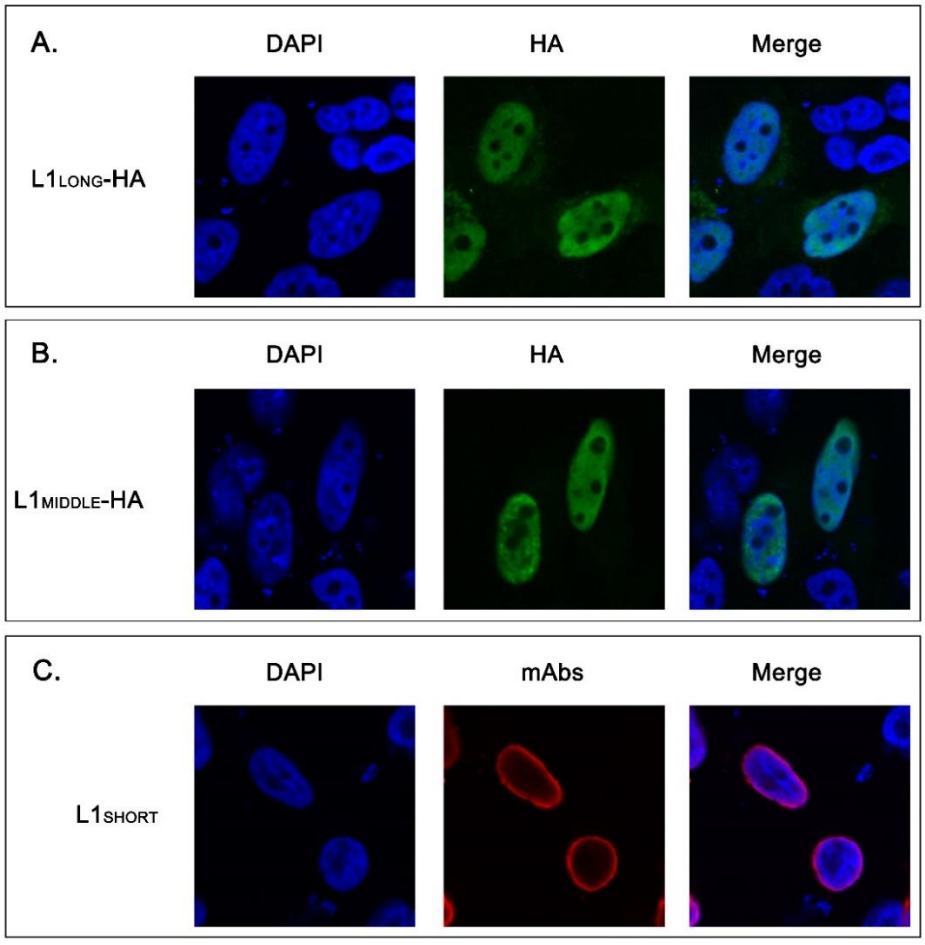

Figure 4.3.5: Localization of L1 proteins. HeLa cells were fixed and processed for the detection of DAPI (blue), HA (green) and mAbs mixture (red, mAbs 2E2, mAbs 2D11 and mAbs 3H8) 48h after transfection of pPK-L1LONG-HA plasmid **(A)**, pPK-L1MIDDLE plasmid **(B)** or pPK-L1SHORT plasmid **(C)**. The L1LONG and L1MIDDLE proteins with HA tag were detected by anti-HA antibody and donkey anti-rat Alexa Fluor 488. The L1SHORT protein was detected by mAbs mixture and goat anti-mouse IgG2a (γ2a) Alexa Fluor 594.

To test a putative interaction with L1SHORT, pPK plasmids expressing L1LONG and L1MIDDLE were co-transfected with pPK-L1SHORT plasmid in HeLa cells. The co-expression with L1SHORT revealed a strong effect on L1LONG and L1MIDDLE localization. As shown in Fig. 4.3.6, a colocalization can be observed, where L1LONG-HA and L1MIDDLE-HA fusion proteins can now be found together with L1SHORT in the cytoplasm or at the nuclear rim.

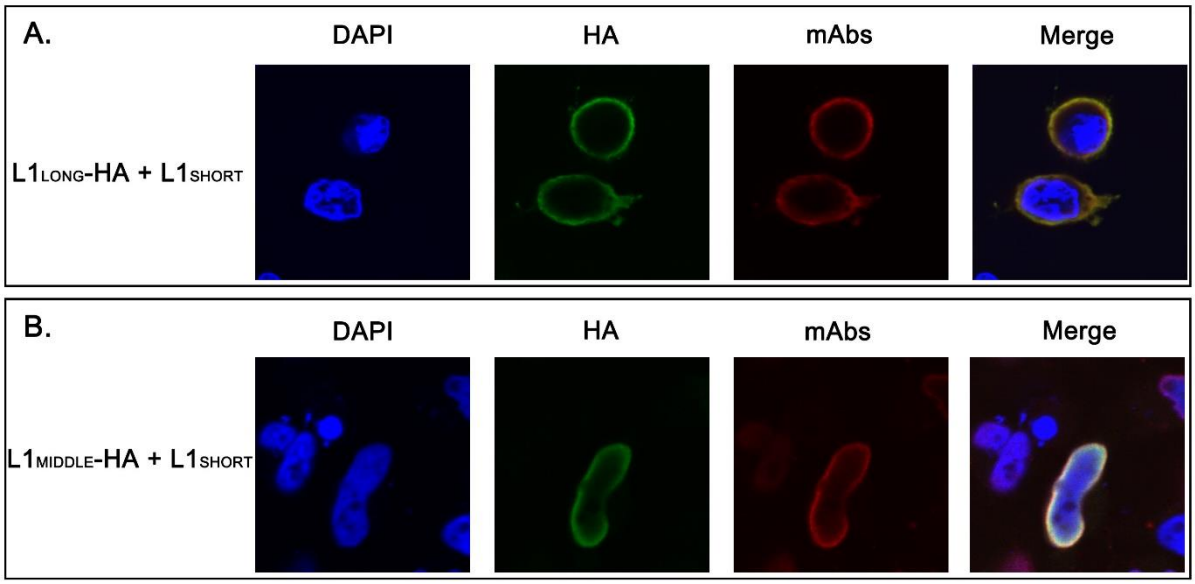

Figure 4.3.6: Colocalization of L1 proteins in the HeLa cells. Cells were fixed and processed for the detection of DAPI (blue), HA (green) and mAbs mixture (red, mAbs 2E2, mAbs 2D11 and mAbs 3H8) 48h after co-transfection of pPK-L1LONG-HA plasmid and pPK-L1SHORT plasmid **(A)**, or pPK-L1MIDDLE plasmid and pPK-L1SHORT plasmid **(B)**. The L1LONG and L1MIDDLE proteins with HA-tag were detected by anti-HA antibody and donkey anti-rat Alexa Fluor 488. The L1SHORT protein was detected by mAbs mixture and goat anti-mouse IgG2a (γ2a) Alexa Fluor 594.

In conclusion, competition assays in PsVs production revealed that the capsid formation process by L1SHORT might be inhibited in the presence of L1LONG protein. A possible direct interaction with L1SHORT is further inferred by changes in the intracellular localization when L1LONG or L1MIDDLE is co-expressed together with L1SHORT.

5. Discussion

5.1 Alternative initiation translation codons of MnPV L1 protein

Alignment of translation initiation codons for PVs major capsid protein L1 revealed that cervical carcinoma-associated types (HPV 16, 18, 45, 52, 54, 58) possess additional ATGs, while non-cancer-causing types do not (HPV 3, 7, 6b, 11, 13, 42) [32]. Notably, similar to high-risk HPV types, MnPV L1 ORF also contains three ATG codons at its N-terminus (**Fig. 4.1.1**). According to several following ribosome scanning mechanisms, these different L1 isoforms might be formed. **(1).** 40S ribosomal subunits are recruited to the capped 5'-end of mRNA and move linearly until the first AUG is found, whereupon translation initiation can start [124]. It is believed that the initiation/scan-through ratio depends on the nucleotide context in the vicinity of the AUG. Once the context does not match with the Kozak sequence, a proportion of scanning complexes may be inclined to skip this AUG and initiate translation at the next AUG (so-called leaky scanning mechanism) [125, 126]. **(2).** Alternatively, after termination of a small reading frame, some ribosomes remain attached to the mRNA and resume scanning in 3' direction, regaining competence to reinitiate translation at a downstream AUG codon (so-called "termination-reinitiation mechanism") [127, 128]. **(3).** A third mechanism exists that enables a cap-independent initiation through the internal ribosome entry sites (IRES), which has been proven in several cellular genes, hepatitis C virus and picornaviruses [129]. **(4).** Another translation initiation mechanism (so-called "ribosomal shunting") relies on cap-dependent discontinuous scanning. Here, ribosomes first bind to the 5' end of mRNA and start scanning for a short distance, then bypass the intervening sequences and initiate translation at a downstream site. This has been observed in adenovirus, Sendai virus, HPVs, cauliflower mosaic virus and others [130-133]. Based on these different possible mechanisms, there is a high likelihood that several different MnPV L1 isoforms can be translated from a transcript containing multiple in-frame AUGs.

Using *in vitro* expression systems, the expression of $L1_{LONG}$, $L1_{MIDDLE}$ and $L1_{SHORT}$ in insect cells as well as in mammalian cells was confirmed in SDS-PAGE gels with their corresponding sizes (**Fig. 4.1.2, Fig. 4.1.6 and Fig. 4.1.7**). However, the short L1 mRNA had significantly higher translation efficiency than $L1_{LONG}$ and $L1_{MIDDLE}$ starting from the first and second ATG, respectively. Similarly, it is also reported that HPV58 $L1_{SHORT}$ proteins were more abundant than $L1_{LONG}$ in keratinocytes after transient transfection with L1 expression constructs. This might be due to a

stem-loop structure with high ΔG value downstream of the first AUG codon in its mRNA secondary structure, which might prevent efficient binding of ribosomes to the mRNA thus blocking the long L1 translation [134]. Therefore, this might also be the case for MnPV L1 expression.

Analysis of the assembled MnPV transcriptome showed that there is a major monocistronic transcript which codes for L1SHORT, driven by the late promoter. However, L1LONG and L1MIDDLE are potentially encoded by other polycistronic mRNA isoforms along with the early and late genes which are controlled by the early promoter [135]. The Kozak consensus sequence for L1LONG and L1MIDDLE ORF is equivalent or superior to the short L1 isoform in the polycistronic transcripts, as has been previously described for HPV 16, 18, 45, 52, 54, 58 [32]. There might be an expression preference for L1LONG and L1MIDDLE compared to the short version from such transcripts. The late gene expression of mucosal high-risk HPV such as HPV16 and 31 only occurs in the differentiated uppermost granular layer, but cutaneous HPVs such as HPV1 and 63 start capsid proteins synthesis much closer to the basal layer [136, 137]. Therefore, it is likely that L1LONG is translated from a polycistronic mRNA which carries several ORFs of viral proteins driven by an early promoter during the early infection. It is therefore tempting to speculate that there might be a switch from long to short L1 expression during the viral infection stage, which could be caused by the early and late viral promoter switch during different infection phases or a change in the ratios of respective transcripts. Seroreactivity of MnPV-infected animals showed that strong MnPV L1LONG immune responses, which had no reactivity with the intact capsids, occurred during the early infection period (**Fig. 4.2.2**). This indicates that the expression of L1LONG might be achieved in the early infection stage *in vivo*. The expression of L1LONG in the early infection phase elicits a production of antibodies that are not neutralizing, which might be due to the fact that L1LONG hardly induces capsid formation (**Chapter 4.1**). The functional antibodies that are capable of neutralizing virus might appear after a switch to massive transcript expression towards L1SHORT at the late infection stage, when virus capsids are efficiently assembled. With this strategy, virus might escape the host defense systems by avoiding the neutralizing antibodies at the beginning of viral infection, thus facilitating a productive infection. This immune evasion mechanism will be discussed in detail in Chapter 5.3.

5.2 Different capsid formation ability of L1LONG, L1MIDDLE and L1SHORT

The different capsid formation ability of MnPV L1 isoforms was verified by various cell systems including VLPs production in insect cells and PsVs production in 293TT cells (**Chapter 4.1**). One difference between these two systems is that minor capsid protein L2 is incorporated into PsVs to mimic the native viral capsids, which might facilitate capsid formation [119, 138]. An indispensable L1 intercapsomeric disulfide bond for virion stability is formed between cysteines 426 in the C-terminal arm and cysteines 171 on a subunit of neighboring capsomere. This bond is only formed in cell lysis in an oxidizing environment during intracellular assembly [47]. Therefore, an extra PsVs maturation step is performed by incubation of the cell lysate at 37°C overnight for the strengthening of such disulfide bonds between the neighboring L1 molecules, thus supporting the capsid stability and solubility [139]. However, even with these advanced procedures, the capsid assembly of different L1 isoforms still remained the same in both systems:

No particles with classic capsomeres subunits were identified from L1LONG and L1MIDDLE indicating that both proteins hardly self-assemble into correct VLPs. Moreover, even with the help of L2, these proteins still lack the ability to accurately assemble viral particles. In contrast, L1SHORT strongly induced uniformly shaped VLPs with typical capsomeres as well as infectious particles during PsVs production (**Fig. 4.1.4 - Fig. 4.1.7**). A similar situation was reported in several studies. Only the recombinant HPV16 L1 protein derived from the second initiation codon (5637 nt) was able to produce high quantities of VLPs [41, 140] [141]. However, VLPs production was unsuccessful when the first initiation codon (5559 nt) was used [142, 143]. The self-assembly ability of VLPs derived from different MusPV L1 ORFs was previously investigated in the baculovirus expression system. MusPV L1 protein starting from the second ATG hardly folded into VLPs, whereas the L1 proteins derived from the 3rd and 4th translation initiation codon successfully generated correct VLPs that were able to elicit neutralizing antibodies [33]. These results indicate that capsids efficiently form only when the translation of L1 is started at the correct methionine. It is reported that capsids can only be successfully assembled from L1 protein in which the methionine is located close to a consensus Wx_7YLPP motif [33]. In the MnPV L1 ORF, only the methionine of L1SHORT is close to this motif. Therefore, it is obvious that the N-terminal residues of MnPV L1 play a critical role for the capsid assembly, because the addition of residues leads to insufficient capsid formation.

Chen et al. demonstrated that N-terminally truncated L1 protein favors formation of a small VLP (12-pentameric icosahedral particle, T = 1) instead of a T = 7 icosahedral lattice, indicating an essential role for the N-terminal peptides in the intercapsomeric binding [36]. Furthermore, residues 1 - 20 of the HPV16 L1SHORT N-terminal moiety are thought to form a β-hairpin structure and serve as interpentameric contacts to fill the gap in the virus capsid shell, which is important for maintaining the capsid stability [35]. Therefore, it is reasonable to assume that the different capsid assembly abilities of L1LONG and L1MIDDLE might be due to alterations in protein structure caused by the N-terminal residues. In the naturally infected *M.coucha* colony, anti-L1LONG antibodies were shown to be directed against the conformational epitopes of the 41 amino acids and were unable to recognize the 31 amino acids from the N-terminus (**Fig. 4.2.6**). Presumably, the additional N-terminal arm might form a loop that completely changes the functional structure of L1 protein. Since no capsomeres-like structures were observed following L1LONG and L1MIDDLE VLPs production, this loop might prevent the binding between pentamers or even make it difficult to form capsomeres, thus avoiding complete assembly of the closed icosahedral particles.

To further investigate the capsid assembly capacity of different L1 isoforms, capsid formation was examined in HeLa cells. Viral particles as well as specific structures such as tubes were exclusively observed in L1SHORT expressing cells (**Fig. 4.1.8**), while absent in the L1LONG and L1MIDDLE transfected cells. The tubular structures have been also found in human and rabbit papillomavirus wart extracts [144], HPV 33 VLPs extract [145] as well as in murine polyomavirus (PyV)-infected tissue culture cells [146, 147]. Besides, it is reported that tubular structures were adjacent to clusters of assembled virions in the nucleus of PyV-infected mouse fibroblasts [148]. One hypothesis on the function of these tube structures is that capsomeres firstly polymerize into tubes and the interior of tubular structures is then traversed by the viral chromatin. Finally, the icosahedral particles are shed from the ends of this structure. Consistent with previous studies for human polyomavirus JC [149, 150], tubes in particle-containing cells were dominantly found near the periphery of cellular compact chromatin, indicating that capsid proteins and DNA might interact in a coordinated manner to form viral particles. Therefore, the specific structures in MnPV particle-containing cells suggest that the virion assembly occurs at specific intracellular sites which might function as virus factories [151, 152]. This result might also shed light on the different capsid formation ability of L1 isoforms. The N-terminal residues of L1 protein cause the

inability of capsid formation, indicated by the fact that only L1SHORT-transfected cells harbor this specific virus machinery.

5.3 Immune responses in the naturally infected animals

The most effective strategy to escape from host surveillance is that viruses become invisible to the host immune system, which inhibits the triggering of effective antiviral responses, such as the production of neutralizing antibodies. Raising neutralizing antibodies with high titer against surface epitopes of virions has long been considered the primary mechanism of protection, since these antibodies can inhibit virus infection by the association with viral particles. Many neutralizing antibodies can abrogate viral particles attachment to the cells prior to the entry process. Some antibodies can also interfere with the interplay between virus and cellular endocytic machinery after attachment. Moreover, after viral endocytosis, neutralizing antibodies also have been shown to have negative effects on viral internalization, uncoating, trafficking, nuclear import and virion transcriptase activity [153-161]. In the whole *Mastomys* colony, 44 of 60 naturally infected animals in total developed antibodies against virus proteins including E2, L1LONG and L1SHORT during their life (**Fig. 4.2.1 and 4.2.2**). However, only 8 animals produced conformation-dependent neutralizing anti-L1SHORT antibodies (**Fig. 4.2.3 and 4.2.5**). This might represent an immune escape, since non-neutralizing antibodies (anti-L1LONG antibodies) are dominant in the early infection stage. In other words, once animals become infected with MnPV shown by strong E2 seroresponses, L1LONG seroreactivity is immediately elicited which however lacks the ability to prevent virus infection. The absence of protective antibodies in the early infection phase might facilitate virus replication and virions escape from recognition by the immune system. These results are consistent with the finding that the HPV16 L1 neutralizing antibodies developed late (8 and 9 months after the first HPV positive DNA detection) [77, 162] [163]. Besides, this virus evasion scenario is also in line with past observations in JC polyomavirus where mutations in the surface loops of the major capsid protein VP1 might enable the virus to avoid antibody-mediated neutralization [164].

As shown in Fig. 4.2.3, two major patterns of immune responses can be found among LSHORT seropositive animals. L1LONG and/or E2 seroresponses occurred during the early time and L1SHORT immune responses showed later (**Pattern 1**). This pattern perfectly fits to an immune

evasion mechanism as described before. Conversely, L1SHORT immune responses were detected without L1LONG and E2 seroresponses at the early time points (**Pattern 2**). This pattern can be explained as follows:

No E2 seroresponses in the early time after infection might indicate that the majority of the original virions would be presented to the dendritic cells for stimulation of cell-mediated immunity, which are finally eliminated by the T cells without virus genome replication [165, 166]. L1SHORT seroreactivity might be caused by infection of virions that are not completely cleared by the cellular immunity. After exposure of viral surface epitopes and with the help of T helper cells through CD40, B cells eventually differentiate into plasma cells that generate antibodies against conformational epitopes of L1SHORT [167]. This process is similar to VLPs vaccination against HPV, which results in the production of the antibodies against conformational epitopes on the surface of virial capsids after injection [168]. This pattern also supports the mentioned immune escape hypothesis that once anti-L1SHORT antibodies (against VLPs) are developed without virus replication (no E2 and L1LONG seroresponses) in the early stage, they can efficiently inhibit the propagation of virus infection, indicated by the lack or delay of E2 seroresponses in the whole-time frame. In accordance with findings previously reported, patients with development of antibodies against HPV16 VLPs in the early stage were found to be less likely to develop a recurrence or die of invasive cancer [169].

Humoral immune responses against viral proteins under immunocompetence and systemic immunosuppression (CsA diet, UV irradiation) were additionally measured to investigate the impact of different immune conditions on L1 seroconversion (**Fig. 4.2.4**). Only few animals (3 of 8) developed anti-L1SHORT antibodies in the immunocompetent control group, which is the same situation in the naturally infected colony without any treatment (8 of 60). Compared to the control group, there were more animals exhibited L1SHORT seroresponses in the CsA and UV treatment groups, which can be explained by the following reasons. CsA as an immunosuppressive drug is able to suppress T cells activity [100, 170, 171]. Furthermore, the exposure of skin to UVB with wavelength of 290-320 nm leads to alteration of the local and systemic immune system by changing the epidermal cytokine profile, hereby inhibiting infection clearance by suppressing cellular immunity [172-175]. Since PVs infection can be cleared by T cells, the massive production of anti-L1SHORT antibodies suggest that virions are largely produced in the late infection phase due

to the immunosuppression condition by CsA and UV treatment. The escape from neutralization in the early infection period might increase the efficacy of virus propagation under circumstances where T-cell mediated immunity is impaired. Therefore, the status of immune system is essential for immune recognition and responses.

5.4 Characterization of anti-L1LONG and anti-L1SHORT antibodies

Anti-L1LONG antibodies in the early infection stage did not react with either GST-L1SHORT antigen or VLPs, and anti-L1SHORT antibodies failed to recognize epitopes on GST-L1LONG fusion protein (**Fig. 4.2.2 and Fig. 4.2.3**). As already demonstrated, correct capsid formation can only be induced by L1SHORT rather than L1LONG (**Chapter 4.1**). These results suggest that L1LONG and L1SHORT antibodies recognize different epitopes on their corresponding antigens, which might be caused by the different proteins structures presented to immune system. Anti-L1LONG antibodies might bind to specific epitopes at the N-terminus (**Fig. 4.2.6**). Probably, a loop formed by 41 amino acids from the N-terminal peptide is the dominant region that is exposed on the exterior surface of protein that fails to form correct capsid but easily identified by the immune system. Especially, 9 amino acids after the third methionine of L1LONG N-terminus would contribute to epitope recognition of anti-L1LONG antibodies. Moreover, since serum contained a mixture of polyclonal antibodies and some positive L1LONG sera did not react with 41 amino acids, anti-L1LONG antibodies might be also directed against epitopes completely within the short ORF, which are not exposed on the surface of the normal capsids. Overall, all the above reasons can explain why anti-L1LONG antibodies cannot neutralize virus due to the fact that neutralizing antibodies only recognize epitopes on the intact viral capsids. This is also a crucial aspect to explain how viruses evade the host defense system by producing non-neutralizing antibodies in the early infection phase.

Since anti-L1SHORT antibodies are conformation-dependent neutralizing antibodies (**Chapter 4.2.3 and 4.2.4**), they might be directed against epitopes on the loops extending toward the outer surface of capsomeres as well as C-terminal arm. It has been reported that passive immunization of sera from MnPV VLPs-vaccinated to naturally infected animals prevents viral infection, indicating that neutralizing anti-L1SHORT antibodies are sufficient for protection [100]. There are several neutralizing antibodies types to elucidate the different mechanisms for neutralization. For example, BPV mAb#9 can bind to the pentavalent and hexavalent capsomeres, thus blocking the

virus binding to the host cells. The main neutralizing function of BPV mAb#5B6 might be the prevention of virus capsid internalization rather than the significant inhibition of the viral binding to the cells surface. This might be due to the fact that mAb#5B6 can only bind monovalently and bivalently to the hexavalent capsomeres sides [176]. The HPV11 H11.B2 mAb is directed against epitopes within the center of capsomere, which coincides with L2 location on the capsid [177]. The HPV16 H16.V5 has a higher affinity to the hexavalent capsomeres than the pentavalent capsomeres and is able to recognize epitopes (17 residues) located on the five exterior flexible loops (BC, DE, FG, EF, and HI loop) from two neighboring L1 molecules [178]. HPV16.U4 is mapped to the intercapsomeric C-terminal region of L1 and blocks the binding to the cell surface rather than the extracellular matrix (ECM) [156] [179]. Therefore, the elicited anti-L1$_{SHORT}$ antibodies in the naturally infected colony might also recognize either of the mentioned conformational epitopes, thus exhibiting neutralization. Even though there are several mechanisms for neutralizing antibodies to prevent virus infection, it is still unknown how they reach the basal epidermal layers to intervene in infection. There are two major transport mechanisms for IgG antibodies to reach the genital mucosa: the neonatal Fc receptor-mediated bidirectionally transcytoses of IgG and exudation of antibodies at the site of pathogen entry [180, 181]. In the context of the skin, the exudation mechanism seems the most likely way, because B cells and IgG can enter the skin under certain circumstances [182-184]. This mechanism is also consistent with the fact that the PVs infect the basal epithelial layer at the traumatized epithelium [101, 185].

It is very difficult to identify these specific epitopes of anti-L1 antibodies by the epitope mapping method because of limitations of the method (**Fig. 4.2.9**). The synthesized linear peptides and cyclic peptides cannot mimic the epitopes for anti-L1$_{LONG}$ and L1$_{SHORT}$ antibodies, which might be due to the complex of the discontinuous and conformation epitopes (discussed above). However, several linear epitopes were identified from sera which were mixed from five tumor-bearing animals. This result indicates that L1 antibodies against linear epitopes can be largely generated when the viral particles are massively produced. The identified ITGHPLY, DYLGMSK and KRSLPASRN peptide is located on the putative DE loop, FG loop and C-terminal arm, respectively, when MnPV L1 amino acid sequence is aligned to HPV16 L1 sequence. This result is in line with reports that linear epitopes are located on the VLPs surface [186, 187]. For example, HPV 2, 27

and 57 type-specific monoclonal antibodies against linear epitopes, were mapped to the VLPs hypervariable surface loop regions [188].

5.5 The interaction between L1LONG and L1SHORT

L1LONG protein might facilitate the virus to evade the adaptive immune system in the early infection stage by the production of non-neutralizing antibodies. However, it is unknown how L1LONG can influence the appearance of these non-neutralizing antibodies and when it works as an antigen: either from the original virions or after virus replication from the first round of infection. Therefore, several hypotheses and related experiments are discussed in detail as follows:

Hypothesis 1: Anti-L1LONG antibodies are raised by virions which are formed by both L1 isoforms but with low copy numbers of L1LONG. It is known that typical capsids are composed of L1SHORT and L2 proteins. However, with the help of L1SHORT, a proportion of particles might be able to incorporate L1LONG, thus leading to a production of antibodies against the exposed N-terminal arm. This hypothesis can first be supported by the mass spectrometry analysis of the PsVs samples, where an N-terminal peptide of L1LONG was detected (**Fig. 4.3.1**). However, a drawback of this experiment is that there might be free over-expressed L1LONG proteins purified together with the cellular proteins after ultracentrifugation. Furthermore, the immunofluorescence staining of PsVs-infected cells showed that L1LONG-HA and L1MIDDLE-HA fusion proteins do not take part in the capsid formation even with help of L1SHORT and L2 (**Fig. 4.3.3**). Therefore, it is very important to know whether the lack of HA-tag signal on the PsVs here is due to the defective capsid formation ability of L1LONG and L1MIDDLE or interruption of capsid assembly by the additional peptides at the C-terminus. According to several publications, peptide fusing to the C-terminal region, in which the same part was replaced, did not influence the capsid formation (VLPs still can be formed) [37, 39, 189, 190]. Besides, the mAbs mixture staining of L1SHORT-HA fusion protein might represent the assembled capsid proteins, since they are neutralizing antibodies against MnPV VLPs [123]. There was a perfect colocalization of HA signal and mAbs mixture by detection of L1SHORT-HA fusion protein, which might indicate the HA-tag at the C-terminus does not interrupt the capsid formation of the L1 protein. However, to confirm the above assumption, capsid formation of L1SHORT-HA fusion protein has to be checked in the future. Besides, specific antibodies against L1LONG need to be produced for the detection of L1LONG on capsids as well as the expression pattern

in 3D raft culture or tissue sections. Overall, even though hypothesis 1 is possible, more supportive evidences have to be provided.

Hypothesis 2: Anti-L1LONG antibodies are generated following the expression of L1LONG after virus infection. The absence of anti-L1SHORT antibodies in the early infection stage might be caused by the expression pattern which has not yet switched from long to short (**see discussion in Chapter 5.1**). Apart from this reason, if both L1 proteins are expressed, the interference of L1LONG protein with the capsid formation process might also lead to the absence of L1SHORT seroresponses. This hypothesis is supported by the detection of L1LONG N-terminal peptide in PsVs extract when L1LONG is co-expressed with L1SHORT (**Fig. 4.3.1**) and further demonstrated by fewer infectious particles formed in the "L1L + L1S + L2" PsVs production (**Fig. 4.3.4**). Moreover, in addition to an interaction of L1LONG/L1MIDDLE and L1SHORT, co-localization was demonstrated at the nuclear rim or cytoplasm of transfected cells which was induced by an outward shift of the nuclear L1LONG and L1MIDDLE in the presence of L1SHORT (**Fig. 4.3.6**). Little has been reported about an interaction between different virus capsid protein variants. However, it was demonstrated that small molecule 'assembly effectors' can interfere with capsid assembly by changing conformation, interrupting subunit-subunit interaction or crosslinking of protein and DNA [191, 192]. For example, peptides can interfere with HIV capsid substructure interaction, inhibit capsid maturation and trigger disassembly [191]. Small molecules are able to prevent HBV capsid assembly by altering the geometry of interactions between subunits or strengthening these interactions, leading to malformed or empty capsid, respectively [193, 194]. Therefore, L1LONG protein might also serve as an assembly effector that modulates capsid assembly, thus inhibiting effective capsid formation by L1SHORT. Overall, based on the above results, this scenario remains highly possible.

5.6 Conclusion and perspectives

Mastomys coucha, which is latently infected with MnPV, is a useful preclinical model to investigate the role of papillomavirus-induced skin carcinogenesis. Apparently, there is immune tolerance after virus infection, since some animals develop cutaneous lesions such as papillomas or keratoacanthomas that can even progress to non-melanoma skin cancer. Considering a fundamental role of different L1 isoforms in virus infection, the present study shows an immune escape scenario, indicated by the deficiency of serum antibodies capable of neutralizing viruses in the early infection phase (**Fig. 5.1**). The L1 expression switch from a long to a short variant, the inability of L1LONG and L1MIDDLE to form correct capsids and interference with capsid formation might contribute to minimizing the exposure of viral particles to immune and epithelial cells, thus leading to low diversity of plasma cells secreting conformation-dependent neutralizing antibodies. With this strategy, viruses are able to evade the host immune system in the beginning of an infection, thus facilitating efficient encapsidation and productive infection at later stages of the viral life cycle.

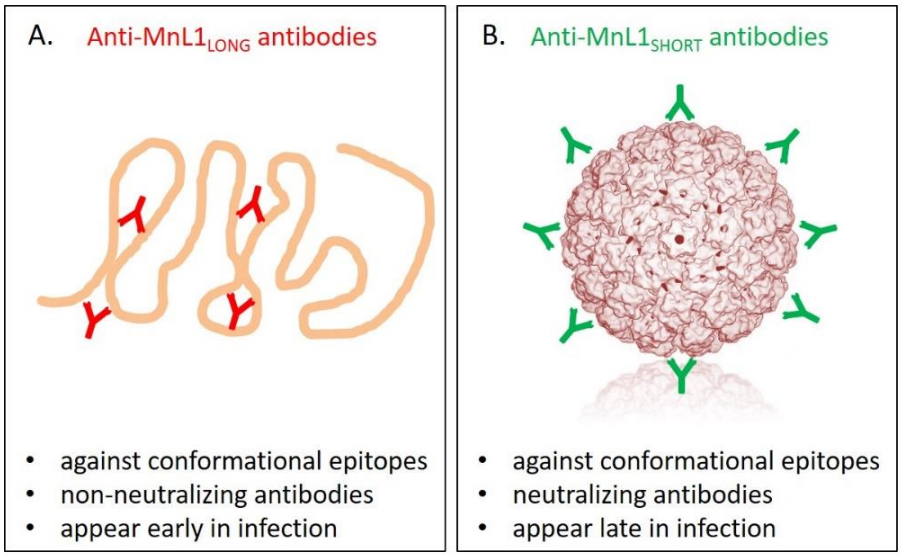

Figure 5.1: Schematic overview of the characterization of anti-L1LONG and L1SHORT antibodies. (A). Antibodies directed against the MnPV L1LONG protein in the early infection stage are neither reactive nor protective against the native capsids, but possibly against the conformational epitopes on a loop formed by 41 amino acids at the L1LONG N-terminus. **(B).** Neutralizing antibodies which recognize conformational epitopes against the L1SHORT protein only arose during the late phase of infection.

With regard to the fact that immune responses of non-neutralizing L1 antibodies are dominant in the MnPV early infection stage, it is also noteworthy to examine the early L1 immune responses in unvaccinated but sexually active young women with infection of high-risk

HPV types, which contain alternative translation initiation codons in the L1 ORF as well. It will be of importance to elucidate immune escape mechanism during the history of HPV infection.

Furthermore, since there were different immune responses patterns of anti-L1$_{LONG}$ and L1$_{SHORT}$ antibodies in the naturally infected colony, the immunogenicity of different L1 isoforms needs to be further investigated. The injection of plasmids exclusively expressing different L1 isoforms and purified proteins from the baculovirus expression system will be performed with a tattoo gun and subcutaneous injection in virus-free animals. Such studies will be of great help to further understand the structure of L1$_{LONG}$ and L1$_{SHORT}$ as well as their capsid formation ability. Besides, future evaluation of the neutralizing capacity of anti-L1$_{LONG}$ and L1$_{SHORT}$ antibodies will be strengthened by passive immunization, which will be performed in virus-free animals by using the above generated L1 antibodies.

6. References

1. Doorbar, J., et al., *Human papillomavirus molecular biology and disease association.* Rev Med Virol, 2015. **25 Suppl 1**: p. 2-23.
2. Van Doorslaer, K., et al., *The Papillomavirus Episteme: a central resource for papillomavirus sequence data and analysis.* Nucleic Acids Res, 2013. **41**(Database issue): p. D571-8.
3. Bernard, H.U., et al., *Classification of papillomaviruses (PVs) based on 189 PV types and proposal of taxonomic amendments.* Virology, 2010. **401**(1): p. 70-9.
4. de Villiers, E.M., et al., *Classification of papillomaviruses.* Virology, 2004. **324**(1): p. 17-27.
5. Van Doorslaer, K., *Evolution of the papillomaviridae.* Virology, 2013. **445**(1-2): p. 11-20.
6. Egawa, N., et al., *Human Papillomaviruses; Epithelial Tropisms, and the Development of Neoplasia.* Viruses, 2015. **7**(7): p. 3863-90.
7. de Villiers, E.M., *Cross-roads in the classification of papillomaviruses.* Virology, 2013. **445**(1-2): p. 2-10.
8. Moody, C.A. and L.A. Laimins, *Human papillomavirus oncoproteins: pathways to transformation.* Nat Rev Cancer, 2010. **10**(8): p. 550-60.
9. Egawa, N. and J. Doorbar, *The low-risk papillomaviruses.* Virus Res, 2017. **231**: p. 119-127.
10. Chabeda, A., et al., *Therapeutic vaccines for high-risk HPV-associated diseases.* Papillomavirus Res, 2017. **5**: p. 46-58.
11. zur Hausen, H., *Papillomaviruses and cancer: from basic studies to clinical application.* Nat Rev Cancer, 2002. **2**(5): p. 342-50.
12. Favre, M., et al., *Chromatin-like structures obtained after alkaline disruption of bovine and human papillomaviruses.* J Virol, 1977. **21**(3): p. 1205-9.
13. Stanley, M.A., *Epithelial cell responses to infection with human papillomavirus.* Clin Microbiol Rev, 2012. **25**(2): p. 215-22.
14. Bravo, I.G. and A. Alonso, *Mucosal human papillomaviruses encode four different E5 proteins whose chemistry and phylogeny correlate with malignant or benign growth.* J Virol, 2004. **78**(24): p. 13613-26.
15. Ustav, M., et al., *Identification of the origin of replication of bovine papillomavirus and characterization of the viral origin recognition factor E1.* EMBO J, 1991. **10**(13): p. 4321-9.

16. Ustav, E., et al., *The bovine papillomavirus origin of replication requires a binding site for the E2 transcriptional activator.* Proc Natl Acad Sci U S A, 1993. **90**(3): p. 898-902.

17. Lee, D., et al., *Identification of sequence requirement for the origin of DNA replication in human papillomavirus type 18.* Virus Res, 1997. **52**(1): p. 97-108.

18. Bergvall, M., T. Melendy, and J. Archambault, *The E1 proteins.* Virology, 2013. **445**(1-2): p. 35-56.

19. McBride, A.A., *The papillomavirus E2 proteins.* Virology, 2013. **445**(1-2): p. 57-79.

20. Frattini, M.G. and L.A. Laimins, *Binding of the human papillomavirus E1 origin-recognition protein is regulated through complex formation with the E2 enhancer-binding protein.* Proc Natl Acad Sci U S A, 1994. **91**(26): p. 12398-402.

21. Lambert, P.F., B.A. Spalholz, and P.M. Howley, *A transcriptional repressor encoded by BPV-1 shares a common carboxy-terminal domain with the E2 transactivator.* Cell, 1987. **50**(1): p. 69-78.

22. Lim, D.A., et al., *Competition for DNA binding sites between the short and long forms of E2 dimers underlies repression in bovine papillomavirus type 1 DNA replication control.* J Virol, 1998. **72**(3): p. 1931-40.

23. Ammermann, I., et al., *Inhibition of transcription and DNA replication by the papillomavirus E8-E2C protein is mediated by interaction with corepressor molecules.* J Virol, 2008. **82**(11): p. 5127-36.

24. Bryan, J.T. and D.R. Brown, *Association of the human papillomavirus type 11 E1()E4 protein with cornified cell envelopes derived from infected genital epithelium.* Virology, 2000. **277**(2): p. 262-9.

25. Doorbar, J., *The E4 protein; structure, function and patterns of expression.* Virology, 2013. **445**(1-2): p. 80-98.

26. DiMaio, D. and L.M. Petti, *The E5 proteins.* Virology, 2013. **445**(1-2): p. 99-114.

27. Dyson, N., *The regulation of E2F by pRB-family proteins.* Genes Dev, 1998. **12**(15): p. 2245-62.

28. Cheng, S., et al., *Differentiation-dependent up-regulation of the human papillomavirus E7 gene reactivates cellular DNA replication in suprabasal differentiated keratinocytes.* Genes Dev, 1995. **9**(19): p. 2335-49.

29. Demers, G.W., C.L. Halbert, and D.A. Galloway, *Elevated wild-type p53 protein levels in human epithelial cell lines immortalized by the human papillomavirus type 16 E7 gene.* Virology, 1994. **198**(1): p. 169-74.
30. Doorbar, J., *The papillomavirus life cycle.* J Clin Virol, 2005. **32 Suppl 1**: p. S7-15.
31. Buck, C.B., P.M. Day, and B.L. Trus, *The papillomavirus major capsid protein L1.* Virology, 2013. **445**(1-2): p. 169-74.
32. Webb, E., J. Cox, and S. Edwards, *Cervical cancer-causing human papillomaviruses have an alternative initiation site for the L1 protein.* Virus Genes, 2005. **30**(1): p. 31-5.
33. Joh, J., et al., *Searching for the initiating site of the major capsid protein to generate virus-like particles for a novel laboratory mouse papillomavirus.* Exp Mol Pathol, 2014. **96**(2): p. 155-61.
34. Li, Z., et al., *The C-Terminal Arm of the Human Papillomavirus Major Capsid Protein Is Immunogenic and Involved in Virus-Host Interaction.* Structure, 2016. **24**(6): p. 874-85.
35. Modis, Y., B.L. Trus, and S.C. Harrison, *Atomic model of the papillomavirus capsid.* EMBO J, 2002. **21**(18): p. 4754-62.
36. Chen, X.S., et al., *Structure of small virus-like particles assembled from the L1 protein of human papillomavirus 16.* Mol Cell, 2000. **5**(3): p. 557-67.
37. Peng, S., et al., *Papillomavirus virus-like particles can deliver defined CTL epitopes to the MHC class I pathway.* Virology, 1998. **240**(1): p. 147-57.
38. Paintsil, J., et al., *Carboxyl terminus of bovine papillomavirus type-1 L1 protein is not required for capsid formation.* Virology, 1996. **223**(1): p. 238-44.
39. Muller, M., et al., *Chimeric papillomavirus-like particles.* Virology, 1997. **234**(1): p. 93-111.
40. Baker, T.S., et al., *Structures of bovine and human papillomaviruses. Analysis by cryoelectron microscopy and three-dimensional image reconstruction.* Biophys J, 1991. **60**(6): p. 1445-56.
41. Kirnbauer, R., et al., *Papillomavirus L1 major capsid protein self-assembles into virus-like particles that are highly immunogenic.* Proc Natl Acad Sci U S A, 1992. **89**(24): p. 12180-4.
42. Hagensee, M.E., N. Yaegashi, and D.A. Galloway, *Self-assembly of human papillomavirus type 1 capsids by expression of the L1 protein alone or by coexpression of the L1 and L2 capsid proteins.* J Virol, 1993. **67**(1): p. 315-22.

43. Hanumantha Rao, N., et al., *Expression of codon optimized major capsid protein (L1) of human papillomavirus type 16 and 18 in Pichia pastoris; purification and characterization of the virus-like particles.* Vaccine, 2011. **29**(43): p. 7326-34.

44. Belnap, D.M., et al., *Conserved features in papillomavirus and polyomavirus capsids.* J Mol Biol, 1996. **259**(2): p. 249-63.

45. Day, P.M., et al., *Establishment of papillomavirus infection is enhanced by promyelocytic leukemia protein (PML) expression.* Proc Natl Acad Sci U S A, 2004. **101**(39): p. 14252-7.

46. Buck, C.B., et al., *Arrangement of L2 within the papillomavirus capsid.* J Virol, 2008. **82**(11): p. 5190-7.

47. Wolf, M., et al., *Subunit interactions in bovine papillomavirus.* Proc Natl Acad Sci U S A, 2010. **107**(14): p. 6298-303.

48. Yang, J., Y.L. Wang, and L.S. Si, *Predicting the nuclear localization signals of 107 types of HPV L1 proteins by bioinformatic analysis.* Genomics Proteomics Bioinformatics, 2006. **4**(1): p. 34-41.

49. Merle, E., et al., *Nuclear import of HPV11 L1 capsid protein is mediated by karyopherin alpha2beta1 heterodimers.* J Cell Biochem, 1999. **74**(4): p. 628-37.

50. Finnen, R.L., et al., *Interactions between papillomavirus L1 and L2 capsid proteins.* J Virol, 2003. **77**(8): p. 4818-26.

51. Florin, L., et al., *Assembly and translocation of papillomavirus capsid proteins.* J Virol, 2002. **76**(19): p. 10009-14.

52. Schafer, F., L. Florin, and M. Sapp, *DNA binding of L1 is required for human papillomavirus morphogenesis in vivo.* Virology, 2002. **295**(1): p. 172-81.

53. Zhao, K.N., et al., *DNA packaging by L1 and L2 capsid proteins of bovine papillomavirus type 1.* Virology, 1998. **243**(2): p. 482-91.

54. Roden, R.B., et al., *Positively charged termini of the L2 minor capsid protein are necessary for papillomavirus infection.* J Virol, 2001. **75**(21): p. 10493-7.

55. Wang, J.W. and R.B. Roden, *L2, the minor capsid protein of papillomavirus.* Virology, 2013. **445**(1-2): p. 175-86.

56. Heino, P., J. Zhou, and P.F. Lambert, *Interaction of the papillomavirus transcription/replication factor, E2, and the viral capsid protein, L2.* Virology, 2000. **276**(2): p. 304-14.

57. Rose, R.C., et al., *Expression of human papillomavirus type 11 L1 protein in insect cells: in vivo and in vitro assembly of viruslike particles.* J Virol, 1993. **67**(4): p. 1936-44.

58. Harper, D.M., et al., *Efficacy of a bivalent L1 virus-like particle vaccine in prevention of infection with human papillomavirus types 16 and 18 in young women: a randomised controlled trial.* Lancet, 2004. **364**(9447): p. 1757-65.

59. Schwartz, S., *Regulation of human papillomavirus late gene expression.* Ups J Med Sci, 2000. **105**(3): p. 171-92.

60. Buck, C.B., et al., *Efficient intracellular assembly of papillomaviral vectors.* J Virol, 2004. **78**(2): p. 751-7.

61. Conway, M.J. and C. Meyers, *Replication and assembly of human papillomaviruses.* J Dent Res, 2009. **88**(4): p. 307-17.

62. Sapp, M., et al., *Organization of the major and minor capsid proteins in human papillomavirus type 33 virus-like particles.* J Gen Virol, 1995. **76 (Pt 9)**: p. 2407-12.

63. Mach, H., et al., *Disassembly and reassembly of yeast-derived recombinant human papillomavirus virus-like particles (HPV VLPs).* J Pharm Sci, 2006. **95**(10): p. 2195-206.

64. Li, M., et al., *Intercapsomeric disulfide bonds in papillomavirus assembly and disassembly.* J Virol, 1998. **72**(3): p. 2160-7.

65. Kines, R.C., et al., *The initial steps leading to papillomavirus infection occur on the basement membrane prior to cell surface binding.* Proc Natl Acad Sci U S A, 2009. **106**(48): p. 20458-63.

66. Richards, R.M., et al., *Cleavage of the papillomavirus minor capsid protein, L2, at a furin consensus site is necessary for infection.* Proc Natl Acad Sci U S A, 2006. **103**(5): p. 1522-7.

67. Johnson, K.M., et al., *Role of heparan sulfate in attachment to and infection of the murine female genital tract by human papillomavirus.* J Virol, 2009. **83**(5): p. 2067-74.

68. Day, P.M., D.R. Lowy, and J.T. Schiller, *Heparan sulfate-independent cell binding and infection with furin-precleaved papillomavirus capsids.* J Virol, 2008. **82**(24): p. 12565-8.

69. Wilson, V.G., et al., *Papillomavirus E1 proteins: form, function, and features.* Virus Genes, 2002. **24**(3): p. 275-90.

70. Stubenrauch, F. and L.A. Laimins, *Human papillomavirus life cycle: active and latent phases.* Semin Cancer Biol, 1999. **9**(6): p. 379-86.

71. Lambert, P.F., *Papillomavirus DNA replication.* J Virol, 1991. **65**(7): p. 3417-20.

72. Chen, J.J., et al., *Interaction of papillomavirus E6 oncoproteins with a putative calcium-binding protein.* Science, 1995. **269**(5223): p. 529-31.

73. Flores, E.R., et al., *Establishment of the human papillomavirus type 16 (HPV-16) life cycle in an immortalized human foreskin keratinocyte cell line.* Virology, 1999. **262**(2): p. 344-54.

74. Chow, L.T., T.R. Broker, and B.M. Steinberg, *The natural history of human papillomavirus infections of the mucosal epithelia.* APMIS, 2010. **118**(6-7): p. 422-49.

75. Doorbar, J., *Papillomavirus life cycle organization and biomarker selection.* Dis Markers, 2007. **23**(4): p. 297-313.

76. Bravo, I.G. and M. Felez-Sanchez, *Papillomaviruses: Viral evolution, cancer and evolutionary medicine.* Evol Med Public Health, 2015. **2015**(1): p. 32-51.

77. Gutierrez-Xicotencatl, L., et al., *Humoral Immune Response Against Human Papillomavirus as Source of Biomarkers for the Prediction and Detection of Cervical Cancer.* Viral Immunol, 2016. **29**(2): p. 83-94.

78. Chen, R., et al., *Presence of DNA of human papillomavirus 16 but no other types in tumor-free tonsillar tissue.* J Clin Microbiol, 2005. **43**(3): p. 1408-10.

79. Malcolm, K., et al., *Multiple conformational epitopes are recognized by natural and induced immunity to the E7 protein of human papilloma virus type 16 in man.* Intervirology, 2000. **43**(3): p. 165-73.

80. Vonka, V., et al., *Prospective study on cervical neoplasia IV. Presence of HPV antibodies.* Int J Cancer, 1999. **80**(3): p. 365-8.

81. Reuschenbach, M., et al., *Characterization of humoral immune responses against p16, p53, HPV16 E6 and HPV16 E7 in patients with HPV-associated cancers.* Int J Cancer, 2008. **123**(11): p. 2626-31.

82. Viladiu, P., et al., *Human papillomavirus DNA and antibodies to human papillomaviruses 16 E2, L2, and E7 peptides as predictors of survival in patients with squamous cell cervical cancer.* J Clin Oncol, 1997. **15**(2): p. 610-9.

83. Dillner, J., et al., *Mapping of linear epitopes of human papillomavirus type 16: the L1 and L2 open reading frames.* Int J Cancer, 1990. **45**(3): p. 529-35.

84. Carter, J.J. and D.A. Galloway, *Humoral immune response to human papillomavirus infection.* Clin Dermatol, 1997. **15**(2): p. 249-59.

85. Urquiza, M., et al., *Two L1-peptides are excellent tools for serological detection of HPV-associated cervical carcinoma lesions.* Biochem Biophys Res Commun, 2005. **332**(1): p. 224-32.

86. Schafer, K., et al., *Serological markers for papillomavirus infection and skin tumour development in the rodent model Mastomys coucha.* J Gen Virol, 2011. **92**(Pt 2): p. 383-94.

87. Doorbar, J., *Model systems of human papillomavirus-associated disease.* J Pathol, 2016. **238**(2): p. 166-79.

88. Shope, R.E. and E.W. Hurst, *Infectious Papillomatosis of Rabbits : With a Note on the Histopathology.* J Exp Med, 1933. **58**(5): p. 607-24.

89. Campo, M.S., *Animal models of papillomavirus pathogenesis.* Virus Res, 2002. **89**(2): p. 249-61.

90. Lange, C.E. and C. Favrot, *Canine papillomaviruses.* Vet Clin North Am Small Anim Pract, 2011. **41**(6): p. 1183-95.

91. Jahan-Parwar, B., et al., *Development of a canine model for recurrent respiratory papillomatosis.* Ann Otol Rhinol Laryngol, 2003. **112**(12): p. 1011-3.

92. Wilgenburg, B.J., et al., *Characterization of immune responses during regression of rabbit oral papillomavirus infections.* Comp Med, 2005. **55**(5): p. 431-9.

93. Suzich, J.A., et al., *Systemic immunization with papillomavirus L1 protein completely prevents the development of viral mucosal papillomas.* Proc Natl Acad Sci U S A, 1995. **92**(25): p. 11553-7.

94. Kruppa, T.F., et al., *Mastomys natalensis or Mastomys coucha. Correct species designation in animal experiments.* Trop Med Parasitol, 1990. **41**(2): p. 219-20.

95. Muller, H. and L. Gissmann, *Mastomys natalensis papilloma virus (MnPV), the causative agent of epithelial proliferations: characterization of the virus particle.* J Gen Virol, 1978. **41**(2): p. 315-23.

96. Nafz, J., et al., *A novel rodent papillomavirus isolated from anogenital lesions in its natural host.* Virology, 2008. **374**(1): p. 186-97.

97. Reinacher, M., et al., *Localization of papillomavirus and virus-specific antigens in the skin of tumor-bearing Mastomys natalensis (GRA Giessen).* Med Microbiol Immunol, 1978. **165**(2): p. 93-9.

98. Burtscher, H., W. Grunberg, and G. Meingassner, *[Infectious keratoacanthomas of the epidermis in Praomys (Mastomys) natalensis].* Naturwissenschaften, 1973. **60**(4): p. 209-10.

99. Smit, A., et al., *Biochemical genetic markers to identify two morphologically similar South African Mastomys species (Rodentia: Muridae).* Biochem Syst Ecol, 2001. **29**(1): p. 21-30.

100. Vinzon, S.E., et al., *Protective vaccination against papillomavirus-induced skin tumors under immunocompetent and immunosuppressive conditions: a preclinical study using a natural outbred animal model.* PLoS Pathog, 2014. **10**(2): p. e1003924.

101. Nafz, J., et al., *Persistence of Mastomys natalensis papillomavirus in multiple organs identifies novel targets for infection.* J Gen Virol, 2007. **88**(Pt 10): p. 2670-8.

102. Rudolph, R. and W. Thiel, *[Pathological anatomy and histology of spontaneous, epithelial skin tumors in Mastomys natalensis].* Zentralbl Veterinarmed A, 1976. **23**(05): p. 429-41.

103. Rudolph, R.L., et al., *Morphology of experimentally induced so-called keratoacanthomas and squamous cell carcinomas in 2 inbred-lines of Mastomys natalensis.* J Comp Pathol, 1981. **91**(1): p. 123-34.

104. Hasche, D., et al., *The interplay of UV and cutaneous papillomavirus infection in skin cancer development.* PLoS Pathog, 2017. **13**(11): p. e1006723.

105. Steinbach, A. and A.B. Riemer, *Immune evasion mechanisms of human papillomavirus: An update.* Int J Cancer, 2018. **142**(2): p. 224-229.

106. Senba, M. and N. Mori, *Mechanisms of virus immune evasion lead to development from chronic inflammation to cancer formation associated with human papillomavirus infection.* Oncol Rev, 2012. **6**(2): p. e17.

107. Schafer, K., T. Waterboer, and F. Rosl, *A capture ELISA for monitoring papillomavirus-induced antibodies in Mastomys coucha.* J Virol Methods, 2010. **163**(2): p. 216-21.

108. Salvermoser, M.S.G., *The Mastomys natalensis papillomavirus transcriptome in skin: implications for pathogenicity*. 2012, Ludwig-Maximilians-Universität München.

109. Bieniossek, C., et al., *MultiBac: expanding the research toolbox for multiprotein complexes.* Trends Biochem Sci, 2012. **37**(2): p. 49-57.

110. Bieniossek, C., T.J. Richmond, and I. Berger, *MultiBac: multigene baculovirus-based eukaryotic protein complex production.* Curr Protoc Protein Sci, 2008. **Chapter 5**: p. Unit 5 20.

111. Fitzgerald, D.J., et al., *Protein complex expression by using multigene baculoviral vectors.* Nat Methods, 2006. **3**(12): p. 1021-32.

112. Berger, I., D.J. Fitzgerald, and T.J. Richmond, *Baculovirus expression system for heterologous multiprotein complexes.* Nat Biotechnol, 2004. **22**(12): p. 1583-7.

113. Trowitzsch, S., et al., *New baculovirus expression tools for recombinant protein complex production.* J Struct Biol, 2010. **172**(1): p. 45-54.

114. Luckow, V.A., et al., *Efficient generation of infectious recombinant baculoviruses by site-specific transposon-mediated insertion of foreign genes into a baculovirus genome propagated in Escherichia coli.* J Virol, 1993. **67**(8): p. 4566-79.

115. Luckow, V.A., *Baculovirus systems for the expression of human gene products.* Curr Opin Biotechnol, 1993. **4**(5): p. 564-72.

116. Pelosse, M., et al., *MultiBac: from protein complex structures to synthetic viral nanosystems.* BMC Biol, 2017. **15**(1): p. 99.

117. Biryukov, J. and C. Meyers, *Papillomavirus Infectious Pathways: A Comparison of Systems.* Viruses, 2015. **7**(8): p. 4303-25.

118. Holmgren, S.C., et al., *The minor capsid protein L2 contributes to two steps in the human papillomavirus type 31 life cycle.* J Virol, 2005. **79**(7): p. 3938-48.

119. Ishii, Y., et al., *Human papillomavirus 16 minor capsid protein L2 helps capsomeres assemble independently of intercapsomeric disulfide bonding.* Virus Genes, 2005. **31**(3): p. 321-8.

120. Kondo, K., et al., *Neutralization of HPV16, 18, 31, and 58 pseudovirions with antisera induced by immunizing rabbits with synthetic peptides representing segments of the HPV16 minor capsid protein L2 surface region.* Virology, 2007. **358**(2): p. 266-72.

121. Roden, R.B., et al., *In vitro generation and type-specific neutralization of a human papillomavirus type 16 virion pseudotype.* J Virol, 1996. **70**(9): p. 5875-83.

122. Schäfer, K., *Mastomys coucha as animal model for vaccines against papillomavirus-induced skin tumors*. 2010, University Heidelberg: Heidelberg.

123. Schmitt, L.K., *Development and characterization of monoclonal antibodies against the major capsid protein of Mastomys natalensis papillomavirus*. 2012, Mannheim University of Applied Sciences.

124. Kochetov, A.V., *[Alternative translation start sites and their significance for eukaryotic proteome].* Mol Biol (Mosk), 2006. **40**(5): p. 788-95.

125. Kozak, M., *The scanning model for translation: an update.* J Cell Biol, 1989. **108**(2): p. 229-41.

126. Kochetov, A.V., *Alternative translation start sites and hidden coding potential of eukaryotic mRNAs.* Bioessays, 2008. **30**(7): p. 683-91.

127. Kozak, M., *Structural features in eukaryotic mRNAs that modulate the initiation of translation.* J Biol Chem, 1991. **266**(30): p. 19867-70.

128. Stacey, S.N., et al., *Leaky scanning is the predominant mechanism for translation of human papillomavirus type 16 E7 oncoprotein from E6/E7 bicistronic mRNA.* J Virol, 2000. **74**(16): p. 7284-97.

129. Jackson, R., *A comparative view of initiation site selection mechanisms.* COLD SPRING HARBOR MONOGRAPH SERIES, 1996. **30**: p. 71-112.

130. Dominguez, D.I., et al., *Ribosome shunting in cauliflower mosaic virus. Identification of an essential and sufficient structural element.* J Biol Chem, 1998. **273**(6): p. 3669-78.

131. Futterer, J., Z. Kiss-Laszlo, and T. Hohn, *Nonlinear ribosome migration on cauliflower mosaic virus 35S RNA.* Cell, 1993. **73**(4): p. 789-802.

132. Latorre, P., D. Kolakofsky, and J. Curran, *Sendai virus Y proteins are initiated by a ribosomal shunt.* Mol Cell Biol, 1998. **18**(9): p. 5021-31.

133. Xi, Q., R. Cuesta, and R.J. Schneider, *Regulation of translation by ribosome shunting through phosphotyrosine-dependent coupling of adenovirus protein 100k to viral mRNAs.* J Virol, 2005. **79**(9): p. 5676-83.

134. Wang, X., et al., *Expression of HPV 58 long and short L1 capsid proteins in primary mouse keratinocyte cultures.* Protein Pept Lett, 2009. **16**(1): p. 65-74.

135. Salvermoser, M., et al., *Transcriptome analysis of Mastomys natalensis papillomavirus in productive lesions after natural infection.* J Gen Virol, 2016. **97**(7): p. 1658-69.

136. Peh, W.L., et al., *Life cycle heterogeneity in animal models of human papillomavirus-associated disease.* J Virol, 2002. **76**(20): p. 10401-16.

137. Graham, S.V., *Keratinocyte Differentiation-Dependent Human Papillomavirus Gene Regulation.* Viruses, 2017. **9**(9).

138. Chen, H.S., et al., *Papillomavirus capsid proteins mutually impact structure.* Virology, 2011. **412**(2): p. 378-83.

139. Buck, C.B., et al., *Maturation of papillomavirus capsids.* J Virol, 2005. **79**(5): p. 2839-46.

140. Biemelt, S., et al., *Production of human papillomavirus type 16 virus-like particles in transgenic plants.* J Virol, 2003. **77**(17): p. 9211-20.

141. Zhao, Q., et al., *Disassembly and reassembly of human papillomavirus virus-like particles produces more virion-like antibody reactivity.* Virol J, 2012. **9**: p. 52.

142. Cason, J., et al., *Detection of protein aggregates, but not virus-like particles, when the major (L1) coat protein of a wild-type human papillomavirus type 16 (HPV-16) is expressed in insect cells.* Biochem Soc Trans, 1994. **22**(3): p. 335S.

143. Xi, S.Z. and L.M. Banks, *Baculovirus expression of the human papillomavirus type 16 capsid proteins: detection of L1-L2 protein complexes.* J Gen Virol, 1991. **72 (Pt 12)**: p. 2981-8.

144. Kiselev, N.A. and A. Klug, *The structure of viruses of the papilloma-polyoma type. V. Tubular variants built of pentamers.* J Mol Biol, 1969. **40**(2): p. 155-71.

145. Volpers, C., et al., *Assembly of the major and the minor capsid protein of human papillomavirus type 33 into virus-like particles and tubular structures in insect cells.* Virology, 1994. **200**(2): p. 504-12.

146. Baker, T.S., D.L. Caspar, and W.T. Murakami, *Polyoma virus 'hexamer' tubes consist of paired pentamers.* Nature, 1983. **303**(5916): p. 446-8.

147. Baker, T.S. and D.L. Caspar, *Computer image modeling of pentamer packing in polyoma virus "hexamer" tubes.* Ultramicroscopy, 1984. **13**(1-2): p. 137-51.

148. Erickson, K.D., et al., *Virion assembly factories in the nucleus of polyomavirus-infected cells.* PLoS Pathog, 2012. **8**(4): p. e1002630.

149. Shishido-Hara, Y., et al., *Major and minor capsid proteins of human polyomavirus JC cooperatively accumulate to nuclear domain 10 for assembly into virions.* J Virol, 2004. **78**(18): p. 9890-903.

150. Shishido-Hara, Y., et al., *Promyelocytic leukemia nuclear bodies provide a scaffold for human polyomavirus JC replication and are disrupted after development of viral inclusions in progressive multifocal leukoencephalopathy.* J Neuropathol Exp Neurol, 2008. **67**(4): p. 299-308.

151. Wileman, T., *Aggresomes and pericentriolar sites of virus assembly: cellular defense or viral design?* Annu Rev Microbiol, 2007. **61**: p. 149-67.

152. Novoa, R.R., et al., *Virus factories: associations of cell organelles for viral replication and morphogenesis.* Biol Cell, 2005. **97**(2): p. 147-72.

153. Lowy, D.R. and J.T. Schiller, *Prophylactic human papillomavirus vaccines.* J Clin Invest, 2006. **116**(5): p. 1167-73.

154. Hangartner, L., R.M. Zinkernagel, and H. Hengartner, *Antiviral antibody responses: the two extremes of a wide spectrum.* Nat Rev Immunol, 2006. **6**(3): p. 231-43.

155. Klasse, P.J. and Q.J. Sattentau, *Mechanisms of virus neutralization by antibody.* Curr Top Microbiol Immunol, 2001. **260**: p. 87-108.

156. Day, P.M., et al., *Neutralization of human papillomavirus with monoclonal antibodies reveals different mechanisms of inhibition.* J Virol, 2007. **81**(16): p. 8784-92.

157. Che, Z., et al., *Antibody-mediated neutralization of human rhinovirus 14 explored by means of cryoelectron microscopy and X-ray crystallography of virus-Fab complexes.* J Virol, 1998. **72**(6): p. 4610-22.

158. Possee, R.D., G.C. Schild, and N.J. Dimmock, *Studies on the mechanism of neutralization of influenza virus by antibody: evidence that neutralizing antibody (anti-haemagglutinin) inactivates influenza virus in vivo by inhibiting virion transcriptase activity.* J Gen Virol, 1982. **58**(Pt 2): p. 373-86.

159. Varghese, R., et al., *Postentry neutralization of adenovirus type 5 by an antihexon antibody.* J Virol, 2004. **78**(22): p. 12320-32.

160. Virgin, H.W.t., M.A. Mann, and K.L. Tyler, *Protective antibodies inhibit reovirus internalization and uncoating by intracellular proteases.* J Virol, 1994. **68**(10): p. 6719-29.

161. Zhuge, W., et al., *Antibodies that neutralize SIV(mac)251 in T lymphocytes cause interruption of the viral life cycle in macrophages by preventing nuclear import of viral DNA.* Virology, 2001. **287**(2): p. 436-45.

162. Carter, J.J., et al., *Comparison of human papillomavirus types 16, 18, and 6 capsid antibody responses following incident infection.* J Infect Dis, 2000. **181**(6): p. 1911-9.

163. Ho, G.Y., et al., *Natural history of human papillomavirus type 16 virus-like particle antibodies in young women.* Cancer Epidemiol Biomarkers Prev, 2004. **13**(1): p. 110-6.

164. Ray, U., et al., *JC polyomavirus mutants escape antibody-mediated neutralization.* Sci Transl Med, 2015. **7**(306): p. 306ra151.

165. Nicholls, P.K., et al., *Regression of canine oral papillomas is associated with infiltration of CD4+ and CD8+ lymphocytes.* Virology, 2001. **283**(1): p. 31-9.

166. Monnier-Benoit, S., et al., *Immunohistochemical analysis of CD4+ and CD8+ T-cell subsets in high risk human papillomavirus-associated pre-malignant and malignant lesions of the uterine cervix.* Gynecol Oncol, 2006. **102**(1): p. 22-31.

167. Stanley, M., *HPV - immune response to infection and vaccination.* Infect Agent Cancer, 2010. **5**: p. 19.

168. Wang, J.W. and R.B. Roden, *Virus-like particles for the prevention of human papillomavirus-associated malignancies.* Expert Rev Vaccines, 2013. **12**(2): p. 129-41.

169. Skiba, D., et al., *Prognostic significance of serum antibodies to HPV-16 L1 virus-like particles in patients with invasive cervical cancer.* Anticancer Res, 2006. **26**(6C): p. 4921-6.

170. Jauhari, H., et al., *Cyclosporine trough levels in renal graft recipients.* J Indian Med Assoc, 1999. **97**(11): p. 476-7.

171. Gafter-Gvili, A., et al., *Cyclosporin A-induced hair growth in mice is associated with inhibition of calcineurin-dependent activation of NFAT in follicular keratinocytes.* Am J Physiol Cell Physiol, 2003. **284**(6): p. C1593-603.

172. Clydesdale, G.J., G.W. Dandie, and H.K. Muller, *Ultraviolet light induced injury: immunological and inflammatory effects.* Immunol Cell Biol, 2001. **79**(6): p. 547-68.

173. Wei, J., et al., *Photodamage: all signs lead to actinic keratosis and early squamous cell carcinoma.* Curr Probl Dermatol, 2015. **46**: p. 14-9.

174. Noonan, F.P. and E.C. De Fabo, *Ultraviolet-B dose-response curves for local and systemic immunosuppression are identical.* Photochem Photobiol, 1990. **52**(4): p. 801-10.

175. Norval, M. and G.M. Halliday, *The consequences of UV-induced immunosuppression for human health.* Photochem Photobiol, 2011. **87**(5): p. 965-77.

176. Booy, F.P., et al., *Two antibodies that neutralize papillomavirus by different mechanisms show distinct binding patterns at 13 A resolution.* J Mol Biol, 1998. **281**(1): p. 95-106.

177. Zhao, Q., et al., *Characterization of virus-like particles in GARDASIL(R) by cryo transmission electron microscopy.* Hum Vaccin Immunother, 2014. **10**(3): p. 734-9.

178. Lee, H., et al., *A cryo-electron microscopy study identifies the complete H16.V5 epitope and reveals global conformational changes initiated by binding of the neutralizing antibody fragment.* J Virol, 2015. **89**(2): p. 1428-38.

179. Zhang, X., et al., *Functional assessment and structural basis of antibody binding to human papillomavirus capsid.* Rev Med Virol, 2016. **26**(2): p. 115-28.

180. Li, Z., et al., *Transfer of IgG in the female genital tract by MHC class I-related neonatal Fc receptor (FcRn) confers protective immunity to vaginal infection.* Proc Natl Acad Sci U S A, 2011. **108**(11): p. 4388-93.

181. Rath, T., et al., *Regulation of immune responses by the neonatal fc receptor and its therapeutic implications.* Front Immunol, 2014. **5**: p. 664.

182. Geherin, S.A., et al., *The skin, a novel niche for recirculating B cells.* J Immunol, 2012. **188**(12): p. 6027-35.

183. El-Rachkidy, R.G., et al., *Humoral autoimmune responses to the squamous cell carcinoma antigen protein family in psoriasis.* J Invest Dermatol, 2008. **128**(9): p. 2219-24.

184. Majewski, S. and S. Jablonska, *Possible involvement of epidermodysplasia verruciformis human papillomaviruses in the immunopathogenesis of psoriasis: a proposed hypothesis.* Exp Dermatol, 2003. **12**(6): p. 721-8.

185. Roberts, J.N., et al., *Genital transmission of HPV in a mouse model is potentiated by nonoxynol-9 and inhibited by carrageenan.* Nat Med, 2007. **13**(7): p. 857-61.

186. Christensen, N.D., et al., *Surface conformational and linear epitopes on HPV-16 and HPV-18 L1 virus-like particles as defined by monoclonal antibodies.* Virology, 1996. **223**(1): p. 174-84.

187. Combita, A.L., et al., *Identification of two cross-neutralizing linear epitopes within the L1 major capsid protein of human papillomaviruses.* J Virol, 2002. **76**(13): p. 6480-6.

188. Senger, T., et al., *Identification of B-cell epitopes on virus-like particles of cutaneous alpha-human papillomaviruses.* J Virol, 2009. **83**(24): p. 12692-701.

189. Wakabayashi, M.T., et al., *Comparison of human papillomavirus type 16 L1 chimeric virus-like particles versus L1/L2 chimeric virus-like particles in tumor prevention.* Intervirology, 2002. **45**(4-6): p. 300-7.

190. Paz De la Rosa, G., et al., *An HPV 16 L1-based chimeric human papilloma virus-like particles containing a string of epitopes produced in plants is able to elicit humoral and cytotoxic T-cell activity in mice.* Virol J, 2009. **6**: p. 2.

191. Prevelige, P.E., Jr., *New approaches for antiviral targeting of HIV assembly.* J Mol Biol, 2011. **410**(4): p. 634-40.

192. Zlotnick, A. and S. Mukhopadhyay, *Virus assembly, allostery and antivirals.* Trends Microbiol, 2011. **19**(1): p. 14-23.

193. Katen, S.P., et al., *Trapping of hepatitis B virus capsid assembly intermediates by phenylpropenamide assembly accelerators.* ACS Chem Biol, 2010. **5**(12): p. 1125-36.

194. Katen, S.P., et al., *Assembly-directed antivirals differentially bind quasiequivalent pockets to modify hepatitis B virus capsid tertiary and quaternary structure.* Structure, 2013. **21**(8): p. 1406-16.

7. Appendix

A

aa	Amino acid
APS	Ammonium persulfate
ATG	Start codon

B

bp	Base pairs
BPV	Bovine papillomavirus
BSA	Bovine serum albumin

C

CBB	Casein blocking buffer
°C	Degree Celsius
cDNA	complementary DNA
CDS	protein coding sequence
CIN	Cervical intraepithelial neoplasia
cm	Centimeter
CmPV1	Chelonia mydas papillomavirus type 1
CMV	Cytomegalovirus
CO2	carbon dioxide
COPV	Canine oral papillomavirus
CPV1	Canine papillomavirus type 1
CRPV	Cottontail rabbit papillomavirus
CsA	Cyclosporine A
C-terminus	Carboxyl-terminus

D

DAPI	4', 6'-diamidino-2-phenylindol
DCs	Dendritic cells
ddH2O	doubly distilled water
DMEM	Dulbecco's modified Eagle's medium
DMSO	Dimethyl sulfoxide
DNA	Deoxyribonucleic acid
dNTP	Deoxynucleotide triphosphate
dNTPs	Deoxyribonucleotide triphosphates
DPBS	Dublecco's phosphate buffered saline
DTT	Dithiothreitol

E

E. coli	*Escherichia coli*
ECL	Enhanced Chemiluminescence Substrate

ECM	Extracellular matrix
EDTA	Ethylenediaminetetraacetic acid
EM	Electron microscopy
ELISA	Enzyme-linked immunosorbent assay
F	
FCS	Fetal calf serum
Fig.	Figure
G	
GFP	Green fluorescent protein
GI	Gastrointestinal
GST	Glutathione S-transferase
H	
h	Hour(s)
H_2SO_4	Sulfuric acid
HA	Hemagglutinin
HEPES	4-(2-hydroxyethyl)-1-piperazine-ethanesulfonicacid
HPV(s)	Human papillomavirus(es)
HPSGs	Heparin sulfate proteoglycans
HRP	Horseradish peroxidase
I	
IgG	Immunoglobulin G
IgM	Immunoglobulin M
IPTG	Isopropylß-D-1-thiogalactopyranoside
K	
Kan	Kanamycin
kb	Kilobases
KCl	Potassium chloride
kDa	Kilodalton
KH_2PO_4	Potassium dihydrogen phosphate
L	
L1	Papillomavirus major capsid protein
L2	Papillomavirus minor capsid protein
LB	lysogeny broth
LCs	Langerhans cells
LT	Large T antigen
M	
M	Mol
mA	Miliampère

mAbs	Monoclonal antibodies
McPV2	*Mastomys coucha* papillomavirus 2
MEFs	Mouse embryonic fibroblasts
MgCl2	Magnesium chloride
MgSO4	Magnesium sulfate
min	Minute(s)
mJ/cm2	Millijoule per square centimeter
ml	Milliliter
mM	Millimol
MmuPV	Murine Papillomavirus
MnPV	*Mastomys natalensis* papillomavirus
mRNA	Messenger RNA

N

Na_2HPO_4	Sodium dihydrogen phosphate
NaCl	Sodium chloride
NaOH	Sodium hydroxide
NLS	Nuclear localization signal
NMSC	Non-melanoma skin cancer
nm	Nanometer
NP-40	Nonidet P-40
nt	Nucleoride
NT	N-terminus
N-terminus	Amino-terminus

O

OD	Optical density
ORFs	Open reading frame(s)
Ori	Origin of replication

P

PAGE	Polyacrylamide gel electrophoresis
PBS	Phosphate-buffered saline
PCR	Polymerase chain reaction
PFA	Paraformaldehyde
PML	Promyelocytic leukemia protein
PMSF	Phenylmethylsulfonyl fluoride
P/S	Penicillin/Streptavidine
PRM	Parallel reaction monitoring
PsVs	Pseudovirions
pUC	pBR322-derived vector
PV	Papillomavirus
PVDF	Polyvinylidene fluoride

PyV	Polyomavirus
R	
Rb	retinoablastoma
RNA	Ribonucleic acid
rpm	rounds per minute
S	
SD	Standard deviation
SDS	Sodium dodecyl sulfate
sec	Second(s)
SEM	Standard error of the mean
Sf9	*Spodoptera frugiperda* 9
SOC	Super optimal broth
SPF	Specified pathogen-free
SPP	Synthetic papillomavirus particles
SV40	Simian Virus 40
T	
TAE	Tris acetate EDTA
Taq	Thermus aquaticus
TBS	Tris-buffered saline
TBST	Tris-buffered saline + Tween20
TEMED	Tetramethylethylenediamine
Th1/2	T helper 1/2
TMB	3,3',5,5'-Tetramethylbenzidine
TN-High-5	*Trichoplusia ni* High-5
URR	Upstream regulatory region
U	
UV	Ultraviolet light
URR	upstream regulatory region
V	
V	Volt
VLPs	Virus-like particles
v/v	Volume per volume
W	
WB	Western blot
µM	Micromol
µm	Micrometer

8. Acknowledgments

I would like to express my gratitude to Prof. Dr. Frank Rösl for his support and excellent supervision during my time as a PhD student. Thank you very much for giving me the possibility to work on this very interesting and challenging project to accomplish my PhD thesis.

Furthermore, I would like to thank:

China Scholarship Council (CSC) to give me the opportunity to study and pursue my doctoral degree overseas.

Prof. Dr. Martin Müller for his kindness to share great scientific knowledge and technical support. Thank you very much for your generous guidance and help all the time.

Prof. Dr. Baki Akgül who joined my TAC committee and always participated with good scientific discussion and advice.

Prof. Dr. Ralf Bartenschlager and PD. Dr. Karin Müller-Decker for attending my thesis evaluation committee.

Dr. Sabrina Vinzón who guided me to the *Mastomys* project in the beginning of my project.

Dr. Karsten Richter and Dr. Michelle Neßling for their excellent work on the Electron micrographs. Special thanks to Dr. Karsten Richter for teaching me how to handle the Electron microscopy and images processing.

Dr. Damir Krunic who taught me how to handle the confocal fluorescence microscopes and always being willing to help me to solve all the problems I had.

PD. Dr. Bischoff Ralf for epitope mapping and providing advice on data analysis.

Rui Cao and Ruwen Yang who supported me through my whole PhD with positively scientific communication and help whenever it was needed.

Dr. Martina Niebler, Dr. Daniel Hasche, Ilona Braspenning-Wesch, Elke Göckel-Krzikalla, and Sonja Stephan for their continuous support in the lab.

Other lab members of F030 (Linhan Zhuang, Regina Ly and Diana Schalk) for the nice working atmosphere and much-appreciated scientific support throughout my time in the lab.

Finally, I am grateful to my family: my parents for their continuous and unconditional love and support all over these years. Special thanks to my husband Guochao for his unparalleled trust, love, help and support.